



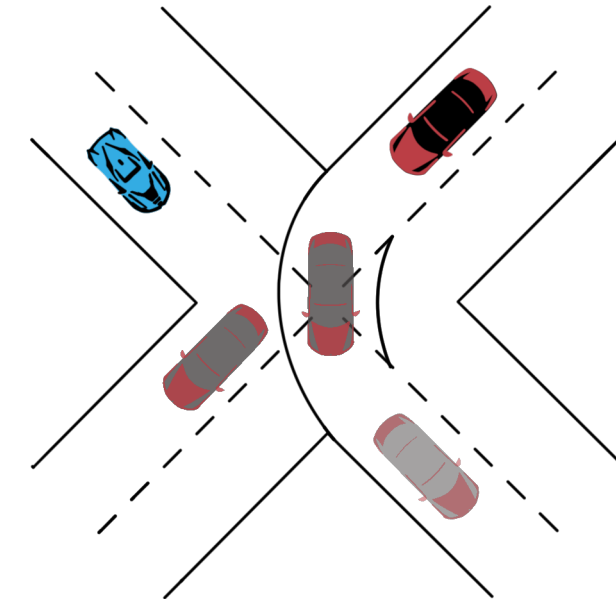
Our means of transportation are undergoing a remarkable evolution, with autonomous driving (AD) technology poised to play a pivotal role in this transformation. Imagine a future where autonomous vehicles (AVs) seamlessly optimize traffic flow, reducing congestion and revolutionizing urban mobility. By intelligently scheduling commercial transports outside of peak hours, AVs have the potential to significantly enhance traffic efficiency. Moreover, they could alleviate the strain on parking infrastructure by autonomously relocating to less crowded areas when not in use.

Machine learning (ML) has been instrumental in driving the rapid progress of AV technology. Advanced ML techniques enable AVs to perceive their surroundings with unprecedented accuracy. However, navigating complex scenarios such as busy

intersections remains a challenge, as it requires intricate interaction with other road users. Human drivers possess the ability to assess the environment, identify traffic signals, and make split-second decisions based on various factors. Yet, human error still leads to numerous accidents annually, underscoring the need for more sophisticated decision-making algorithms for AVs.

The focus of this thesis revolves around the development of decision-making algorithms that go beyond merely adhering to traffic rules, but also anticipate and adapt to the actions of other drivers. Leveraging reinforcement learning (RL) methods, this thesis proposes the creation of a decision-making agent capable of navigating intersections while taking into account the intentions of other drivers. Additionally, two approaches to estimating uncertainty are proposed. This uncertainty estimate serves as a crucial tool for avoiding poor decisions and ensuring the implementation of a safer driving strategy.

TOMMY FUJITA TRAM • Learning When To Drive in Uncertrain Scenarios • 2024



Learning When To Drive in Uncertrain Scenarios

A deep Q-learning approach

TOMMY FUJITA TRAM

THESIS FOR THE DEGREE OF DOCTOR OF PHILOSOPHY

Learning When To Drive in Uncertain Scenarios

A deep Q-learning approach

TOMMY FUJITA TRAM

Department of Electrical Engineering
Chalmers University of Technology
Gothenburg, Sweden, 2024

Learning When To Drive in Uncertain Scenarios

A deep Q-learning approach

TOMMY FUJITA TRAM

ISBN 978-91-7905-623-0

© 2024 TOMMY FUJITA TRAM

All rights reserved.

Doktorsavhandlingar vid Chalmers tekniska högskola

Ny serie nr 5089

ISSN 0346-718X

Department of Electrical Engineering

Chalmers University of Technology

SE-412 96 Gothenburg, Sweden

Phone: +46 (0)31 772 1000

Email: tommy.tram@chalmers.se; tommy.tram@gmail.com

Cover:

An illustration of two vehicles approaching an intersection. The blue vehicle has to make a decision to yield or drive while the intention of the red vehicle is uncertain.

Printed by Chalmers Reproservice

Gothenburg, Sweden, June 2024

To my loving family

Learning When To Drive in Uncertain Scenarios

A deep Q-learning approach

TOMMY FUJITA TRAM

Department of Electrical Engineering

Chalmers University of Technology

Abstract

The main topic for this thesis is tactical decision making for autonomous driving through intersections with other road users. A human driver are able to drive in diverse environments and situations even though they have never driven there before. The same is expected of an AV. Specifically, this thesis studies the problem of navigating through an intersection where the intention of other drivers are unknown. These intentions depend on a variety of factors such as the mood or attention of the driver, right of way, traffic signs or lights. By generalizing the future action of the driver to intention, the autonomous vehicle will be able to handle more complicated scenarios such as a driver running a red light. The large amount of environments and possible scenarios makes it hard to manually specify a reaction for every possible situation. Therefore, a learning-based strategy is considered in this thesis, which will introduce different approaches based on RL.

The problem is formulated as a POMDP to account for the unknown intentions and a general decision making agent derived from the DQN algorithm is proposed. With few modifications, this method can be applied to different environments, which is demonstrated for various simulated intersection scenarios.

Keywords: Autonomous driving, reinforcement learning, decision making, uncertain environments, Partially observable Markov decision process, deep Q-learning, transfer learning, model predictive control, neural networks

List of Publications

This thesis is based on the following publications:

- [A] Tommy Tram, Anton Jansson, Robin Grönberg, Mohammad Ali, and Jonas Sjöberg, “Learning Negotiating Behavior Between Cars in Intersections using Deep Q-Learning”. *Published in 2018 21st International Conference on Intelligent Transportation Systems (ITSC)*.
- [B] Tommy Tram, Ivo Batković, Mohammad Ali, and Jonas Sjöberg, “Learning When to Drive in Intersections by Combining Reinforcement Learning and Model Predictive Control”. *Published in 2019 IEEE Intelligent Transportation Systems Conference (ITSC)*.
- [C] Carl-Johan Hoel, Tommy Tram, and Jonas Sjöberg, “Reinforcement Learning with Uncertainty Estimation for Tactical Decision-Making in Intersections”. *Published in 2020 IEEE 23rd International Conference on Intelligent Transportation Systems (ITSC)*.
- [D] Tommy Tram, Maxime Bouton, Jonas Fredriksson, Jonas Sjöberg, and Mykel Kochenderfer, “Belief State Reinforcement Learning for Autonomous Vehicles in Intersections”. *Submitted to IEEE Transactions on Intelligent Vehicles*.
- [E] Hannes Eriksson, Tommy Tram, Debabrota Basu, Mina Alibeigi, and Christos Dimitrakakis, “Reinforcement Learning in the Wild with Maximum Likelihood-based Model Transfer”. *Published in 2024 International Conference on Adaptive Agents and Multi-Agent Systems (AAMAS)*.

Acknowledgments

This thesis is the result of many years of hard work, lots of travel and a great learning experience. Even in times when things did not work as expected or unexpected problems emerged, I never felt that I was alone. That is why I would like to acknowledge the people who have made this work possible and memorable.

First, I want to thank my supervisor and examiner Professor Jonas Sjöberg. Thank you for believing in me and the opportunity of pursuing a doctoral degree as your student. It has been an honor and a pleasure.

A special thanks to my industrial supervisor Dr. Mohammad Ali, who chose and encouraged me to pursue a PhD in this field. I still remember the pitch that convinced me to do it. You said: "Pilot assist is mostly done now, we need someone to look towards the future of decision making and control". We had a lot of fun in the beginning of this journey and I will always be grateful for the guidance and support you provided, and most of all for believing in me.

The work presented in this thesis would not have been possible without the financial support from VCC, Zenuity, Zenseact, and the Wallenberg AI, Autonomous Systems and Software Program (WASP). I am also grateful for the community and environment created by both Zenseact and WASP. The Advanced Graduate Program led by Dr. Mats Nordlund and Dr. Carl Lindberg created an environment within the company created a safe space to share ideas, talk amongst peers and fun to go to work in the morning.

I would especially like to thank Dr. Carl Lindberg for the coaching during these final years of my PhD. At the start of the pandemic, you paid attention to our casual conversations, identified problems and proposed solutions I did not think was possible, but more importantly you cared. Thanks to you, I was able to finish my final year of my PhD together with my wife on the other side of the world and as a direct result of that, I now have a beautiful son. For this, I am eternally grateful.

I especially want to thank my great friends and co-authors with whom I embarked on this PhD journey with. Carl-Johan Hoel, my research twin, thank you for all the support over the years, the enlightening conversations and most of all for being a friend. Ivo Batkovic, thank you for all the good times we shared. I have always admired your determination and focus working with you has been a pleasure and a privilege. I am happy to call you my friend. I would also like to thank Anton Jansson and Robin Grönberg for their well executed

master thesis from where I found the direction of this thesis. We started out as supervisor and master thesis students but ended up as friends. Special thanks go to Christian Rodriguez for being a great friend and supporting me whenever times were tough.

I would like to thank WASP for all the interesting study trips, courses, and events that not only widened my skills, but also introduced me to a vast network of colleagues and friends across the world. In addition, the WASP exchange program gave me the opportunity to spend six months as a visiting research student at the Stanford Intelligent Systems Laboratory. To that end, I am deeply grateful to Professor Mykel Kochenderfer who thought me that life is a POMDP and gave me the opportunity to spend time and work with his research group. Additionally, special thanks to Maxime Bouton for the fun we had during my time at SISL. I learned a lot, both on and off campus.

*Tommy Tram,
Göteborg, June, 2024.*

Acronyms

AD:	Autonomous driving
ADAS:	Advanced driving assistance systems
AV:	Autonomous vehicles
CNN:	Convolutional neural network
DQN:	Deep Q-network
EQN:	Ensabmle quantile networks
IDM:	Intelligent driver
LSTM:	Long short-term memory
MDP:	Markov descision process
MPC:	Model predictive control
POMDP:	Partially observable Markov descision process
RL:	Reinforcement learning

Contents

Abstract	i
List of Papers	iii
Acknowledgements	v
Acronyms	vii
I Overview	1
1 Introduction	3
1.1 Autonomous Driving Levels	4
1.2 Intersections, intention and scenarios	5
1.3 Research questions	7
1.4 Scope and limitations	7
1.5 Contributions	7
1.6 Thesis outline	8
2 Related work	9
2.1 Rule-based methods	9
2.2 Planning methods	10

2.3	Learning based methods	10
3	Technical background	13
3.1	Markov decision process	13
3.1.1	Partially observable Markov decision process	15
3.2	Reinforcement learning	15
3.2.1	Deep Q-learning	16
4	Modeling Intersection Driving Scenarios	19
4.1	POMDP formulation	19
4.1.1	State space	20
4.1.2	Action space	21
4.1.3	Transition model	21
4.1.4	Observation model	22
4.1.5	Reward function	22
4.2	Deep Q-learning approach	22
4.3	Results from simulation	23
4.4	Discussion	23
5	Accounting for the uncertainty	27
5.1	Estimating the uncertainty of the Q-value	28
5.1.1	Results for scenarios within the training set	29
5.1.2	Results for scenarios outside the training set	31
5.2	Estimating the uncertainty of the input	32
5.2.1	Results within the training set	33
5.2.2	Results for scenarios outside the training set	34
6	Generalizing over different scenarios	35
6.1	Approach	36
6.2	Results and discussion	36
7	Discussion	37
7.1	Guaranteeing safety	37
8	Concluding remarks and future work	41
8.1	Conclusions	41
8.2	Future work	42

9	Summary of included papers	43
9.1	Paper A	43
9.2	Paper B	44
9.3	Paper C	44
9.4	Paper D	45
9.5	Paper E	46
	References	47
	II Papers	51
A	Learning Negotiating Behavior Between Cars in Intersections using Deep Q-Learning	A1
1	Introduction	A3
2	Overview	A4
3	Problem formulation	A4
3.1	System architecture	A5
3.2	Actions as Short Term Goals	A5
3.3	Observations that make up the state	A7
3.4	Partially Observable Markov Decision Processes	A8
4	Finding the optimal policy	A8
5	Method	A9
5.1	Deep Q-learning	A9
5.2	Experience Replay	A9
5.3	Dropout	A10
5.4	Long short term memory	A10
6	Implementation	A11
6.1	Simulation environment	A11
6.2	Reward function tuning	A12
6.3	Neural Network Setup	A12
7	Results	A14
7.1	Effect of using Experience replay	A15
7.2	Effect of using Dropout	A16
7.3	Comparing DQN and DRQN	A16
7.4	Effect of sharing weights in the network	A16
8	Conclusion	A17

References	A19
B Learning When to Drive in Intersections by Combining Reinforcement Learning and Model Predictive Control	B1
1 Introduction	B3
2 System	B5
3 Problem formulation	B6
3.1 Partially Observable Markov Decision Process	B6
3.2 Deep Q-Learning	B6
4 Agents	B7
4.1 MPC agent	B7
4.2 Sliding mode agent	B11
4.3 Intention agents	B11
5 Implementation	B12
5.1 Deep Q-Network	B12
5.2 Q-masking	B14
5.3 Simulation environment	B14
5.4 Reward function tuning	B15
6 Results	B17
7 Discussion	B17
8 Conclusion	B19
References	B20
C Reinforcement Learning with Uncertainty Estimation for Tactical Decision-Making in Intersections	C1
1 Introduction	C3
2 Approach	C5
2.1 Reinforcement learning	C5
2.2 Bayesian reinforcement learning	C6
2.3 Confidence criterion	C7
3 Implementation	C8
3.1 Simulation setup	C8
3.2 MDP formulation	C9
3.3 Fallback action	C11
3.4 Network architecture	C12
3.5 Training process	C12
3.6 Baseline method	C13

4	Results	C13
4.1	Within training distribution	C14
4.2	Outside training distribution	C17
5	Discussion	C17
6	Conclusion	C20
	References	C20

D Belief State Reinforcement Learning for Autonomous Vehicles in Intersections

		D1
1	Introduction	D3
2	Mathematical preliminaries	D6
2.1	Partially observable Markov decision process	D6
2.2	Behavior model	D8
3	Proposed approach	D9
3.1	POMDP formulation	D9
3.2	Belief state representation using a particle filter	D11
3.3	Belief state reinforcement learning algorithms	D13
4	Experiments	D17
4.1	Simulator setup	D18
4.2	Designing the reward function	D18
5	Results / Results and discussion	D19
5.1	Traffic density experiment	D20
5.2	Probability distribution of the intention state	D21
5.3	Oracle DQN	D22
5.4	QMDP-IE and QMDP results	D23
5.5	QPF and QID results	D24
5.6	Overtake agent	D24
5.7	Discussion	D25
6	Conclusion	D26
	References	D26

E Reinforcement Learning in the Wild with Maximum Likelihood-based Model Transfer

		E1
1	Introduction	E3
2	Related Work	E6
3	Background	E8
3.1	Markov Decision Process	E8

3.2	Maximum Likelihood Estimation	E8
4	A Taxonomy of Model Transfer RL	E9
4.1	MTRL: Problem Formulation	E10
4.2	Three Classes of MTRL Problems	E10
5	MLEMTRL: MTRL with Maximum Likelihood Model Transfer	E13
5.1	Stage 1: Model Estimation	E13
5.2	Stage 2: Model-based Planning	E15
6	Theoretical Analysis of MLEMTRL	E16
7	A Meta-Algorithm for MLEMTRL under Non-realisability . .	E17
8	Experimental Analysis	E18
9	Discussions and Future Work	E22
	References	E23

Part I

Overview

CHAPTER 1

Introduction

The way we transport ourselves is currently evolving, and autonomous driving (AD) technology is expected to have a big impact on this transformation [1], [2]. With autonomous vehicles (AV) the efficiency of traffic can be improved by scheduling commercial transports outside of rush hours [3]. Number of parking spots in cities can be reduced if the vehicles can autonomously drive itself to a less crowded area when not in use and drive back when needed. Congestion and traffic jams could also be reduced if a large amount of vehicles in traffic are autonomous and optimize around the same goal e.g., traffic flow or fuel efficiency.

The rapid success of machine learning (ML) during the last decades has lead to major progress towards deploying AVs in the real world. One clear benefactor of these new ML technics are the perception systems [4]. Better perception enables more accurate representation of the environment. However, navigating complex scenarios such as urban intersections and roundabouts with dense traffic remain challenging for AVs because it requires a higher level of interaction between road users, as summarized in a review paper [5]. When a human driver approach an intersection, they observe the environment to identify the traffic light, signs and other approaching vehicles. Then assess the

situation to determine *who has the right of way?* Before deciding whether to drive or yield. But human drivers are not perfect, according to the Insurance Institute for Highway Safety [6], in 2019, an estimated 115,741 people were injured by drivers running a red light, whereas 928 of them were killed. While these accidents were mainly caused by driver inattention or reckless driving, it motivates the development of decision-making algorithms for AVs which not only follow the traffic rules but can also take into account other drivers future actions and inattention, which is the main focus in this thesis.

1.1 Autonomous Driving Levels

When talking about autonomous driving, it is first important to specify which level of autonomy that is being discussed. The Society of Automotive Engineers has classified these different levels of autonomy ranging from zero to five [7], also referred to as L0-L5. The first level L0 is a vehicle with no autonomy, whereas a fully AV that can operate in any environment and without any human supervision is defined as L5. Popular advance driver assistance systems (ADAS) functions today, like lane centering or adaptive cruise control are classified as L1, while the Volvo Pilot Assist and Tesla Autopilot that provide both steering and acceleration/breaking are classified as level 2. The main criteria for L2 systems is that the driver is in control and only supported by the system. This puts a requirement on the driver to always supervise the vehicle and take over when needed to ensure safety. For L3 and higher the responsibility of driving is shifted to the system. At L3, the driver still has to take control over the vehicle but at only the request of the system, and at L4 and L5 the autonomous driving features no longer require the driver to take over. Finally, the main difference between L4 and L5 is the capability of driving anywhere, under all conditions. Examples of L4 are robot taxis developed by Waymo, Zoox, cruise and Toyota which only operate in a specified area or city.

The AV making the decisions in this work are referred to as the ego vehicle, while other traffic participants are assumed to be vehicles driven by other human drivers but could be extended to pedestrians bicyclist and other AVs. The methods presented in this thesis are aimed at an autonomy level L5. At this level the system is expected to handle all aspects of driving within a specific task such as crossing an intersection.

1.2 Intersections, intention and scenarios

When it comes to the scenarios considered in this work. This section aims to clarify the use of the words' intersection, intention and scenario.

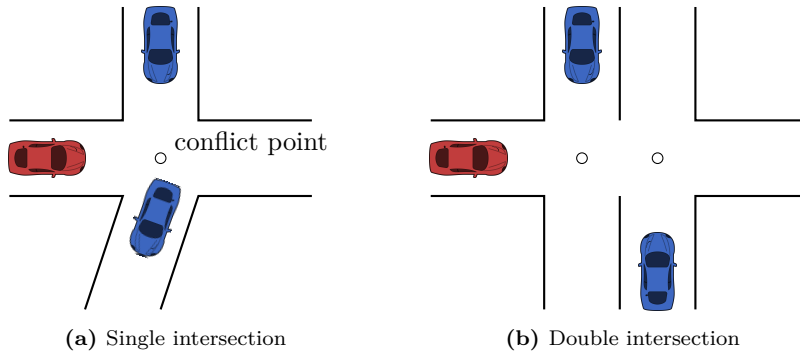


Figure 1.1: Examples of different intersections

Let's begin by defining the terms *intersection*, *intention*, and *scenario* within the context of this thesis. An intersection refers to the geometric layout of roads intersecting each other, encompassing elements such as the number of junctions, conflict points, turns, and angles of incidence, as illustrated in Figure 1.1. Intersections can be categorized as signalized or unsignalized. A signalized intersection is equipped with infrastructure to designate the right-of-way, such as regulatory signs (e.g., STOP or YIELD) or traffic signals, while an unsignalized intersection lacks such features. However, as emphasized in the introduction, human drivers do not always follow these right-of-way rules, which can result in accidents. Therefore, this thesis defines intentions as the anticipated actions of other vehicles in the future, such as stopping or proceeding through the intersection.

Figure 1.2 illustrates how velocity profiles can differ for three different intentions. In this example, distinguishing between the 'give way' and 'take way' intentions is straightforward, as the velocity begins to decelerate at time 0. However, identifying the 'cautious' intention poses a challenge, as the agent cannot be certain until the other vehicle comes to a complete stop.

If intentions are known, intersections can be treated as unsignalized, as the right-of-way can be inferred from the intentions rather than relying solely on

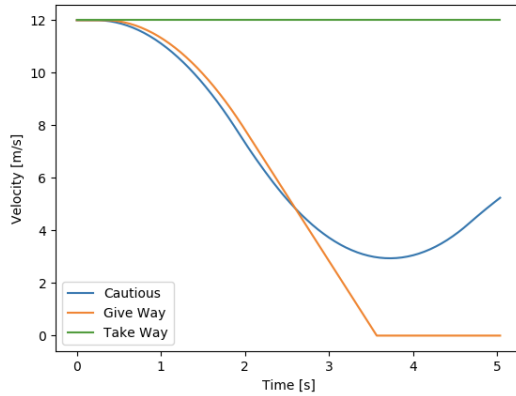


Figure 1.2: An illustration showing velocity profiles for agents with three distinct intentions. Each agent shares the same initial position and velocity while approaching a common intersection.

infrastructure. A reinforcement learning (RL) approach has the potential to ensure safety even in situations where another vehicle disregards traffic rules, such as running a red light, as a cautious agent will prioritize safety and stop accordingly.

1.3 Research questions

The work presented in this thesis investigate the following research questions:

- Q1.** How can RL techniques be used to develop a decision-making agent that effectively navigates intersections without explicitly estimating the intention state of other vehicles? (PAPER A and B)
- Q2.** How can an RL agent utilize the uncertainty in its predictions and actions to enhance decision-making in complex environments? (PAPER C and D)
- Q3.** How do can a RL agent handle situations it has not been trained on? (PAPER C and E)

1.4 Scope and limitations

The following aspects of creating a tactical decision-making agent for autonomous driving in uncertain environments are not considered in this thesis.

1. Guaranteeing safety in AD systems is an important open question that is out of scope for this thesis.
2. The work in this thesis is tested in simulation environments and not real world.
3. This work considers the control of one vehicle and not multiple agents.

1.5 Contributions

The main contributions of this thesis are:

1. A deep Q-learning approach for creating a decision-making agent navigating intersection that considers the intentions of other drivers.
2. A neural network architecture that is invariant to permutations of the order of which surrounding traffic participants are observed, which speeds up training and improves the quality of the trained agent.

3. REWRITE: A belief state representation using a particle filter and a comparison and analysis of different algorithms that utilize the belief state.
4. Extension of RL methods that provide an uncertainty estimate of the proposed decisions and use it to create a confidence criterion that can identify situations with high uncertainty.
5. Method for choosing between a set of fully trained policies.

1.6 Thesis outline

The outline of the thesis is as follows: in Chapter 2 other research in the same field is presented. In Chapter 3 introduce the mathematical framework Markov Decision Process (MDP) and partially observable Markov decision process (POMDP) with a brief theory of RL and deep Q-learning. Chapter 4 is where the problem is formulated by defining the components of the POMDP. Results from using deep Q-learning to solve the POMDP is presented and later combined with a model predictive control (MPC) to improve the actions. Later in Chapter 5 two approaches to handle the uncertainty is presented. First the uncertainty in the decisions from the RL algorithm and then an empirical study of how well a deep Q-network (DQN) can handle uncertainty of others driving intentions. Chapter 6 present an approach to generalize over different MDPs more specifically policies learned from different transfer functions.

CHAPTER 2

Related work

In recent years, decision-making for AVs in structured scenarios like intersections has attracted a lot of attention in the literature. This chapter gives a broad introduction to the main research directions, but it does not aspire to provide a comprehensive survey of each class of approaches.

2.1 Rule-based methods

A skilled engineer can sometimes solve the decision-making problem for structured traffic scenarios using rule-based methods. One example of a rule-based method was implemented using hierarchical state machines to switch between predefined behaviors depending on what scenarios was encountered [8], [9]. These methods was successful for a limited and controlled environment such as the Urban Challenge event, but it is difficult for an engineer to anticipate every situation that may occur in the real world and design a suitable strategy that can solve all of them, in particular when drivers are not following the law [10]. One approach is to use the intelligent driver model (IDM) [11] to infer driver intent in urban intersections Liebner *et al.* [12] and another used a particle filter to estimate the parameters of the IDM Hoermann *et al.* [13],

both works showed promising results when evaluated on real-world data.

2.2 Planning methods

Another group of algorithms treats the decision-making task as a motion planning problem. Commonly, a prediction model is used to predict the motion of the other agents, and then the behavior of the ego vehicle that is being controlled is planned accordingly. One planning method is using Monte Carlo tree search (MCTS) [14], but since the predictions are independent of the ego vehicle plan results in a reactive behavior [15], [16]. Therefore, the interaction between the ego vehicle and other agents is not explicitly considered, but may happen implicitly by frequent replanning.

A third approach to solve the motion planning problem is to use optimization-based techniques, for example optimal control, which was applied to highway driving scenarios by Werling et al. [17]. Since human behavior is complex and varies between individuals, some algorithms use a probabilistic prediction as input to the motion planning. This is for example shown in a study by Damerow et al. [18], which aims to minimize the risk during an intersection scenario. Other approaches to motion planning for autonomous driving are provided in the surveys by González et al. [19] and Paden et al. [20].

2.3 Learning based methods

In order to handle the uncertainty of predicting other traffic participants' behaviors or intentions, the literature formulates the problem of driving under uncertainty as a POMDP [21]. Learning-based approaches, like RL [22], [23], can help relieve the burden of designing hand-crafted solutions for all possible scenarios and Deep recurrent Q-network (DRQN) approaches, [24], [25], showed some promise solving POMDP with non-observable states by leveraging past observations or actions.

Another approach to estimating the intention is to introduce belief states to capture uncertainties in the environment [26]. The belief state can be used to model the probability distribution over the uncertain world states, e.g., the intention of other road users. One paper [27] decoupled the belief state modeling (via unsupervised learning) from policy optimization (via RL) and claimed that having full observability at learning time, combined with knowing

what will not be observable at deployment time, enables an RL agent to learn a policy that is more robust to its unobservable states. One advantage of RL methods, compared to planning based methods, is that a model of the environment is not required, i.e., the transition probabilities between different states are not assumed to be known. Many RL methods provide a general framework and an agent could, in theory, learn how to behave correctly in all possible driving situations.

CHAPTER 3

Technical background

This chapter briefly introduce the MDP framework, its extension POMDP and reinforcement learning. A more comprehensive overview of POMDPs and RL is given in the books by Kochenderfer [21] and Sutton and Barto [22], upon which this chapter is based. The purpose of the chapter is to summarize the most important concepts and introduce the notation that are used in the subsequent chapters.

3.1 Markov decision process

A MDP is a mathematical framework for modeling discrete time sequential decision making problems. It involves an agent making decisions in an environment evolving over time according to a stochastic process. The state of the environment contains all the information necessary about the agent and environment at a given time to be able to transition to any given state. This property is referred to as the Markov property.

The MDP is formally defines as the tuple $(\mathcal{S}, \mathcal{A}, T, R, \gamma)$, described by the following list [21]:

- The state space \mathcal{S} represents the set of all possible states of the environment. This set could consist of both discrete and continuous states.
- The action space \mathcal{A} represents the set of all possible actions the agent can take. The action space can consist of both discrete and continuous actions. Since this thesis focuses on high-level decision-making, only discrete actions are considered.
- The state transition model $T(s' | s, a)$ describes the probability $\Pr(s' | s, a)$ that the system transitions to the next state $s' \in \mathcal{S}$ from state $s \in \mathcal{S}$ when action $a \in \mathcal{A}$ is taken.
- The reward function $R(s, a)$ returns a scalar reward r for each action a an agent takes in a given state s . The design of the reward function should reflect on the overall objective that the agent should maximize.
- The discount factor $\gamma \in [0, 1]$ is a scalar that discounts the value of future rewards. The discount factor γ will affect the results of the optimization problem. A discount factor set close to 0 will make immediate rewards more important while a γ closer to 1 would give some weight to expected future reward as well.

A policy π is defined as the mapping from state s to action a and the goal of the agent is to take a sequence of actions that maximize the accumulated reward r . The value of being in a state while following a policy is described by the value function

$$V^\pi(s) = \mathbb{E} \left[\sum_{k=0}^{\infty} \gamma^k R(s_t, a_t) | s_0 = s, \pi \right]. \quad (3.1)$$

The optimal value function V^* is unique and follows the Bellman equation:

$$V^*(s) = \max_a \left[R(s, a) + \gamma \sum_{s'} T(s, a, s') V^*(s') \right]. \quad (3.2)$$

From the bellman equation one can deduce a state-action value function $Q(s, a)$ that satisfies $V^*(s) = \max_a Q(s, a)$. Given this Q function, a policy can be derived as $\pi(s) = \operatorname{argmax}_a Q(s, a)$.

3.1.1 Partially observable Markov decision process

Sometimes the agent does not have direct access to the entire state of the environment. In these cases, it is more common to use a POMDP, which is an extension to the MDP. A POMDP is defined by the tuple $(\mathcal{S}, \mathcal{A}, \mathcal{O}, T, O, R, \gamma)$, where the state space, action space, transition model, reward and discount factor is the same as the MDP, but a POMDP has two additional elements:

- The observation space \mathcal{O} , which represents all possible observations that the agent can receive. This can be both discrete and continuous.
- The observation model $O(o|s', a)$, which describes the probability of observing $o \in \mathcal{O}$ in a given state s' after taking an action a : $O(o, s', a) = \Pr(o|s', a)$.

For a POMDP, the agent takes an action a from a given state s and the environment transitions to the next state s' according to the transition model T . The agent then receives an observation o related to s' and a according to the observation model O .

In a POMDP, after the agent takes an action a from a given state s and the environment transitions to the next state s' according to the transition model T , the agent receives an observation o . This observation o is drawn according to the observation model $O(o|s', a)$, which specifies the porbability of observing the given new state s' and taken action a .

The observable states in this work are information that sensors on the ego vehicle can provide e.g., distance to intersection, position and speeds of other vehicles. While the unobservable states are the intentions of other drivers that are approaching the same intersection as ego. Chapter 4 formulates the POMDP studied in this work.

3.2 Reinforcement learning

In some problems, the state transition probabilities or the reward function are unknown. These problems can be addressed using reinforcement learning, where the agent learns how to behave by interacting with the environment [21, Ch. 5]. The data available to an RL agent depends on its current policy, necessitating a balance between exploring the environment and exploiting existing knowledge. Moreover, the reward an agent receives might hinge on a

crucial decision made earlier, making it essential to attribute rewards to the correct decisions.

RL algorithms are categorized into model-based and model-free approaches [21, Ch. 5]. In model-based methods, the agent first estimates a representation of the state transition function T and then uses a planning algorithm to find a policy. Conversely, model-free RL algorithms, as the name suggests, do not explicitly construct a model of the environment to determine actions.

Model-free approaches can be further divided into value-based and policy-based techniques. Value-based algorithms, such as Q -learning, aim to learn the value of each state, thereby implicitly defining a policy. Policy-based techniques directly search for the optimal policy within the policy space, either through policy gradient methods or gradient-free methods like evolutionary optimization. Hybrid techniques, such as actor-critic methods, combine both policy and value-based approaches.

RL algorithms typically assume that the environment is modeled as a MDP, where the agent knows the state of the environment. However, in many practical situations, only partial information about the state of the environment is available, which is modeled within the POMDP framework. In such cases, it is common to approximate the state by either the observation or a finite history of observations [22, Ch. 17]. This approximation is referred to as a k -Markov approximation, where k defines the length of the included history. With a sufficiently long history, the Markov property is assumed to approximately hold, even in a partially observable environment.

3.2.1 Deep Q-learning

Q-learning [28] is a model-free and value-based branch of RL, where the objective of the agent is to learn the optimal state-action value function $Q^*(s, a)$. This function is defined as the expected return when taking action a from state s and then following the optimal policy π^* , i.e.,

$$Q^*(s, a) = \max_{\pi} \mathbb{E} \left[\sum_{k=0}^{\infty} \gamma^k R(s_k, a_k) | s_0 = s, a_0 = a, \pi \right]. \quad (3.3)$$

The optimal state-action value function follows the Bellman equation

$$Q^*(s, a) = \mathbb{E}_{s' \sim T(s'|s, a)} \left[R(s, a) + \gamma \max_{a'} Q^*(s', a') \right], \quad (3.4)$$

which recursively defines the Q -values of the state-action pairs (s, a) . The equation can intuitively be understood by the fact that if Q^* is known, the optimal policy is to select the action a' that maximizes $Q^*(s', a')$.

In the DQN algorithm, a neural network (NN) with weights θ is used as a function approximator of the optimal state-action value function, $Q(s, a; \theta) \approx Q^*(s, a)$ [29]. The weights of the network are adjusted to minimize the temporal difference (TD) error in the Bellman equation, typically with some kind of stochastic gradient descent (SGD) algorithm. Mini-batches with size M of experiences, $e = (s, a, r, s')$, are drawn from an experience replay memory, and the loss is calculated as

$$L(\theta) = \mathbb{E}_M \left[(r + \gamma \max_{a'} Q(s', a'; \theta^-) - Q(s, a; \theta))^2 \right]. \quad (3.5)$$

Here, θ^- represents the NN parameters of a target network, which is kept fixed for a number of training steps, in order to stabilize the training process. Several improvements to this vanilla form of DQN have been proposed and are compared by Hessel et al. [30]. See Paper A for the details of the DQN implementation in this study.

CHAPTER 4

Modeling Intersection Driving Scenarios

Navigating an intersection is a sequential decision-making problem that can be mathematically modeled using a MDP, as introduced in Section 3.1. This thesis focuses on driving through intersections in the presence of other drivers, emphasizing not only to follow traffic rules but also the ability to adapt to the intentions of other drivers. Given that current sensors cannot directly observe other drivers' intentions, a POMDP is a more suitable framework for formulating this problem.

4.1 POMDP formulation

Effectively modeling the intersection problem is key for developing an optimal decision-making policy. While specific details of the POMDP may vary between different studies, the general description remains consistent. This section outlines the essential aspects of the POMDP framework as applied to the intersection problem in this thesis.

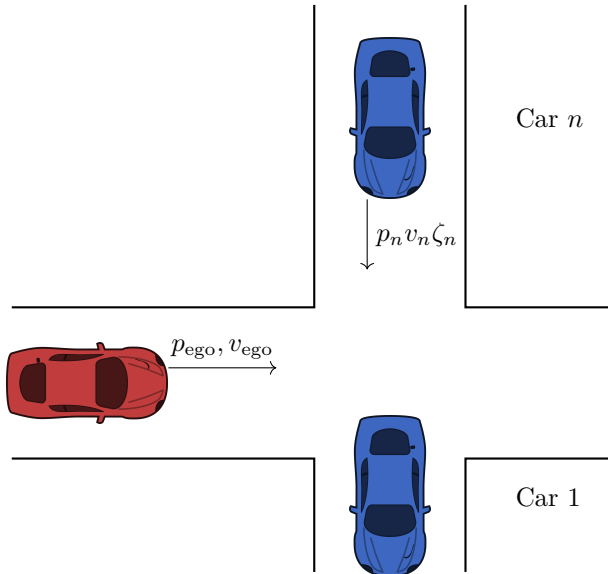


Figure 4.1: General description of the states in a simple intersection. The ego vehicle in red is controlled by the agent, while the blue vehicles are the other vehicles crossing the same intersection. Each blue vehicle is described by an index n , a position p_n , a velocity v_n and hidden intention ζ_n

4.1.1 State space

From Section 3.1, the state space contains all the information necessary about the agent and environment to be able to transition from any given state s to the next state s' . In the scenario shown in Figure 4.1, the red car on the horizontal lane represents the ego vehicle controlled by the agent while the blue cars on the vertical lane are the other vehicles which ego needs to interact with in order to cross the intersection.

A simplified description of the state,

$$s = (p_{\text{ego}}, v_{\text{ego}}, \{p_n, v_n, \zeta_n\}_{n=1}^N), \quad (4.1)$$

consists of positions state p_{ego} and p_n , where subscript (ego) and n denotes ego vehicle and the index of the surrounding vehicle up to N vehicles. Instead

of using a Cartesian coordinate system to describe the position p_{ego} and p_n , relative distance measures are proposed instead. This way, the state space are generalizable to different intersection designs, e.g., the angle of incidence and number of crossing points. The velocity of ego v_{ego} and all other the traffic participants v_n is also necessary to be able to predict what position they will be in the next state. Finally, the intention of all the other participants ζ_n . As mentioned in Section 1.2, ζ_n encapsulates information such as stop sign, traffic light or even inattention in to one state. Paper D shows a comparison between two fully observable MDPs, one with intention and the other one without and the results show that having an intention state reduce number of collisions. Paper A used a long short-term memory (LSTM) network architecture to implicitly predict ζ .

4.1.2 Action space

One limitation of deep Q-learning is the requirement for a discrete action space. In various AD studies [31], it is common practice to define the action space in terms of different acceleration requests. The approach in Paper A proposes using short-term goals as actions: $\{ \text{'take way'}, \text{'yield'}, \text{'follow car } \{1, \dots, N\} \}$.

These short-term goals represent high-level objectives, such as driving through an intersection (take way), stopping at the start of an intersection (yield) or drive behind a specific car (follow car n). Each high-level action is translated into a set of parameters that are input into a sliding mode controller in Paper A and a MPC in Paper B , which then generates the appropriate acceleration to control the ego car.

4.1.3 Transition model

The transition model is initially unknown, and RL is employed to learn this model by taking actions in the environment from different states, recording the resulting rewards, and noting the subsequent state transitions. In this work, the environment is a simulator, and the primary objective for the agent is to learn the transition dynamics of other vehicles, which depend on their intentions ζ . These intentions are modeled as predetermined actions, governed by an IDM. Using the IDM to guide predetermined actions makes the interactions between vehicles more complex, which complicates the learning process. For more details on the simulation environment see Paper A .

4.1.4 Observation model

The observation space typically mirrors the state space, excluding the intention state ζ , as there are no sensors capable of directly detecting other drivers' intentions. This observation

$$o = (p_{\text{ego}}, v_{\text{ego}}, \{p_n, v_n\}_{n=1}^N), \quad (4.2)$$

encompasses all elements of the state space, from (4.1), that are observable through the sensors in the car, except for the intention state ζ .

4.1.5 Reward function

The design of the reward function is pivotal as it determines the value associated with each state, ultimately shaping the driving policy of the agent. A well-crafted reward function is instrumental in guiding the agent towards achieving its objectives effectively. The reward model in this work is formulated based on terminal states, including reaching the goal, collision events, and timeouts. These terminal states play a critical role in defining the success or failure of the agent's driving behavior and are accordingly reflected in the reward structure.

4.2 Deep Q-learning approach

To find a driving policy π for the POMDP detailed in the previous section, both Paper A and Paper B used deep Q-learning, described Chapter 3.2.1. Paper A proposed a DQN structure with shared weights and LSTM layer to approximate the Q-function. Because the scenarios has up to N cars that with same type of states, the shared weight is an effective way to reduce the input space the agent need to explore. While the LSTM layer has the role of utilizing the previous states to implicitly estimate a hidden state that could possibly encapsulate the intention of other cars.

As mentioned in Chapter 4.1.2, the actions in Paper A are controlled by a sliding mode controller while Paper B use a MPC to generate a velocity profile for a short time horizon. Instead of specifying which car to drive behind, the action in this context determines which gap between cars the vehicle should drive through. This gap is then translated into constraints that the MPC uses to create the velocity profile.

MPC excels at creating plans within given constraints but faces challenges with mixed integer problems, making the calculation of the optimal path for all possible actions computationally intensive. On the other hand, Q-learning is effective at estimating the value of an action given a state, but it requires exploring many suboptimal actions before converging on a good one. By combining RL and MPC, an agent can efficiently select a good action, which the MPC can then use to generate a safe and efficient velocity profile.

The agents from Paper A and Paper B are evaluated on both a single intersection, shown in Figure 1.1, and a double intersection with two crossing points, shown in Figure 1.1a. The results are summarized in Table 4.1.

4.3 Results from simulation

The results from Table 4.1 showed that the proposed DQN agent from Paper A found a policy that successfully crossed a single intersection 96.1% of the time, with 2.8% resulting in collisions and 1.1% resulting in timeouts. When comparing agents trained with and without an LSTM layer, those with the LSTM succeeded in 3 out of 4 attempts where those without it would fail. This demonstrates that deep Q-learning has great potential for creating decision-making agents capable of navigating intersections. Additionally, the results from Figure 4.2 indicate that using a network structure with shared weights between cars significantly improved the convergence speed of the network. Shared weights, along with other enhancements like dropout and experience replay, are essential components for this improvement.

As mentioned previously, the controller from Paper A could only consider one car at a time, which placed a heavy burden on the DQN compensate by frequently switching actions. In contrast, in Paper B , the MPC showed significant improvement in handling more complex intersections. For instance, in the double intersection, the MPC agent succeeded 95.2% of the time with a collision rate of 3.6%, compared to the sliding mode controller, which only succeeded 90.9% of the time with a collision rate of 8.3%.

4.4 Discussion

Observing the behavior of a fully trained agent from Paper A and Paper B provides the insight that the path of the ego vehicle can be segmented into

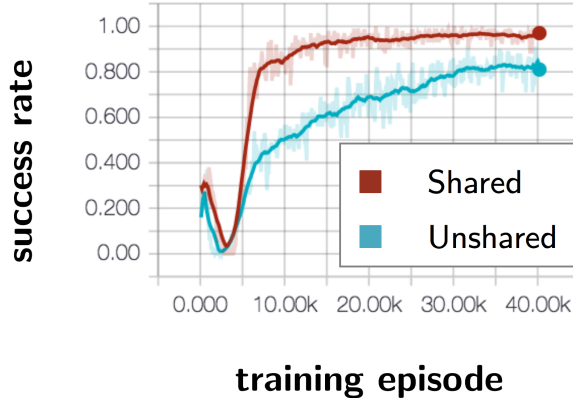


Figure 4.2: The figure shows that the success rate for a network with shared weights (brown line) converge faster than the fully connected network structure which do not share weights (turquoise line).

Controller	Success Rate		Collision Rate	
	Single	Double	Single	Double
SM (Paper A)	96.1%	90.9%	2.8%	8.3%
MPC (Paper B)	97.3%	95.2%	1.2%	3.6%

Table 4.1: Average success rates and collision rates for a fully trained DQN agent driving though a single and double intersections.

four zones, illustrated in Figure 4.3. Starting from the right, Zone 0 represents the ‘safe zone,’ where the ego vehicle is out of danger and can resume nominal driving. Zone 1 is the ‘conflict zone,’ where a collision with another vehicle is possible. Zone 2, the ‘critical decision zone,’ is the final opportunity for the vehicle to either stop or proceed through the intersection. The size of zone 2 is determined by the minimum distance required for the vehicle to come to a complete stop before entering the conflict zone, ensuring sufficient time for safe decision-making. Lastly, Zone 3, the ‘information gathering zone,’ is situated furthest from the intersection. Here, the agent can observe how other vehicles behave over time to estimate their intentions.

The goal is to reach Zone 0. To achieve this, the agent aims to minimize the

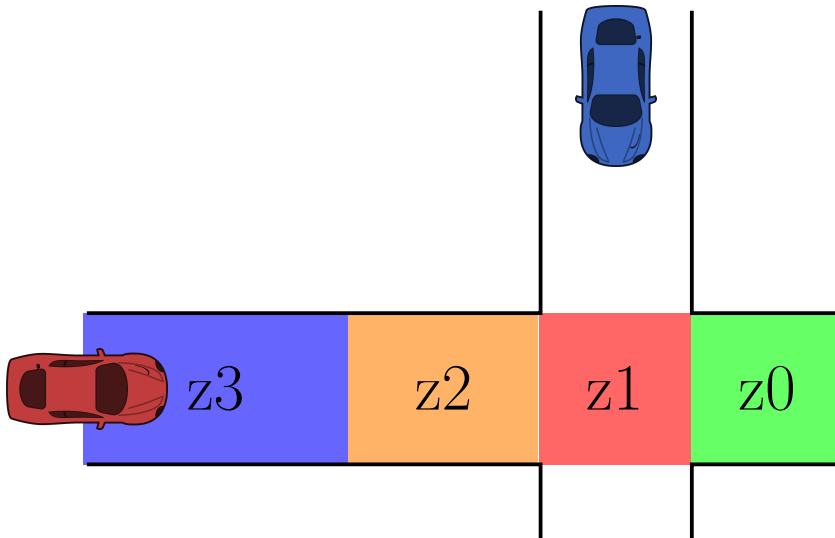


Figure 4.3: Intersection scenario divided into zones describing what is required of the decision maker in different zones

time spent in Zone 1 if there is a chance of intersection with another car. Our actions are formulated as short-term goals, designed for comfortable use with lower acceleration rates. The size of Zone 2 depends on the vehicle's current speed, which is influenced by its behavior in Zone 3.

Now, two conflicting strategies emerge: to minimize time in Zone 1, the agent desires a high speed entering the intersection. However, it also seeks a low speed to reduce the size of Zone 2 and the critical decision period. If the intentions of other vehicles are known, the stochasticity in Zone 1 would be eliminated, transforming the problem into a scheduling task aimed at creating a velocity profile that minimizes the time required to cross. However, since the intentions of other vehicles are inherently stochastic, the next chapter offers a promising approach by accounting for this uncertainty and optimizing decision-making in dynamic traffic scenarios.

CHAPTER 5

Accounting for the uncertainty

The previous chapter formulated the POMDP and introduced how deep Q-learning methods can be utilized to create decision-making agents capable of navigating intersections. A significant advantage of RL methods is their scalability to different scenarios through appropriate training. However, a drawback of deep Q-learning methods, is the use of neural networks, which provide a black-box solution without indicating any confidence or uncertainty in their decisions.

This chapter presents two approaches to estimating the uncertainty: Paper C addresses the uncertainty in the output of the DQN, and Paper D addresses the uncertainty in the intention estimation that is fed as an input to the DQN. To demonstrate the effect of accounting for uncertainty, the results include two types of experiments. In the first type, the trained agent is evaluated on scenarios within the training set. In the second type, the agent is evaluated on scenarios outside the training set.

5.1 Estimating the uncertainty of the Q-value

To estimate the uncertainty of Q -estimate from the DQN, Paper C employed statistical bootstrapping to train an ensemble of neural networks on different subsets of the available experience. This ensemble provides a distribution over the estimated Q -values. A better Bayesian posterior is obtained by adding different randomized prior functions (RPF) to each ensemble member [32]. The Q -values of each ensemble member k is then calculated as the sum of two neural networks, f and p , with the same architecture, i.e.,

$$Q_k(s, a) = f(s, a; \theta_k) + \beta p(s, a; \hat{\theta}_k). \quad (5.1)$$

Here, the weights θ_k of network f are trainable, and the weights $\hat{\theta}_k$ of the prior network p are fixed to the randomly initialized values. A parameter β scales the importance of the networks. With the two networks, the loss function in Eq. 3.5 becomes

$$\begin{aligned} L(\theta_k) = \mathbb{E}_M & \left[(r + \gamma \max_{a'} (f_{\theta_k^-} + \beta p_{\hat{\theta}_k})(s', a') \right. \\ & \left. - (f_{\theta_k} + \beta p_{\hat{\theta}_k})(s, a))^2 \right]. \end{aligned} \quad (5.2)$$

The training process of an ensamble RPF is described by Algorithm 1. An ensemble of K DQN are first initialized randomly. Each ensemble member is also assigned a separate experience replay memory buffer m_k . For each new episode, a random ensemble member ν is selected and used to take greedy actions throughout the episode, which corresponds to an approximate Thompson sampling approach to the exploration vs. exploration dilemma. Each new experience $e = (s_i, a_i, r_i, s_{i+1})$ is then added to the separate replay buffers m_k with probability p_{add} . The trainable weights of each ensemble member are then updated by uniformly sample a mini-batch M of experiences and using SGD.

The agent's uncertainty in choosing different actions can be defined as the coefficient of variation $c_v(s, a)$ of the Q -values of the ensemble members. $c_v(s, a)$ is then used to create a hard threshold c_{safe} , which determines if an action has an acceptable level of uncertainty. A high uncertainty, where $c_v(s, a) > c_v^{\text{safe}}$, indicates that (s, a) is outside the training distribution. When the agent is fully trained, the policy π chooses actions by maximizing the mean of the

Algorithm 1 Ensemble RPF training process

```

1: for  $k \leftarrow 1$  to  $K$  do
2:   Initialize  $\theta_k$  and  $\hat{\theta}_k$  randomly
3:    $m_k \leftarrow \{\}$ 
4:    $i \leftarrow 0$ 
5:   while networks not converged do
6:      $s_i \leftarrow$  initial random state
7:      $\nu \sim \mathcal{U}\{1, K\}$ 
8:     while episode not finished do
9:        $a_i \leftarrow \text{argmax}_a Q_\nu(s_i, a)$ 
10:       $s_{i+1}, r_i \leftarrow \text{STEPENVIRONMENT}(s_i, a_i)$ 
11:      for  $k \leftarrow 1$  to  $K$  do
12:        if  $p \sim \mathcal{U}(0, 1) < p_{\text{add}}$  then
13:           $m_k \leftarrow m_k \cup \{(s_i, a_i, r_i, s_{i+1})\}$ 
14:         $M \leftarrow$  sample mini-batch from  $m_k$ 
15:        update  $\theta_k$  with SGD and loss  $L(\theta_k)$ 
16:       $i \leftarrow i + 1$ 

```

Q -values of the ensemble members, with the restriction $c_v(s, a) < c_v^{\text{safe}}$, i.e.,

$$\begin{aligned} \pi = \underset{a}{\text{argmax}} \frac{1}{K} \sum_{k=1}^K Q_k(s, a), \\ \text{s.t. } c_v(s, a) < c_v^{\text{safe}}. \end{aligned} \quad (5.3)$$

If no action within the action space satisfy the restriction, a safe action a_{safe} is chosen instead. This a_{safe} can be something like a collision avoidance measure, such as emergency braking.

5.1.1 Results for scenarios within the training set

This section shows the results of ensemble RPF method compared to the DQN method used in Paper A , but without the LSTM layer. The ensemble RPF method outperforms the DQN method, both in terms of training speed and final performance, when the resulting agents are tested on scenarios that are similar to the training scenarios. When the fully trained ensemble RPF agent is exposed to situations that are outside the training distribution, the agent

indicates a high uncertainty and chooses safe actions, whereas the DQN agent collides with other vehicles.

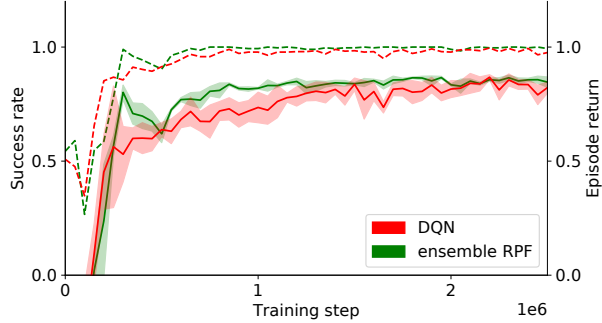


Figure 5.1: Proportion of test episodes where the ego vehicle reached its goal (dashed), and episode return (solid), over training steps for the ensemble RPF and DQN methods. The shaded areas show the standard deviation for 5 random seeds.

The average return and the average proportion of episodes where the ego vehicle reached the goal, as a function of number of training steps, is shown in Figure 5.1, for the test episodes. The figure also shows the standard deviation for 5 random seeds, which generates different sets of initial parameters of the networks and different training episodes, whereas the test episodes are kept fixed. The results show that the ensemble RPF method both learns faster, yields a higher return, and causes less collisions than the DQN method.

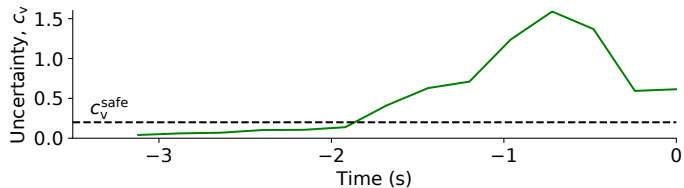
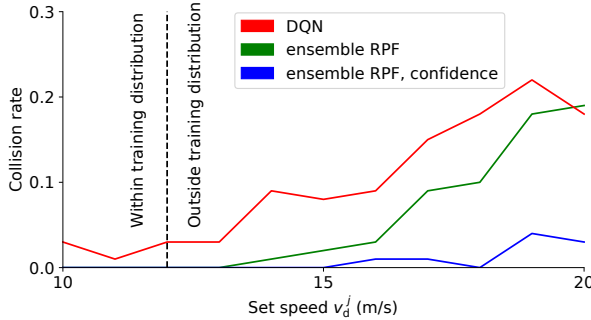


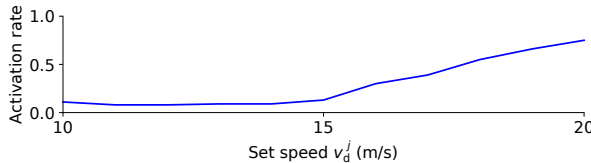
Figure 5.2: Uncertainty c_v during the time steps before one of the collisions in the test episodes, within the training distribution. The collision occurs at $t = 0$ s.

As shown in Figure 5.1, occasional collisions still occur during the test episodes when deploying the fully trained ensemble RPF agent. In one particular example of a collision, using the zones from Figure 4.3, the agent fails to brake enough in zone 3 and take an incorrect action in zone 2, which leads to a collision in zone 1. However, Figure 5.2 show that the estimated uncertainty increases significantly during the time before the collision (zone 2), when the incorrect actions are taken. When applying the confidence criterion, the agent, aware of high uncertainty, brakes early enough in zone 2, thus avoiding collisions. The confidence criterion was applied to all test episodes, effectively eliminating all collisions for scenarios within the training set.

5.1.2 Results for scenarios outside the training set



(a) Proportion of collisions.



(b) Proportion of episodes where a_{safe} was used at least once.

Figure 5.3: Performance of the ensemble RPF agent, with and without the confidence criterion, and the DQN agent, in test episodes with different set speeds v_d^j for the surrounding vehicles.

To evaluate the agents' ability to detect unseen situations, a fully trained

ensemble RPF agent was tested in scenarios outside the training distribution. The same testing scenarios as in the previous section were used, with the exception that the speed of the surrounding vehicles was set to a single deterministic value, which was varied during different runs in the range $v_n = [10, 20]$ m/s. The proportion of collisions as a function of set speed of the surrounding vehicles is shown in Figure 5.3, along with the proportion of episodes where the confidence criterion was violated at least once. The figure demonstrates that by accounting for the uncertainty of the Q -value and the use of the confidence criterion some collisions can be avoided.

5.2 Estimating the uncertainty of the input

The ensemble RPF agent avoided collisions by not taking a bad action in zone 2, by accounting for the uncertainty of the Q -value estimate. However, is it possible reduce the number of collisions by accounting for the uncertainty of the input when in zone 3? In Paper D , the uncertainty about the intention state ζ_n is represented by a belief state, which is a probability distribution over possible true states. A particle-filter was used to give the probability distribution, henceforth referred to as intention distributions.

Using the intention distributions, two methods were proposed: QMDP-IE and QID. QID trained the intention distributions as the intention state ζ_n , while QMDP-IE is derived from the QMDP algorithm [33]. By assuming that the intention state ζ_n can be derived by looking at the history after crossing the intersection, allows the QMDP algorithm to combine elements of both POMDPs and MDPs. In QMDP-IE and QMDP the NN is trained using true intention state and the QMDP calculates the Q -value for each belief state (potential true state). QMDP then computes the expected Q -value for each action by taking the weighted average of the Q -values, while QMDP-IE chooses one intention state using a threshold $\zeta_{\text{threshold}}$ on the intention distribution.

QMDP-IE, in particular, offered adjustable aggressiveness post-training, yielding a collision rate close to the Oracle DQN with an optimal threshold value $\zeta_{\text{threshold}}$. Furthermore, QID policies collision rate was comparable to QMDP-IE for scenarios outside the training set.

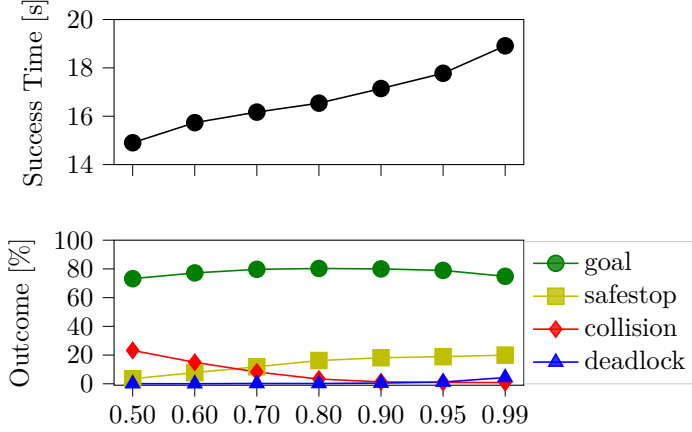


Figure 5.4: QMDP-IE success time for different $\zeta_{\text{threshold}}$ values. Increasing $\zeta_{\text{threshold}}$ lowers the collision rate while at the same time increasing the safe stop rate and the time it takes to reach a success state.

5.2.1 Results within the training set

The results from the experiments show that QMDP-IE outperformed QID.

Starting with QMDP-IE, we first demonstrate how the $\zeta_{\text{threshold}}$ is chosen and then compare its results with QMDP. Both algorithms use the same network weights as the Oracle DQN, but QMPD-IE is less computational than QMDP since the threshold $\zeta_{\text{threshold}}$ transforms the set of particles into a point estimate of the intention state. Therefore, the choice of $\zeta_{\text{threshold}}$ is an important hyperparameter that directly correlates with the aggressiveness of the agent.

As opposed to QMDP-IE and QMDP, QID and QPF algorithms do not require access to the true intent during training time. While QPF trains a network using all particles, QID only uses the intention distribution from the particles, which reduces the size of the network while keeping information about the uncertainty of the intention state. Looking at 5.1, QPF has the highest collision rate at 12.15 % and the second lowest success time out of all considered algorithms, making it the most aggressive policy out of all four algorithms. QID collided more than QMDP-IE but still less than QMDP. This shows that training on ground truth is preferred, but QID is a good algorithm

Table 5.1: Result summary for scenarios within the training set

Experiments	Goal reached	Safe stop	Collision	Deadlock	Success time
	%	%	%	%	s
Oracle DQN	84.50	14.45	1.05	0.00	15.49
QMDP-IE	80.00	18.15	1.35	0.50	17.14
QMDP	71.95	15.05	5.70	7.30	20.56
QID	85.60	10.40	3.70	0.30	16.64
QPF	63.50	21.80	12.15	2.55	16.61

Table 5.2: Results with an overtaking agent

Experiments	Goal reached	Safe stop	Collision	Deadlock	Success time
	%	%	%	%	s
Oracle DQN	89.80	0.15	10.05	0.00	16.01
QMDP-IE	94.55	0.20	4.60	0.65	16.62
QMDP	79.70	10.20	5.95	4.15	19.84
QID	96.89	0.11	2.53	0.47	16.38
QPF	96.15	0.10	3.70	0.05	17.62

to use when ground truth data is not available.

5.2.2 Results for scenarios outside the training set

In the overtaking scenario, both QID and QPF have relatively low collision rates at 2.53% and 3.7% respectively, which is lower when compared to the trained scenarios in 5.1. While the collision rate for QMDP-IE and QMDP is 4.6% and 5.95% respectively, which is higher than what they got on the trained scenario but it is also higher than QID and QPF. This indicates that QID and QPF are better at handling some scenarios outside the training set than QMDP-IE and QMDP. QMDP also has the highest safe stop and deadlock rate at 10.2% and 4.15%, making it the most passive policy.

CHAPTER 6

Generalizing over different scenarios

Now lets us consider that a company designing Level 5 AD agents, as mentioned in Section 1.1 L5 requires the AV to be able to drive anywhere. The company has designed two RL agents that have learned to drive at L4 in the USA and UK. Now, the company wants to deploy a new RL agent in India. Though all the RL agents are concerned with the same task, i.e. driving, the models encompassing driver behaviors, traffic rules, signs, etc., can differ for each. For example, UK and India have left-handed traffic, while the USA has right-handed traffic. However, learning a new controller specifically for every new geographic location is computationally expensive and time-consuming, as both data collection and learning take time. Thus, the company might use the models learned for UK and USA, to estimate the model for India, and use it further to build a new AD agent (RL agent). Hence, being able to transfer the source models to the target environment allows the company to use existing knowledge to build an efficient agent faster and resource efficiently. This problem of model transfer from source models to a target environment to plan efficiently is address in Paper E .

6.1 Approach

Our approach is to use transfer RL to identify where we are in the convex hull of MDPs and then choose the policy for MDP we are closest too. Given at set of MDPs, a convex hull is created using the MDPs as the boudries. The goal is then to identity where in the convex hull of MPDs the agent is existing or which MDP is the closest. This does require some number of MDPs to span out the convex hull of models. This can find a policy between MDPs. Identify which MDP is closest. For example Downtown driving in one country may be similar to the driving stile to another.

6.2 Results and discussion

How can we accurately construct a model using a set of source models for an RL agent deployed in the wild? Our answer to the first question is by adopting the Model Transfer Reinforcement Learning framework and weighting existing knowledge together with data from the novel task. We accomplished this by following a maximum likelihood-based approach. This has led to a novel algorithm, MLEMTRL, consisting of a model identification stage and a model-based planning stage.

Does the constructed model allow us to perform efficient planning and yield improvements over learning from scratch? the model allows generalising to novel tasks, given that the tasks are similar enough to the existing task(s). We motivate the use of our framework in settings where an agent is to be deployed in a new domain that is similar to existing, known, domains.

CHAPTER 7

Discussion

7.1 Guaranteeing safety

Safety is the most important factor of a AD system, but since RL is a data driven approach it is very difficult to guarantee safety **tbd** in the same way e.g., a MPC can. That is why this section will clarify where the work in this thesis would fit in by first defining a system architecture for AD, its modules and a short summary of the ISO 26262 standard. Then, place itself within the system and motivate how safety can be guaranteed.

The architecture of an autonomous driving system can be divided into perception, planning and control [5], [34]. The perception module is responsible for sensing and mapping the environment with the use of sensors such as LIDARs, cameras, radars etc. The raw data from the sensors are then processed through various sensor fusion techniques to generate a representation of the environment, e.g., position, velocity of other traffic participants while also describing the road such as width and distance to the next intersection. This information is then used by the planner to create a driving strategy of how to transverse through the world. However, the information from the sensors are often noisy, with false positives and false negatives making it difficult for the

planner.

Tactical planning can be divided into three categories, the proactive, active and reactive. A proactive module would be something like a precautionary safety module that interprets the information about the environment and create constraints that is sent to the active planner, like driveable area, allowed speeds and actions. These constraints are generated from a set of safety goals and rules, making this the first layer of protection that can ensure safety. The role of the active planner is to take this sets of allowed actions and prescribe the behavior of the vehicle through decisions such as drive, yield or stop. The goal of these high level decisions is to optimize metrics such as comfort, fuel consumption and time to goal. These decisions are then sent to a motion planner that generates a safe dynamically feasible path for the vehicle for a shorter planning horizon of around 0.1s. At the same time, a reactive, collision avoidance, module make sure that the chosen decision and path does lead to any collisions. Unlike the decision maker, the collision avoidance module main goal is to identify imminent danger and therefore has access to more aggressive actions like emergency breaking to ensure safety.

In the industry today the main standard for functional safety in motorized vehicles is the ISO 26262 standard, titled "Road vehicles – Functional safety" [35]. It uses a Automotive Safety Integrity Level (ASIL) to classify the inherent safety risk in an automotive system and the functions or modules of such a system. The ASIL classification is used to express the level of risk reduction required to prevent a specific hazard, from ASIL D to ASIL A. ASIL D represents the highest hazard level and ASIL A the lowest. There is a level with no safety relevance and only standard Quality Management processes are required, this level is referred to as QM.

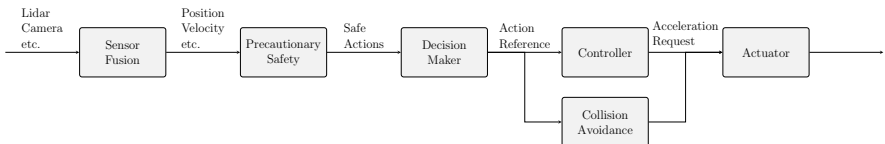


Figure 7.1: Representation of the system architecture.

Although safety is the most important requirement for enabling autonomous driving, the work in this paper does not make any safety guarantees. Instead, it is proposed that the decision-making algorithms presented in this paper be

used in the system architecture shown in Figure 7.1. This approach allows higher ASIL to be applied to the precautionary safety and collision avoidance modules, while the decision-making algorithms focus primarily on comfort. As a result, the ASIL classification for the decision-making components could be at lower levels, potentially even classified as QM in the best case.

CHAPTER 8

Concluding remarks and future work

8.1 Conclusions

Looking at the research questions we posted in the beginning:

- Q1.** How can RL techniques be used to develop a decision-making agent that effectively navigates intersections without explicitly estimating the intention state of other vehicles?
- A1.** By formulating the problem as a POMDP with an unobservable intention state. Deep Q-learning showed some potential of finding a good policy when using a combination of techniques e.g., shared weights, experience replay and a LSTM layer.
- Q2.** How can an RL agent utilize the uncertainty in its predictions and actions to enhance decision-making in complex environments?
- A2.** By creating estimate of the uncertainty of the Q-value from a DQN a threshold value was able to reduce the number of simulated collisions. Another threshold value can also be put on the on estimate of the

intention state which directly affected how much disk the driving policy took.

Q3. How do can a RL agent handle situations it has not been trained on?

A3. If we have a set of pretrained DQN, transfer learning can be used to switch models whenever it is identified that the agent is in an environment it has not been trained on.

8.2 Future work

Implementation in the real world. using transofrmr and attention to estimate the intention state. Other network structures like DVRL to replace lstm.

CHAPTER 9

Summary of included papers

This chapter provides a summary of the included papers.

9.1 Paper A

Tommy Tram, Anton Jansson, Robin Grönberg, Mohammad Ali, and Jonas Sjöberg

Learning Negotiating Behavior Between Cars in Intersections using Deep Q-Learning

Published in 2018 21st International Conference on Intelligent Transportation Systems (ITSC),

pp. 3169–3174, Nov. 2018.

©2018 IEEE DOI: 10.1109/ITSC.2018.8569316.

This paper concerns automated vehicles negotiating with other vehicles, typically human driven, in crossings with the goal to find a decision algorithm by learning typical behaviors of other vehicles. The vehicle observes distance and speed of vehicles on the intersecting road and use a policy that adapts its speed along its pre-defined trajectory to pass the crossing efficiently. Deep Q-

learning is used on simulated traffic with different predefined driver behaviors and intentions. The results show a policy that is able to cross the intersection avoiding collision with other vehicles 98% of the time, while at the same time not being too passive. Moreover, inferring information over time is important to distinguish between different intentions and is shown by comparing the collision rate between a Deep Recurrent Q-Network at 0.85% and a Deep Q-learning at 1.75%.

9.2 Paper B

Tommy Tram, Ivo Batković, Mohammad Ali, and Jonas Sjöberg
Learning When to Drive in Intersections by Combining Reinforcement Learning and Model Predictive Control
Published in 2019 IEEE Intelligent Transportation Systems Conference (ITSC),
pp. 3263–3268, Oct. 2019.
©2019 IEEE DOI: 10.1109/ITSC.2019.8916922.

In this paper, we propose a decision making algorithm intended for automated vehicles that negotiate with other possibly non-automated vehicles in intersections. The decision algorithm is separated into two parts: a high-level decision module based on reinforcement learning, and a low-level planning module based on model predictive control. Traffic is simulated with numerous predefined driver behaviors and intentions, and the performance of the proposed decision algorithm was evaluated against another controller. The results show that the proposed decision algorithm yields shorter training episodes and an increased performance in success rate compared to the other controller.

9.3 Paper C

Carl-Johan Hoel, Tommy Tram, and Jonas Sjöberg
Reinforcement Learning with Uncertainty Estimation for Tactical Decision-Making in Intersections
Published in 2020 IEEE 23rd International Conference on Intelligent Transportation Systems (ITSC),
pp. 1-7, Sep. 2020.

©2020 IEEE DOI: 10.1109/ITSC45102.2020.9294407.

This paper investigates how a Bayesian reinforcement learning method can be used to create a tactical decision-making agent for autonomous driving in an intersection scenario, where the agent can estimate the confidence of its decisions. An ensemble of neural networks, with additional randomized prior functions (RPF), are trained by using a bootstrapped experience replay memory. The coefficient of variation in the estimated Q-values of the ensemble members is used to approximate the uncertainty, and a criterion that determines if the agent is sufficiently confident to make a particular decision is introduced. The performance of the ensemble RPF method is evaluated in an intersection scenario and compared to a standard Deep Q-Network method, which does not estimate the uncertainty. It is shown that the trained ensemble RPF agent can detect cases with high uncertainty, both in situations that are far from the training distribution, and in situations that seldom occur within the training distribution. This work demonstrates one possible application of such a confidence estimate, by using this information to choose safe actions in unknown situations, which removes all collisions from within the training distribution, and most collisions outside of the distribution.

9.4 Paper D

Tommy Tram, Maxime Bouton, Jonas Fredriksson, Jonas Sjöberg, and Mykel Kochenderfer

Belief State Reinforcement Learning for Autonomous Vehicles in Intersections

Submitted to IEEE Transactions on Intelligent Vehicles,

©2023 IEEE DOI: TBD.

This paper investigates different approaches to find a safe and efficient driving strategy through an intersection with other drivers. Because the intentions of the other drivers to yield, stop, or go are not observable, we use a particle filter to maintain a belief state. We study how a reinforcement learning agent can use these representations efficiently during training and evaluation. This paper shows that an agent trained without any consideration of the intentions of others is both slower at reaching the goal and results in more collisions. Four algorithms that use a belief state generated by a particle filter are compared.

Two of the algorithms have access to the intention only during training while the others do not. The results show that explicitly trying to predict the intention gave the best performance in terms of safety and efficiency.

9.5 Paper E

Hannes Eriksson, Tommy Tram, Debabrota Basu, Mina Alibeigi, and Christos Dimitrakakis

Reinforcement Learning in the Wild with Maximum Likelihood-based Model Transfer

Published in 2024 International Conference on Adaptive Agents and Multi-Agent Systems (AAMAS),
pp. 516–524, May. 2024.

For decision-problems with insufficient data, it is imperative to take into account not only what you know but also what you do not know. In this work, ways of transferring knowledge from known, existing tasks to a new setting is studied. In particular, for tasks such as autonomous driving, the optimal controller is conditional on things such as, the physical properties of the vehicle, the local and regional traffic rules and regulations and also on the specific scenario trying to be solved. Having separate controllers for every combination of these conditions is intractable. By assuming problems with similar structure, we are able to leverage knowledge attained from similar tasks to guide learning for new tasks. We introduce a maximum likelihood estimation procedure for solving Transfer Reinforcement Learning (TRL) of different types. This procedure is then evaluated over a set of autonomous driving settings, each of which constitutes an interesting scenario for autonomous driving agents to make use of external information. We prove asymptotic regret bounds for proposed method for general structured probability matrices in a specific setting of interest.

References

- [1] O. Y. I-Cheng Lin and C. Joe-Wong, “Mixed-autonomy era of transportation,” *Traffic21*, Tech. Rep., 2022.
- [2] K. Heineke, N. Laverty, T. Möller, and F. Ziegler, *The future of mobility: Mobility evolves*, Apr. 2023.
- [3] D. J. Fagnant and K. Kockelman, “Preparing a nation for autonomous vehicles: Opportunities, barriers and policy recommendations,” *Transportation Research Part A: Policy and Practice*, vol. 77, pp. 167–181, 2015, ISSN: 0965-8564.
- [4] J. Janai, F. Güney, A. Behl, and A. Geiger, *Computer Vision for Autonomous Vehicles: Problems, Datasets and State of the Art*. Now Publishers Inc., 2020.
- [5] W. Schwarting, J. Alonso-Mora, and D. Rus, “Planning and decision-making for autonomous vehicles,” *Annual Review of Control, Robotics, and Autonomous Systems*, vol. 1, no. 1, pp. 187–210, 2018.
- [6] “2019 traffic safety culture index,” AAA Foundation for Traffic Safety, Washington DC, Tech. Rep. 202-638-5944, 2019.
- [7] “Taxonomy and definitions for terms related to driving automation systems for on-road motor vehicles,” On-Road Automated Driving (ORAD) Committee, Tech. Rep., 2021.
- [8] L. Fletcher *et al.*, “The mit–cornell collision and why it happened,” *Journal of Field Robotics*, vol. 25, pp. 775–807, Oct. 2008.

References

- [9] S. Kammel *et al.*, “Team annieway’s autonomous system for the 2007 darpa urban challenge,” *Journal of Field Robotics*, vol. 25, pp. 615–639, Sep. 2008.
- [10] L. Gressenbuch and M. Althoff, “Predictive monitoring of traffic rules,” in *IEEE International Conference on Intelligent Transportation Systems (ITSC)*, 2021.
- [11] M. Treiber, A. Hennecke, and D. Helbing, “Congested traffic states in empirical observations and microscopic simulations,” *Physical Review E*, vol. 62, pp. 1805–1824, 2 2000.
- [12] M. Liebner, M. Baumann, F. Klanner, and C. Stiller, “Driver intent inference at urban intersections using the intelligent driver model,” in *IEEE Intelligent Vehicles Symposium (IV)*, 2012.
- [13] S. Hoermann, D. Stumper, and K. Dietmayer, “Probabilistic long-term prediction for autonomous vehicles,” in *IEEE Intelligent Vehicles Symposium (IV)*, 2017.
- [14] C. B. Browne *et al.*, “A survey of Monte Carlo tree search methods,” *IEEE Transactions on Computational Intelligence and AI in Games*, vol. 4, no. 1, pp. 1–43, 2012.
- [15] C. Hubmann, M. Becker, D. Althoff, D. Lenz, and C. Stiller, “Decision making for autonomous driving considering interaction and uncertain prediction of surrounding vehicles,” in *IEEE Intelligent Vehicles Symposium (IV)*, 2017.
- [16] Z. N. Sunberg, C. J. Ho, and M. J. Kochenderfer, “The value of inferring the internal state of traffic participants for autonomous freeway driving,” in *American Control Conference (ACC)*, 2017.
- [17] M. Werling, J. Ziegler, S. Kammel, and S. Thrun, “Optimal trajectory generation for dynamic street scenarios in a Frenét frame,” in *IEEE Int. Conf. on Robot. and Automat.*, 2010.
- [18] F. Damerow and J. Eggert, “Risk-aversive behavior planning under multiple situations with uncertainty,” in *IEEE Int. Conf. on Intell. Transp. Syst. (ITSC)*, 2015.

- [19] D. González, J. Pérez, V. Milanés, and F. Nashashibi, “A review of motion planning techniques for automated vehicles,” *IEEE Transactions on Intelligent Transportation Systems*, vol. 17, no. 4, pp. 1135–1145, 2016.
- [20] B. Paden, M. Čáp, S. Z. Yong, D. Yershov, and E. Frazzoli, “A survey of motion planning and control techniques for self-driving urban vehicles,” *IEEE Transactions on Intelligent Vehicles*, vol. 1, no. 1, pp. 33–55, 2016.
- [21] M. J. Kochenderfer, *Decision Making Under Uncertainty: Theory and Application*. MIT Press, 2015.
- [22] R. S. Sutton and A. G. Barto, *Reinforcement Learning: An Introduction*, 2nd ed. MIT Press, 2018.
- [23] D. Isele, R. Rahimi, A. Cosgun, K. Subramanian, and K. Fujimura, “Navigating occluded intersections with autonomous vehicles using deep reinforcement learning,” in *IEEE International Conference on Robotics and Automation (ICRA)*, 2018.
- [24] M. J. Hausknecht and P. Stone, “Deep recurrent q-learning for partially observable mdps,” in *AAAI Conference on Artificial Intelligence (AAAI)*, 2015.
- [25] P. Zhu, X. Li, P. Poupart, and G. Miao, *On improving deep reinforcement learning for pomdps*, 2018.
- [26] M. Bouton, A. Cosgun, and M. J. Kochenderfer, “Belief state planning for autonomously navigating urban intersections,” in *IEEE Intelligent Vehicles Symposium (IV)*, 2017.
- [27] A. Wang, A. C. Li, T. Q. Klassen, R. T. Icarte, and S. A. Mcilraith, “Learning belief representations for partially observable deep RL,” vol. 202, Jul. 2023.
- [28] C. J. C. H. Watkins and P. Dayan, “Q-learning,” *Machine Learning*, vol. 8, no. 3, pp. 279–292, 1992.
- [29] V. Mnih *et al.*, “Human-level control through deep reinforcement learning,” *Nature*, vol. 518, no. 7540, pp. 529–533, 2015.
- [30] M. Hessel *et al.*, “Rainbow: Combining improvements in deep reinforcement learning,” in *AAAI Conference on Artificial Intelligence (AAAI)*, 2018.

References

- [31] M. Bouton, A. Nakhaei, K. Fujimura, and M. J. Kochenderfer, “Cooperation-aware reinforcement learning for merging in dense traffic,” in *IEEE International Conference on Intelligent Transportation Systems (ITSC)*, 2019.
- [32] I. Osband, J. Aslanides, and A. Cassirer, “Randomized prior functions for deep reinforcement learning,” in *Advances in Neural Information Processing Systems (NIPS)*, 2018.
- [33] M. L. Littman, A. R. Cassandra, and L. P. Kaelbling, “Learning policies for partially observable environments: Scaling up,” in *International Conference on Machine Learning (ICML)*, 1995.
- [34] D. Kortenkamp, R. G. Simmons, and D. Brugali, “Robotic systems architectures and programming,” in *Springer Handbook of Robotics, 2nd Ed.*, 2008.
- [35] “Road vehicles — functional safety,” International Organization for Standardization, Standard, Dec. 2018.

Part II

Papers

PAPER A

Learning Negotiating Behavior Between Cars in Intersections using Deep Q-Learning

Tommy Tram, Anton Jansson, Robin Grönberg, Mohammad Ali, and Jonas Sjöberg

*Published in 2018 21st International Conference on Intelligent Transportation Systems (ITSC),
pp. 3169–3174, Nov. 2018.
©2018 IEEE DOI: 10.1109/ITSC.2018.8569316.*

The layout has been revised.

Abstract

This paper concerns automated vehicles negotiating with other vehicles, typically human driven, in crossings with the goal to find a decision algorithm based on learning typical behavior of other vehicles. The vehicle observes distance and speed of vehicles on the intersecting road and use a policy that adapts its speed along its pre-defined trajectory to pass the crossing efficiently. Deep Q-learning is used on simulated traffic and the results show that policies can be trained to successfully drive comfortably through an intersection, avoiding collision with other cars and not being too passive. The policies generalize over different types driver behaviors and intentions. Moreover, to enable inferring information over time, a Deep Recurrent Q-Network is tested and compared to the Deep Q-learning. The results show that a Deep Recurrent Q-Network succeeds in three out of four attempts where a Deep Q-Network fails.

1 Introduction

The development of autonomous driving vehicles is fast and there are regularly news and demonstrations of impressive technological progress, see eg [1]. However, one of the largest challenges does not have to do with the autonomous vehicle itself but with the human driven vehicles in mixed traffic situations. Human drivers are expected to follow traffic rules strictly, but in addition they also interact with each other in a way which is not captured by the traffic rules, [2], [3]. This *informal* traffic behavior is important, since the traffic rules alone may not always be enough to give the safest behavior. This motivates the development of control algorithms for autonomous vehicles which behave in a "human-like" way, and in this paper we investigate the possibilities to develop such behavior by training on simulated vehicles.

In [4] they raises two concerns when using Machine learning, specially Reinforcement learning, for autonomous driving applications: ensuring functional safety of the Driving Policy and that the Markov Decision Process model is problematic, because of unpredictable behavior of other drivers. In the real world, intentions of other drivers are not always deterministic or predefined.

Depending on their intention, different actions can be chosen to give the most comfortable and safe passage through an intersection. They also noted that in the context of autonomous driving, the dynamics of vehicles is Markovian but the behavior of other road users may not necessarily be Markovian. In this paper we solve these two concerns using a Partially Observable Markov Decision Process (POMDP) as a model and Short Term Goals (STG) as actions. With a POMDP the unknown intentions can be estimated using observations and that has shown promising results for other driving scenarios [5]. The POMDP is solved using a model-free approach called Deep (Recurrent) Q-Learning. With this approach a driving policy can be found using only observations without defining the states. Since we do not train on human driven vehicles, the results presented here cannot be considered human-like, but the general approach, to train the algorithms using traffic data, is shown working, and a possible next step could be to start with the pre-tuned policies from this work, and to continue the training in real traffic crossings.

2 Overview

This paper starts by introducing the system architecture and defining the actions, observations and POMDP in Section 3. The final strategy of what action to take at a given situation is called a policy and is described in Section 4. The method used for finding this policy is called Q-learning, which uses a neural network to approximate a Q-value and is described in Section 5 together with techniques used to improve the learning, such as Experience replay, Dropout and a recurrent layer called Long short term memory (LSTM). We then present the simulation, reward function and neural network configurations in Section 6. The results are then presented in Section 7 comparing the effect of the methods mentioned in Section 5. Finally the conclusion and brief discussion is presented in Section 8.

3 Problem formulation

The objective is to drive along a main road that has one or two intersections with crossing traffic and control the acceleration in a way that avoids collisions in a comfortable way. All vehicles are assumed to drive along predefined paths on the road where they can either speed up or slow down to avoid collisions in

the crossings. In this section the system architecture is defined along with the environment, observation and actions.

3.1 System architecture

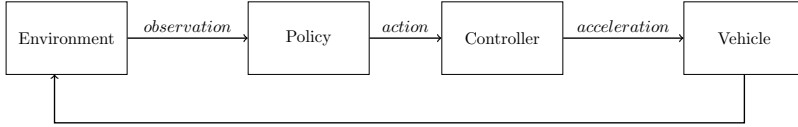


Figure 1: Representation of the architecture

Environment is defined as the world around the ego vehicle, including all vehicles of interest and the shape/type of the intersection. The environment can vary in different ways, e.g. number of vehicles and intersection or the distance to intersections. The environment is defined by the simulation explained in section 6.1. We assume that the ego vehicle receives observations from this environment at each sampling instant, as shown in Fig. 1. A policy then takes these observations and chooses a high level action that is defined in more detail in section 3.3. These actions are sent to a controller that calculates the appropriate acceleration request given to the ego vehicle, which will influence the environment and impact how other cars behave.

3.2 Actions as Short Term Goals

Motivated by the insight that the ego vehicle has to drive before or after other vehicles when passing the intersection, decisions on the velocity profile is modeled by simply keeping a distance to other vehicles until they pass. This is done by defining the actions as Short Term Goals (STG), eg. keep set speed or yield for crossing car. This allows the properties of comfort on actuation and safety to be tuned separately, making the decision a classification problem. The actions are then as followed:

- *Keep set speed:* Aims to keep a specified maximum speed v_{\max} , using a simple P-controller

$$a_p^e = K(v_{\max} - v^e) \quad (\text{A.1})$$

where a_p^e is the acceleration request and v^e is the velocity of ego vehicle towards the center of the intersection, while K is a proportional constant.

- *Keep distance to vehicle N:* Will control the acceleration in a way that keeps a minimum distance to a chosen vehicle N , a *Target Vehicle*, and can be done using a sliding mode controller, where the acceleration request is:

$$a_{sm}^e = \frac{1}{c_2}(-c_1x_2 + \mu sign(\sigma(x_1, x_2))) \quad (\text{A.2})$$

$$\text{where } \begin{cases} x_1 = p^t - p^e \\ x_2 = v^t - v^e \end{cases}$$

where p^e and p^t is the position of ego and target vehicle respectively, shown in Fig. 2, and v^t is the velocity of target vehicle. c_1 together with c_2 are calibration parameters that can be set to achieve wanted performance with a surface plane σ

$$\sigma = c_1x_1 + c_2x_2 \quad (\text{A.3})$$

The final acceleration request a^e is achieved by a min arbitration between eq. A.1 and A.2

$$a^e = \min(a_{sm}^e, a_p^e) \quad (\text{A.4})$$

For more detailed information about sliding mode see [6]. To distinguish between different cars to follow, each other vehicle will have its own action.

- *Stop in front of intersection:* Stops the car at the next intersection. Using the same controller as eq. A.4 while setting $v^t = 0$ and p^t to start of intersection, the controller can bring ego vehicle to a comfortable stop before the intersection.

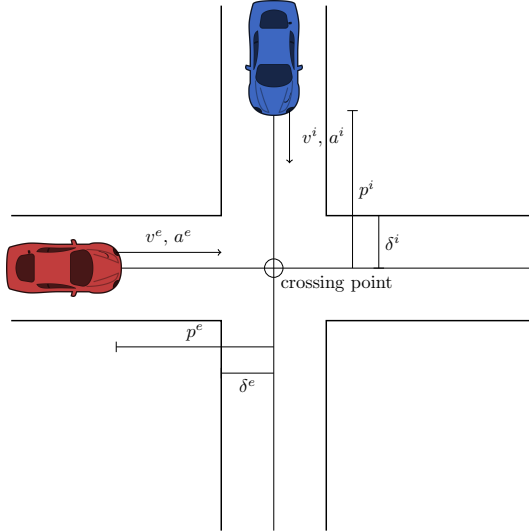


Figure 2: Observations that makes the state

3.3 Observations that make up the state

A human driver is, generally, good at assessing a scenario and it is hard to pin-point what information is used in their assessment. Therefore some assumptions are made on which features that are interesting to observe. The observation o_t at time t is defined as:

$$o_t = [p_t^e \quad v_t^e \quad a_t^e \quad \delta^e \quad p_t^i \quad v_t^i \quad a_t^i \quad \delta^i \quad a_{t+1}^{e,A}]^T \quad (\text{A.5})$$

With notations as follows: consider Fig. 2, position of ego p_t^e and other vehicle p_t^i are defined as distance to common reference point, called *crossing point*, where i is an index of the other vehicle. The start of intersection for ego δ^e and other vehicle δ^i also uses the crossing point as reference. These are relevant in case a driver would choose to yield for other vehicles, then they would most likely stop before the start of intersection. The velocity v^e and acceleration a^e of ego vehicle and velocity v^i and acceleration a^i of the other vehicles are observed to include the dynamics of different actors. The last feature in the observation, $a_{t+1}^{e,A}$, is the ego vehicle's predicted acceleration for each possible action A , which can be used to account for comfort in the

decision.

3.4 Partially Observable Markov Decision Processes

The decision making process in the intersection is modeled as a POMDP. A POMDP works like a Markov Decision Process (MDP) [7] in most aspects, but the full state is not observable.

At each time instant, an action, $a_t \in \mathcal{A}$, is taken, which will influence to which new state vector, s_{t+1} , the system evolves and changes the environment. Each action a_t from a state s_t has a value called the reward r_t , which is given by a reward function \mathcal{R}_t .

One of the unobservable states could be the intentions of other drivers approaching the intersection. The state can only be perceived partially through observations $o_t \in \Omega$ with the probability distribution of receiving observation o_t given an underlying hidden state $s_t : o_t \leftarrow \mathcal{O}(s_t)$, where $\mathcal{O}(s_t)$ is the probability distribution.

4 Finding the optimal policy

Assuming the states are not known, we want a model-free method of finding a policy, and for this we use reinforcement learning. The goal is to have an agent learn how to maximize the future reward by taking different actions in a simulated environment. Details on the simulation environment used is described in Section 6.1. The strategy of which action to take given a state is called a policy π and can be modeled in two ways:

- As stochastic policy $\pi(a|s) = \mathcal{P}[\mathcal{A} = a | \mathcal{S} = s]$
- As deterministic policy $a = \pi(s)$

The standard assumption is made that the future reward is discounted by a factor γ per time step, making the discounted future reward $\mathcal{R}_t = \sum_t^\tau \gamma^{t-1} r_t$, where τ is the time step where the simulation ends, e.g. when the agent crosses an intersection safely.

Similar to [8], the optimal action-value function $Q^*(s_t, a_t)$ is defined as the maximum expected reward achievable by following a policy π given the state s_t and taking an action a_t :

$$Q^*(s_t, a_t) = \max_{\pi} \mathbb{E}[\mathcal{R}_t | s_t, a_t, \pi] \quad (\text{A.6})$$

Using the Bellman equation, $Q^*(s_t, a_t)$ can be defined recursively. If we know $Q^*(s_t, a)$ for all actions a that can be taken in state s_t , then the optimal policy will be one that takes the action a_t that gives the highest immediate and discounted expected future reward $r_t + \gamma Q^*(s_{t+1}, a_{t+1})$. This gives us:

$$Q^*(s_t, a_t) = \mathbb{E}[r_t + \gamma \max_{a_{t+1}} Q^*(s_{t+1}, a_{t+1}) | s_t, a_t] \quad (\text{A.7})$$

The optimal policy π^* is then given by taking actions according to an optimal $Q^*(s_t, a_t)$ function:

$$\pi^*(s_t) = \arg \max_{a_t} Q^*(s_t, a_t) \quad (\text{A.8})$$

5 Method

From eq. A.8, the optimal policy is defined by taking an action that has the highest expected Q-value. Because the Q-value is not known, a non linear function approximation, such as a neural network, is used to estimate the Q-function. The method is known as Deep Q-Learning [8] and in this section we will briefly describe Q-learning and methods used to improve the learning such as, Experience replay, dropout and Long-, Short- Term Memory (LSTM).

5.1 Deep Q-learning

Deep Q-Learning uses a neural network to approximate the Q -function. This neural network is called Deep Q-Network (DQN). The Q -function approximated by the DQN is denoted as $Q(s_t, a_t | \theta^\pi)$, where θ^π are the neural network parameters for policy π . The state s_t is the input to the DQN and the output is the Q -value for each action \mathcal{A} .

5.2 Experience Replay

A problem with Deep Q-Learning, looking at eq. A.8, is that with a small change in the Q -function, can effect the policy drastically. The distribution of future training samples will be greatly influenced by the updated policy. If the network only trains on recent experiences, a biased distribution of samples

is used. Such behavior can cause unwanted feedback loops which can lead to divergence of the trained network [9].

Proposed by [8] in order to make DQN more robust, all observations o , together with taken actions a and their rewards r , are stored in an experience memory E and the agent can sample experiences E' from the experience memory. The sampled experiences are fed to the gradient descent algorithm as a mini-batch. Thus, the agent learns on an average of the experiences in E and is likely to train on the same experiences multiple times, which can speed up the network's convergence and reduce oscillations [10].

5.3 Dropout

Overfitted neural networks have bad generalization performance [11] and to help reduce overfitting a technique called dropout was used. The idea with dropout is to temporarily remove random hidden neurons with their connections from the network, before each training iteration. This is done by, independently, for each neuron, setting its value to 0 with a probability p . For more details, see [12].

5.4 Long short term memory

The effect of changes over time is explored in this paper and is done by adding a recurrent layer to the DQN making it a Deep Recurrent Q-Network (DRQN). A regular Recurrent Neural Network struggle to remember longer sequences due to vanishing gradients, and in [13] LSTM is used to solve this problem. An LSTM is a recurrent network constructed for tasks with long-term dependencies. Instead of storing all information from previous time sample, LSTM stores information in a memory cell and modify this memory by using insert and forget gates. These gates decides if a memory cell should be kept or cleared, and during training, the network learns how to control these gates. As a result of this, both newly seen observations and observations seen a long time ago can be stored and used by the network. A sequence length of 4 is used when training the LSTM, where the first 3 observations are only used to build the internal memory state of the LSTM cells, as described in [14].

6 Implementation

In this section we go through the experiment implementation. A simulation environment was set up to model the interactions. From section 3, both the number of observations and actions are dependent on the maximum number of cars. In this paper we consider up to 4 cars. The Deep Q Network can then also be fully defined with the help of observations from section 3 and finally we go through the reward function that defines our behavior.

6.1 Simulation environment

The simulation environment is set up as an intersection described in section 3.3. The number of other cars that are observable at the same time can vary from 1-4, while their intentions can vary between an aggressive *take way*, passive *give way* or a cautious driver. The take way driver does not slow down or yield for crossing traffic in an intersection, while the give way driver will always yield for other vehicles before continuing through the intersection. The cautious driver on the other hand, will slow down for crossing traffic but not come down to a full stop. With a maximum number of other cars set to 4 all possible actions the ego vehicle can take are:

- α_1 : Keep set speed.
- α_2 : Stop in front of intersection.
- α_3 : Keep distance to vehicle 1.
- α_4 : Keep distance to vehicle 2.
- α_5 : Keep distance to vehicle 3.
- α_6 : Keep distance to vehicle 4.

At the start of an episode, the ego vehicle's position and velocity, the number of other vehicles and their intentions are randomly generated. The episode only ends when the ego vehicle fulfills one out of three conditions: 1. Crossing the intersection and reaching the other side, 2. Colliding with another vehicle. or 3. Running out of time τ_m . Each car follows the control law from eq. A.4,

trying to keep a set speed while keeping a set distance to the vehicle in front of its own lane.

All cars including the ego vehicle in these scenarios have a maximum acceleration set to $5m/s^2$ and was set after comfort and normal driving conditions.

6.2 Reward function tuning

When using a DQN, the reward function is optimally distributed around $[-1, 1]$. If the defined reward values are too large, the Q_π -values can become large and cause the gradients to grow [15]. The reward function is defined as follows:

$$r_t = \hat{r}_t + \begin{cases} 1 - \frac{\tau}{\tau_m} & \text{on success,} \\ -2 & \text{on collision} \\ -0.1 & \text{on timeout, i.e. } \tau \geq \tau_m \\ -\left(\frac{j_t^e}{j_{\max}}\right)^2 \frac{\Delta\tau}{\tau_m} & \text{on non-terminating updates} \end{cases}$$

where $\hat{r}_t = \begin{cases} -1 & \text{if chosen } a_t \text{ is not valid} \\ 0 & \text{otherwise} \end{cases}$

The actions $\alpha_3, \dots, \alpha_6$ described should only be selected when a vehicle is visible and a valid target to follow. To learn when these action are valid, the agent gets punished on invalid choices using \hat{r}_t . Accelerations returned by the controller for different STG can vary, which increases jerk and can make the ride uncomfortable. Therefore the reward function also punishes the agent when acceleration jerk j_t^e is large, where τ is the elapsed time sense the episode started and τ_m is the maximum time has before a timeout.

6.3 Neural Network Setup

The DRQN structure is defined in Fig. 3. Where \mathbf{h} are the hidden layers of the network with weights \mathbf{W} . Because the observations o_t from section 2, are used as input to the DRQN, the number of features must be fixed. With up to four other cars the input vectors ξ are as follows:

- $\xi_1 = [p_t^e \quad v_t^e \quad a_t^e \quad \delta^e \quad p_t^1 \quad v_t^1 \quad a_t^1 \quad \delta^1]^T$
- $\xi_2 = [p_t^e \quad v_t^e \quad a_t^e \quad \delta^e \quad p_t^2 \quad v_t^2 \quad a_t^2 \quad \delta^2]^T$

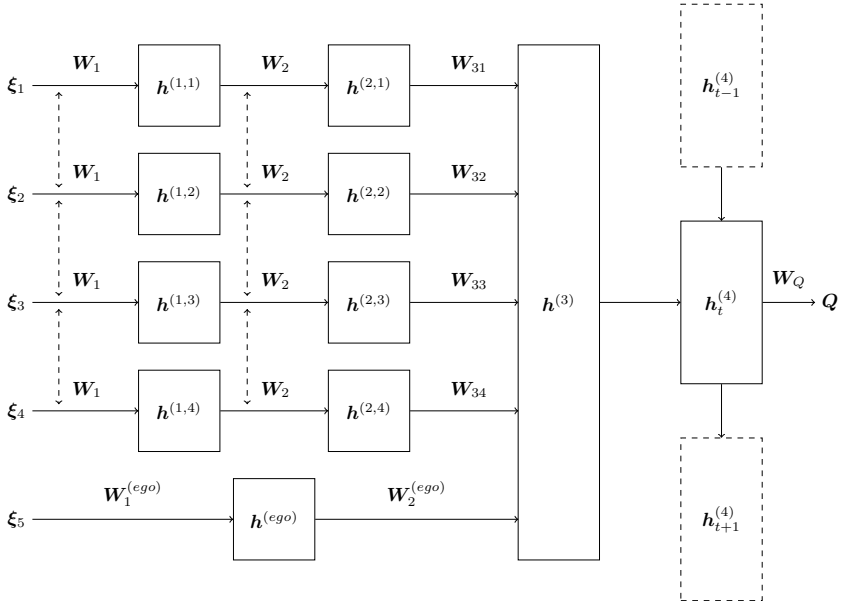


Figure 3: Deep Recurrent Q Network layout with shared weights and a LSTM

- $\xi_3 = [p_t^e \ v_t^e \ a_t^e \ \delta^e \ p_t^3 \ v_t^3 \ a_t^3 \ \delta^3]^T$
- $\xi_4 = [p_t^e \ v_t^e \ a_t^e \ \delta^e \ p_t^4 \ v_t^4 \ a_t^4 \ \delta^4]^T$
- $\xi_5 = [a_{t+1}^{e,1} \ a_{t+1}^{e,2} \ a_{t+1}^{e,3} \ a_{t+1}^{e,4} \ a_{t+1}^{e,5} \ a_{t+1}^{e,6}]^T$

In case a vehicle is not visible, the input vector ξ are set to -1. All vehicle features are scaled to be a value between or close to $[-1, 1]$ by using a car's sight range p_{\max} , maximum speed v_{\max} and maximum acceleration a_{\max} .

The output Q should be independent of which order other vehicles was observed in the input ξ_i . In other words, whether a vehicle was fed into ξ_1 or into ξ_4 , the network should optimally result in the same decision, only based on the features' values. The network is therefore structured such that input features of one car, for instance ξ_1 , are used as input to a sub-network with two layers $\mathbf{h}^{(1,i)}$ and $\mathbf{h}^{(2,i)}$. Each other vehicle has a copy of this sub-network, resulting in them sharing weights (\mathbf{W}_1 and \mathbf{W}_2), as shown in Fig. 3. The first hidden layers are then given by:

$$\mathbf{h}^{(1,i)} = \tanh(\mathbf{W}_1 \boldsymbol{\xi}_i + \mathbf{b}_1) \quad (\text{A.9})$$

$$\mathbf{h}^{(2,i)} = \tanh(\mathbf{W}_2 \mathbf{h}^{(1,i)} + \mathbf{b}_2) \quad (\text{A.10})$$

$$\mathbf{h}^{(ego)} = \tanh(\mathbf{W}_1^{(ego)} \boldsymbol{\xi}_5 + \mathbf{b}^{(ego)}) \quad (\text{A.11})$$

The output of each sub-network, $\mathbf{h}^{(2,i)}$ and $\mathbf{h}^{(ego)}$, is fed as input into a third hidden layer $\mathbf{h}^{(3)}$. The different sub-networks' $\mathbf{h}^{(2,i)}$ outputs are multiplied with different weights $\mathbf{W}_{31}, \dots, \mathbf{W}_{34}$ in order to distinguish different cars for different follow car actions. The ego features are also fed into layer 3 with its own weights $\mathbf{W}_2^{(ego)}$. The neurons in layer $\mathbf{h}^{(3)}$ combine the inputs by adding them together:

$$\mathbf{h}^{(3)} = \tanh\left(\mathbf{W}_2^{(ego)} \mathbf{h}^{(ego)} + \sum_{i=1}^4 \mathbf{W}_{3i} \mathbf{h}^{(2,i)} + \mathbf{b}_3\right) \quad (\text{A.12})$$

The final layer $\mathbf{h}^{(4)}$ uses the LSTM, described in section 5. This layer handles the storage and usage of previous observations, making it the recurrent layer of the network.

$$\mathbf{h}_t^{(4)} = \text{LSTM}\left(\mathbf{h}^{(3)} | \mathbf{h}_{t-1}^{(4)}\right) \quad (\text{A.13})$$

The output of the neural network is then the approximated Q -value:

$$\mathbf{Q} = \mathbf{W}_Q \mathbf{h}^{(4)} + \mathbf{b}_4 \quad (\text{A.14})$$

7 Results

Three metrics were selected for measurement of a training session: success rate, average episodic reward and collision to timeout ratio. With these metrics, the distribution between the three terminating states can be analyzed. Success rate is defined as the success to fail ratio averaged over the last 100 episodes, where both collisions and timeouts are considered as failures. Average episodic reward is the summed reward over a whole episode, then averaged over 100 episodes. The collision to fail ratio displays the ratio between the number of collisions and unsuccessful episodes for the last 100 episodes. From the success rate and collision to fail ratio, a final collision rate is computed, which

is the amount of episodes resulting in a collision, averaged over 100 episodes. The graphs presented are only using evaluation episodes, with a deterministic policy. Every 300 episode, the trained network is evaluated over 300 evaluation episodes.

The improvement of using Dropout and Experience replay, from Section 5, are clearly shown in Fig. 4 and 5. Studying the red curve in Fig. 4, with all methods included, the best policy had a success rate of 99%, average episodic reward 0.8 and collision to timeout ratio at 40%.

7.1 Effect of using Experience replay

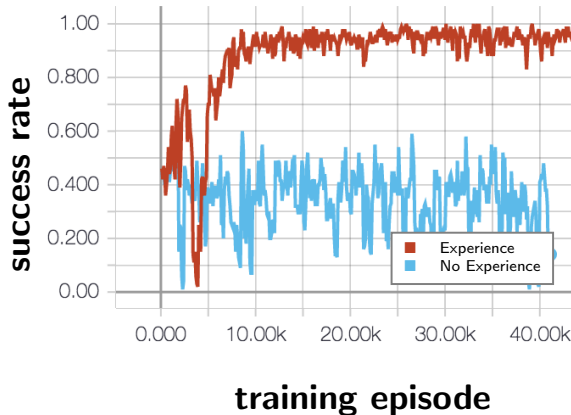


Figure 4: Success rate trend comparing using experience replay (red) and not using experience replay (blue)

Without either method the success rate does not converge to a value higher than 60%. When experience replay was not used, the highest success rate was 53%, average episodic reward -0.1 and collision to timeout ratio at 90%. Compared to not using dropout, not using experience replay has a higher lower variation on the success rate.

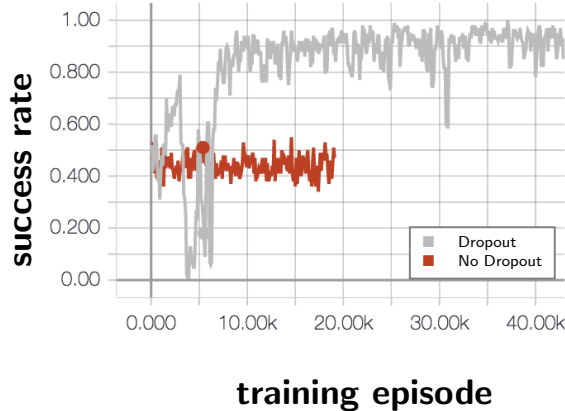


Figure 5: Success rate trend comparing using dropout (grey) and not using dropout (red)

7.2 Effect of using Dropout

In the case of not using Dropout, the best policy had a success rate of 58%, average episodic reward -0.7 and a collision to timeout ratio at 90%.

7.3 Comparing DQN and DRQN

In Fig. 6, we can see the effect off having a recurrent layer by comparing a DQN, without a LSTM layer, and with a DRQN, with LSTM. The faded colored line show actual sampled values and the thick line acts as a trend line which for DRQN converges towards a success rate of around 97.2% and a 0.85% collision rate, compared to a success rate of 87.5% and a collision rate of 1.75% for DQN.

7.4 Effect of sharing weights in the network

When introducing multiple cars in the scenario, the success rate converged considerably slower, as shown in Fig. 7. Using the network structure that share weights between cars, significantly improved how fast the network converged compared to a fully connected DRQN.

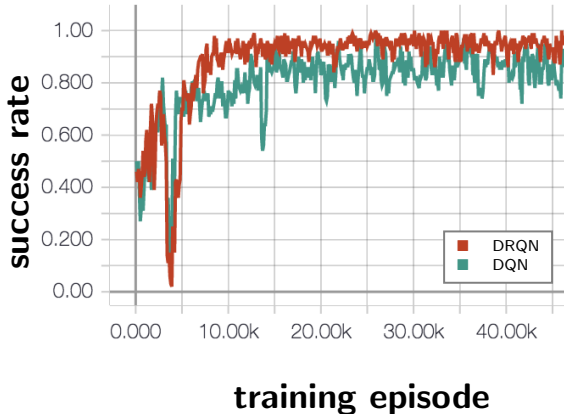


Figure 6: Graphs presenting the performance of a DRQN (red) compared to a DQN with a single observation (green), running on scenarios with cars that have different behaviors. When compared a DRQN succeeds in 3 out of 4 attempts, where a DQN fails.

8 Conclusion

In this paper, Deep Q-Learning was presented in the domain of autonomous vehicle control. The goal of the ego agent is to drive through an intersection, by adjusting longitudinal acceleration using short-term goals. Short-term goals also allowed a smoother and more human-like behavior by controlling the acceleration and comfort with a separate controller. Instead of finding a policy with a continuous control output the problem became a classification problem.

The results also show that trained policies can generalize over different types of driver behaviors. The same policy is able to respond to other vehicles' actions and handle traffic scenarios with a varied number of cars, without knowing traffic rules or the type of intersection it drives in. Multiple observations are needed in order to recognize cars' behaviors, and can be utilized by for instance a DRQN.

There was a significant performance improvement in using a DRQN instead of a DQN with a single observation. In other words, the environment for these scenarios is better modeled as a POMDP instead of an MDP and the agent needs multiple observations in order to draw enough conclusions about other



Figure 7: The figure shows that the success rate for a network with shared weights (brown line) converge faster than the fully connected network structure which do not share weights (turquoise line).

cars' behaviors. Convergence of the neural network was shown to be improved by sharing weights between the first layers to which the target car features are fed, compared to a fully connected neural network structure. The results are still limited to the tested traffic scenarios and driver behaviors, and expanding the domain beyond a simulator is a natural next step. The selected features are also limited to intersections.

The results show a success rate of around 99% for recognizing behaviors. However, the ego vehicle still collides. The ego vehicle is limited to drive comfortably, meaning that in some cases, the ego agent is not allowed to break hard enough. In a complete system, a collision avoidance procedure, which does not have comfort constraints, would need to take over the control to ensure a safe ride. A collision in this paper is defined by two areas overlapping, and in a real world implementation this does not have to mean an actual collision. Instead this could be interpreted as an intervention from a more safety critical system. This way, in the low chances a good action could not be found, the safety of the vehicles can still be guaranteed.

In section 3.2, a sliding mode controller was chosen, but this can be replaced by any controller. One other option could be a Model Predictive Controller, where safer actuation can be achieved by using constraints. Also, the actions in this paper used the same controller tuning for all actions, this does not have to be the case. An action can have the same STG but only differ by the controller’s tuning parameters. This way, the agent gains more flexibility while the comfort can maintain intact, possibly increasing the success rate.

References

- [1] M. Bojarski *et al.*, “End to End Learning for Self-Driving Cars,” 2016.
- [2] M. Liebner, M. Baumann, F. Klanner, and C. Stiller, “Driver intent inference at urban intersections using the intelligent driver model,” in *IEEE Intelligent Vehicles Symposium, Proceedings*, 2012.
- [3] S. Lefevre, C. Laugier, and J. Ibanez-Guzman, “Evaluating risk at road intersections by detecting conflicting intentions,” in *IEEE International Conference on Intelligent Robots and Systems*, 2012.
- [4] S. Shalev-Shwartz, S. Shammah, and A. Shashua, “Safe, multi-agent, reinforcement learning for autonomous driving,” arXiv:1610.03295, 2016.
- [5] S. Brechtel, T. Gindele, and R. Dillmann, “Probabilistic decision-making under uncertainty for autonomous driving using continuous POMDPs,” in *Proceedings of the 17th IEEE International Conference on Intelligent Transportation Systems (ITSC)*, 2014.
- [6] J. J. Moskwa and J. K. Hedrick, “Sliding mode control of automotive engines,” in *American Control Conference (ACC)*, 1989.
- [7] R. Bellman, “A markovian decision process,” English, *Journal of Mathematics and Mechanics*, vol. 6, no. 5, pp. 679–684, 1957.
- [8] V. Mnih *et al.*, “Human-level control through deep reinforcement learning,” *Nature*, vol. 518, no. 7540, pp. 529–533, 2015.
- [9] J. N. Tsitsiklis and B. V. Roy, “An analysis of temporal-difference learning with function approximation,” *IEEE Transactions on Automatic Control*, vol. 42, no. 5, 1997.
- [10] L. J. Lin, “Self-improving reactive agents based on reinforcement learning, planning and teaching,” *Journal of Machine Learning Research*, 1992.

- [11] G. E. Hinton, N. Srivastava, A. Krizhevsky, I. Sutskever, and R. R. Salakhutdinov, “Improving neural networks by preventing co-adaptation of feature detectors,” 2012, ISSN: 9781467394673.
- [12] N. Srivastava, G. Hinton, A. Krizhevsky, I. Sutskever, and R. Salakhutdinov, “Dropout: A simple way to prevent neural networks from overfitting,” *Journal of Machine Learning Research*, vol. 15, pp. 1929–1958, 2014.
- [13] S. Hochreiter and J. Urgen Schmidhuber, “Long short-term memory,” *Neural Computation*, vol. 9, no. 8, pp. 1735–1780, 1997.
- [14] G. Lample and D. S. Chapat, “Playing fps games with deep reinforcement learning,” in *AAAI Conference on Artificial Intelligence (AAAI)*, 2017.
- [15] H. V. Hasselt, A. Guez, M. Hessel, V. Mnih, and D. Silver, “Learning values across many orders of magnitude,” in *Advances in Neural Information Processing Systems (NIPS)*, 2016.

PAPER B

Learning When to Drive in Intersections by Combining Reinforcement Learning and Model Predictive Control

Tommy Tram, Ivo Batković, Mohammad Ali, and Jonas Sjöberg

*Published in 2019 IEEE Intelligent Transportation Systems Conference (ITSC),
pp. 3263–3268, Oct. 2019.
©2019 IEEE DOI: 10.1109/ITSC.2019.8916922.*

The layout has been revised.

Abstract

In this paper, we propose a decision making algorithm intended for automated vehicles that negotiate with other non-automated vehicles in crossings. The decision algorithm is separated into two parts: a high-level decision module based on reinforcement learning, and a low-level planning module based on model predictive control. Traffic is simulated with different predefined driver behaviors and intentions, and evaluate the performance of the proposed decision algorithm and benchmark it against using a sliding mode controller. The results show that the proposed decision algorithm yields faster training times and an increased performance compared to the sliding mode controller.

1 Introduction

Self driving cars is a fast advancing field with Advanced Driver-Assistance Systems becoming a requirement in modern day cars. Decision making for self driving cars can be difficult to solve with simple rule based system in complex scenarios like intersections, while human drivers have a good intuition about when to drive and how to drive comfortably. Sharing the road with other road users requires interaction, which can make rule based decision making complex [1]. Many advancements aim to bring self driving Level 4 to the market by trying to imitate human drivers [2] or predicting what other drivers in traffic are planning to do [3].

Previous research [4] showed that reinforcement learning (RL) can be used to learn a negotiation behavior between cars without vehicle to vehicle communication when driving in an intersection. The method found a policy that learned to drive through an intersection, with crossing traffic, where other vehicles have different intentions and avoided collision. The previous method could use the same algorithm, but trained on different type of intersections and still find a general policy that would get to the other side of the intersection while avoiding collision. By modeling the decision process as a partially observable Markov decision process, uncertainty in the environment or sensing can be accounted for [5] and still be safe [6].

Because the decision policy is separated from the control, high level decision

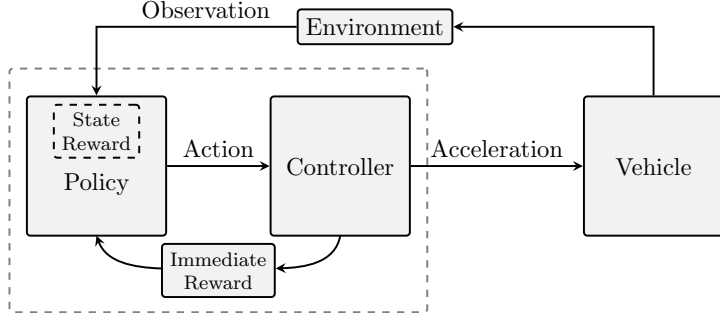


Figure 1: Representation of the decision making architecture

making can focus on the task, when to drive, while the low level control that handles the comfort of passengers in the car by generating a smooth acceleration profile. Previous work showed how this worked for intersections with a single crossing point, where Short Term Goal (STG) actions could choose one car to follow. This gives the RL policy a flexibility to choose actions that can safely transverse through the intersection by switching between different STG.

A simple controller holds well when intersection crossing points are far away from each other, but when there are several crossing points in close succession, a simple controller would have a hard time handling it. In this paper, we instead propose using MPC that can consider multiple vehicles at the same time and generate an optimal trajectory. In contrast to [7], where they prove stability and recursive feasibility using an MPC approach, and assuming that agents can cooperate, we restrict ourselves to non-cooperative scenarios. The MPC is used to plan trajectories around other vehicles using available predictions from other vehicles, and in the worst case, use the prediction as early detection whenever a dangerous situation, e.g., a collision, may appear.

Applying MPC directly to the problem, could lead to a growing complexity with the number of vehicles in the intersection, e.g., which vehicle do we yield for and which vehicle do we drive in front. Therefore, we propose to separate the problem into two parts: the first being a high-level decision maker, which structures the problem, and the second being a low level planner, which optimizes a trajectory given the traffic configuration.

For the high-level decision maker RL is used to generate decisions for how the

vehicle should drive through the intersection, and MPC is used as a low-level planner to optimize a safe trajectory. Compared to [8] where all vehicles are controlled using MPC to stay in a break-safe set based on a model of other vehicles future trajectory, this can be perceived as too conservative for a passenger. By combining RL and MPC, the decision policy will learn which action is optimal by using feedback from the MPC controller into the reward function. Since MPC uses predefined models, e.g. vehicle models and other obstacle prediction models, the performance relies on their accuracy and assumptions. To mitigate this, we use Q-learning, which is a model-free RL approach, to optimize the expected future reward based on its experience during an entire episode which is able to compensate to some extent for model errors, which is explained more in section 5.1.

This paper is structured as follows. Section 2 introduces the system architecture of our framework. The problem formulation, along with the two-layers of the decision algorithm is presented in Section 3. Section 4 present three different used agents for simulation and validation. Implementation details is presented in Section 5 and the results are shown in Section 6 followed by discussion in Section 7. Finally, conclusions and future research are presented in Section 8.

2 System

A full decision architecture system shown in Fig. 1, would include a precautionary safety layer that limits which acceleration values the system can actuate in order to stay safe. Followed by a decisions making system that makes a high level decision for when to drive in order to avoid collision and be comfortable. The policy maker later send that action to a controller that actuates the action turning it into a control signal, e.g., an acceleration request. The environment state, together with the new acceleration request, is sent though a collision avoidance system that checks if the current path has a collision risk, and mitigate if needed. With such a structure, the comfort that is experienced by the passenger is fully controlled by the low-level controller and partially affected by the decision. This paper focuses on the integration between policy and actuation, by having an MPC controller directly giving feedback to the decision maker through immediate actions. This allows the policy to know

how comfortably the controller can handle the action and give feedback sooner if the predicted outcome may be good or bad.

3 Problem formulation

The goal of the ego-vehicle is to drive along a predefined route that has one or two intersections with crossing traffic, where the intent of the other road users is unknown. Therefore, the ego-vehicle needs to assess the driving situation and drive comfortably, while avoiding collisions with any vehicle¹ that may cross. In this section, we define the underlying Partially Observable Markov Decision Process (POMDP) and present how the problem is decomposed using RL for decision making and MPC for planning and control.

3.1 Partially Observable Markov Decision Process

The decision making process is modeled as a Partially Observable Markov Decision Process (POMDP). A POMDP is defined by the 7-tuple $(\mathcal{S}, \mathcal{A}, \mathcal{T}, \mathcal{R}, \Omega, \mathcal{O}, \gamma)$, where \mathcal{S} is the state space, \mathcal{A} an action space that is defined in section 4.1, \mathcal{T} the transition function, \mathcal{R} the reward function $\mathcal{R} : \mathcal{S} \times \mathcal{A} \rightarrow \mathbb{R}$ is defined in 5.4, Ω an observation space, \mathcal{O} the probability of being in state s_t given the observation o_t , and γ the discount factor.

A POMDP is a generalization of the Markov Decision Process (MDP) [9] and therefore works in the same way in most aspects. At each time instant t , an action, $a_t \in \mathcal{A}$, is taken, which will change the environment state s_t to a new state s_{t+1} . Each transition to a state s_t with an action a_t has a reward r_t given by a reward function \mathcal{R} . The Key difference from a regular MDP is that the environment state s_t is not entirely observable because the intention of other vehicles are not known. In order to find the optimal solution for our problem, we need to know the future intention of other drivers. Instead we can only partially perceive the state though observations $o_t \in \Omega$.

3.2 Deep Q-Learning

In the reinforcement learning problem, an agent observes the state s_t of the environment, takes an action a_t , and receives a reward r_t at every time step t .

¹Although our approach can be extended to other road users, for convenience of exposition we'll refer to vehicles.

Through experience, the agent learns a policy π in a way that maximizes the accumulated reward \mathcal{R} in order to find the optimal policy π^* . In Q-learning, the policy is represented by a state action value function $Q(s_t, a_t)$. The optimal policy is given by the action that gives the highest Q-value.

$$\pi^*(s_t) = \arg \max_{a_t} Q^*(s_t, a_t) \quad (\text{B.1})$$

Following the Bellman equation the optimal Q-function $Q^*(s_t, a_t)$ is given by:

$$Q^*(s_t, a_t) = \mathbb{E}[r_t + \gamma \max_{a_{t+1}} Q^*(s_{t+1}, a_{t+1}) | s_t, a_t] \quad (\text{B.2})$$

Because Q-learning is a model-free algorithm and it does not make any assumptions on the environment, even though models are used to simulate the environment, this can be useful when the outcome does not match the prediction models.

4 Agents

This section explains the different agents types. MPC and sliding mode (SM) for the ego vehicle. Observed target vehicles has different intention agents based on SM agent.

4.1 MPC agent

We model the vehicle motion with states $\mathbf{x} \in \mathbb{R}^3$ and control $\mathbf{u} \in \mathbb{R}$, defined as

$$\mathbf{x} := [p^e \ v^e \ a^e]^\top, \quad \mathbf{u} := j^e, \quad (\text{B.3})$$

where we denote the position along the driving path in an Frenet frame as p^e , the velocity as v^e , the acceleration as a^e , and the jerk as j^e , see Fig. 2. In addition, we assume that measurements of other vehicles are provided through an observation \mathbf{o} . We limit the scope of the problem to consider at most four vehicles, and define the observations as

$$\mathbf{o} := [p^1 \ v^1 \ p_{\text{ego}}^{\text{cross},1} \ \dots \ p^4 \ v^4 \ p_{\text{ego}}^{\text{cross},4}]^\top, \quad (\text{B.4})$$

where we denote the position along its path as p , the velocity as v , and $p_{\text{ego}}^{\text{cross},j}$ for $j \in [1, 4]$, as the distance to the ego-vehicle from the intersection point, see Fig. 2.

In this paper, we assume that there exists a lateral controller that stabilizes the vehicle along the driving path. To that end, we only focus on the longitudinal control. Given the state representation, the dynamics of the vehicle is then modeled using a triple integrator with jerk as control input.

The objective of the agent is to safely track a reference, e.g. follow a path with a target speed, acceleration, and jerk profile, while driving comfortably and satisfying constraints that arise from physical limitations and other road users, e.g. not colliding in intersections with crossing vehicles. Hence, we formulate the problem as a finite horizon, constrained optimal control problem

$$J = \min_{\bar{\mathbf{x}}, \bar{\mathbf{u}}} \sum_{k=0}^{N-1} \begin{bmatrix} \bar{\mathbf{x}}_k - \mathbf{r}_k^x \\ \bar{\mathbf{u}}_k - \mathbf{r}_k^u \end{bmatrix}^\top \begin{bmatrix} Q & S^\top \\ S & R \end{bmatrix} \begin{bmatrix} \bar{\mathbf{x}}_k - \mathbf{r}_k^x \\ \bar{\mathbf{u}}_k - \mathbf{r}_k^u \end{bmatrix} \quad (\text{B.5a})$$

$$+ [\bar{\mathbf{x}}_N - \mathbf{r}_N^x]^\top P [\bar{\mathbf{x}}_N - \mathbf{r}_N^x] \quad (\text{B.5b})$$

$$\text{s.t. } \bar{\mathbf{x}}_0 = \hat{\mathbf{x}}_0, \quad (\text{B.5c})$$

$$\bar{\mathbf{x}}_{k+1} = A\bar{\mathbf{x}}_k + B\bar{\mathbf{u}}_k, \quad (\text{B.5d})$$

$$h(\bar{\mathbf{x}}_k, \bar{\mathbf{u}}_k, \bar{\mathbf{o}}_k, a_k) \leq 0, \quad (\text{B.5d})$$

where k is the prediction time index, N is the prediction horizon, Q , R , and S are the stage costs, P is the terminal cost, $\bar{\mathbf{x}}_k$ and $\bar{\mathbf{u}}_k$ are the predicted state and control inputs, \mathbf{r}_k^x and \mathbf{r}_k^u are the state and control input references, $\bar{\mathbf{o}}_k$ denotes the predicted state of vehicles in the environment which need to be avoided, and a is the action from the high-level decision maker. Constraint (B.5b) enforces that the prediction starts at the current state estimate $\hat{\mathbf{x}}_0$, (B.5c) enforces the system dynamics, and (B.5d) enforces constraints on the states, control inputs, and obstacle avoidance.

The reference points, \mathbf{r}_k^x , \mathbf{r}_k^u are assumed to be set-points of a constant velocity trajectory, e.g. following the legal speed-limit on the road. Therefore, we set the velocity reference according to the driving limit, and the acceleration and jerk to zero.

Obstacle prediction

In order for the vehicle planner in (B.5) to be able to properly avoid collisions, it is necessary to provide information about the surrounding vehicles in the environment. Therefore, similarly to [10], we assume that a sensor system

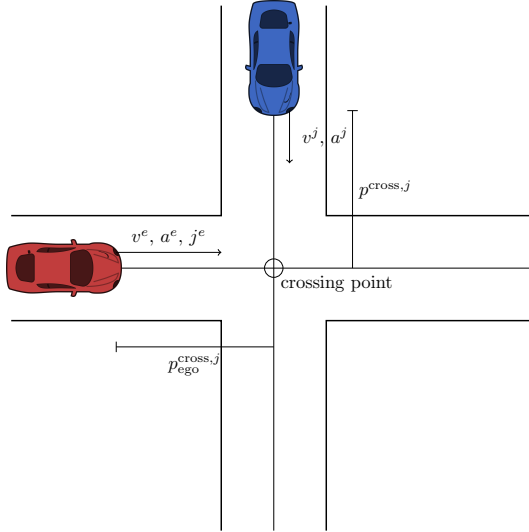


Figure 2: Observations of a scenario

provides information about the environment, and that there exists a prediction layer which generates future motions of other vehicles in the environment. The accuracy of the prediction layer will heavily affect the performance of the planner, hence, it is necessary to have computationally inexpensive and accurate prediction methods.

In this paper, for simplicity the future motion of other agents is estimated by a constant velocity prediction model. The motion is predicted at every time instant for prediction times $k \in [0, N]$, and is used to form the collision avoidance constraints, which we describe in the next section. Even though more accurate prediction methods do exist, e.g. [11], [12], we use this simple model to show the potential of the overall framework.

Collision avoidance

We denote a vehicle j with the following notation $\mathbf{x}^j := [p^j \ v^j \ a^j]^\top$, and an associated crossing point at position $p^{\text{cross},j}$ in its own vehicle frame, which translated into the ego-vehicle frame is denoted as $p_{\text{ego}}^{\text{cross},j}$. With a predefined road topology, we assume that the vehicles will travel along the assigned paths,

and that collisions may only occur at the crossing points $p^{\text{cross},j}$ between an obstacle and the ego vehicle. Hence, for collision avoidance, we use the predictions of the future obstacle states \bar{x}_k^j for times $k \in [0, N]$, provided by a prediction layer outside of the MPC framework. Given the obstacle measurements, the prediction layer will generate future states throughout the prediction horizon. With this information, it is possible to identify the time slots when an obstacle will enter the intersection.

Whenever an obstacle j is predicted to be within a threshold of $p^{\text{cross},j}$, e.g. the width of the intersecting area, the ego vehicle faces a constraint of the following form

$$\bar{p}_k^e \geq p_{\text{ego}}^{\text{cross},j} + \Delta, \quad \underline{p}_k^e \leq p_{\text{ego}}^{\text{cross},j} - \Delta,$$

where Δ ensures sufficient padding from the crossing point that does not cause a collision. The choice of Δ must be at least such that p_k together with the dimensions of the ego-vehicle does not overlap with the intersecting area.

Take way and give way constraint

Since the constraints from the surrounding obstacles become non-convex, we rely on the high-level policy maker to decide through action a how to construct the constraint (B.5d) for Problem (B.5). The take-way action implies that the ego-vehicle drives first through the intersection, i.e., it needs to pass the intersection before all other obstacles. This implies that for any vehicle j that reaches the intersection during prediction times $k \in [0, N]$, the generated constraint needs to lower bound the state p_k according to

$$\max_j p^{\text{cross},j} + \Delta \leq p_k^e. \quad (\text{B.6})$$

Similarly, if the action is to give way, then the position needs to be upper bounded by the closest intersection point so that

$$p_k^e \leq \min_j p_{\text{ego}}^{\text{cross},j} - \Delta, \quad (\text{B.7})$$

for all times k that the obstacle is predicted to be in the intersection.

Following an obstacle

For any action a that results in the following of an obstacle j , the ego-vehicle position is upper bounded by $p_k^e \leq p_{\text{ego}}^{\text{cross},j}$. We construct constraints for obstacles $i \neq j$ according to

- if $p^{\text{cross},i} < p^{\text{cross},j}$ then $p^{\text{cross},i} + \Delta \leq p_k^e$, which implies that the ego-vehicle should drive ahead of all obstacles i that are approaching the intersection;
- if $p^{\text{cross},i} > p^{\text{cross},j}$ then $p_k^e \leq p^{\text{cross},i} - \Delta$, which implies that the ego-vehicle should wait to pass obstacle j and other obstacles i ;
- if $p^{\text{cross},i} = p^{\text{cross},j}$ then the constraints generated for obstacle i becomes an upper or lower bound depending on if obstacle i is ahead or behind the obstacle j into the intersection.

4.2 Sliding mode agent

To benchmark the performance of using MPC, a SM controller that was used in [4] is introduced.

$$a_{\text{sm}}^e = \frac{1}{c_2}(-c_1 x_2 + \mu \text{sign}(\sigma(x_1, x_2))), \quad (\text{B.8a})$$

$$\text{where } \begin{cases} x_1 = p^t - p^e, \\ x_2 = v^t - v^e, \end{cases} \quad (\text{B.8b})$$

$$\sigma = c_1 x_1 + c_2 x_2, \quad (\text{B.8c})$$

$$a_p^e = K(v_{\max} - v^e), \quad (\text{B.8d})$$

$$a^e = \min(a_{\text{sm}}^e, a_p^e). \quad (\text{B.8e})$$

The SM controller aims to keep a minimum distance to a target car with a velocity of v^e , by controlling the acceleration a_{sm}^e . c_1 , c_2 , and μ are tuning parameters to control the comfort of the controller. In case there is no target car, the controller maintains a target velocity v_{\max} with a regular p-controller from (B.8d) with a proportional constant K . The final acceleration is given by (B.8e). For more details about the SM agent see [4].

4.3 Intention agents

There are three different intention agents for crossing traffic with predetermined intentions, three velocity profiles are shown as an example in Fig. 3. All agents were implemented with a SM controller with different target values. The take way intention does not yield for the crossing traffic and simply aim to keep its

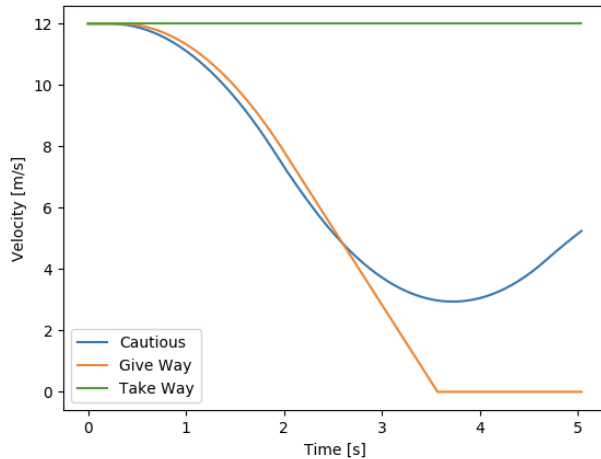


Figure 3: Example of how velocity profile of the different intention agents can look like. All agents has the same starting velocity of 12m/s and are approaching the same intersection

target reference speed. Give way intention however, slow down to a complete stop at the start of the intersection until crossing traffic has passed before continuing through. The third intention is cautious, slowing down but not to a full stop. This makes it difficult for a constant velocity or acceleration model to predict what other agents will do.

5 Implementation

5.1 Deep Q-Network

The deep Q-network is structured as a three layer neural network with shared weights and a Long Short-Term Memory based on previous work [4] and shown in Fig. 4. The input features ξ_n are composed of observations o_t , introduced in section 3.1 and shown in Fig. 2, with up to four observed vehicles:

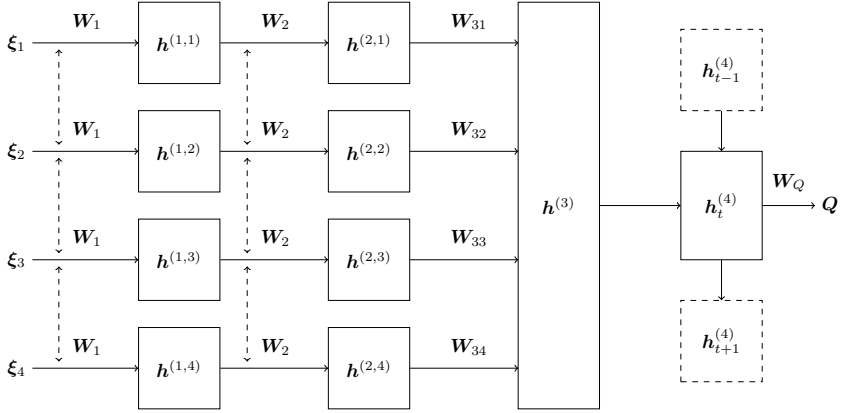


Figure 4: Representation of the network structure

$$\begin{aligned}
 \xi_1 &= [p_t^e \ v_t^e \ a_t^e \ \delta^e \ p_t^1 \ v_t^1 \ a_t^1 \ \delta^1]^T \\
 \xi_2 &= [p_t^e \ v_t^e \ a_t^e \ \delta^e \ p_t^2 \ v_t^2 \ a_t^2 \ \delta^2]^T \\
 \xi_3 &= [p_t^e \ v_t^e \ a_t^e \ \delta^e \ p_t^3 \ v_t^3 \ a_t^3 \ \delta^3]^T \\
 \xi_4 &= [p_t^e \ v_t^e \ a_t^e \ \delta^e \ p_t^4 \ v_t^4 \ a_t^4 \ \delta^4]^T
 \end{aligned} \tag{B.9}$$

Normalization of the input features is done by scaling the features down to values between $[-1, 1]$ using the maximum speed v_{\max} , maximum acceleration a_{\max} and a car's sight range p_{\max} . Empty observation of other vehicles $[p_t^n \ v_t^n \ a_t^n \ \delta^n]$ has a default value of -1 . The input vectors are sent through two hidden layers $\mathbf{h}^{(1,i)}$ and $\mathbf{h}^{(2,i)}$ with shared weights \mathbf{W}_1 and \mathbf{W}_2 respectively

$$\mathbf{h}^{(1,i)} = \tanh(\mathbf{W}_1 \xi_i + \mathbf{b}_1) \tag{B.10}$$

$$\mathbf{h}^{(2,i)} = \tanh(\mathbf{W}_2 \mathbf{h}^{(1,i)} + \mathbf{b}_2). \tag{B.11}$$

A similar study for lane changes on a highway confirmed the importance of having equals weights for inputs that describe the state of interchangeable objects [13]. The output of each sub-network is then sent through a fully connecting layer

$$\mathbf{h}^{(3)} = \tanh \left(\sum_{i=1}^4 \mathbf{W}_{3i} \mathbf{h}^{(2,i)} + \mathbf{b}_3 \right). \tag{B.12}$$

That is then connected to an Long Short-Term Memory (LSTM) [14] that can store and use previous features

$$\mathbf{h}_t^{(4)} = \text{LSTM} \left(\mathbf{h}^{(3)} | \mathbf{h}_{t-1}^{(4)} \right). \quad (\text{B.13})$$

The approximated Q-value is then

$$\mathbf{Q}_{approx} = \mathbf{W}_Q \mathbf{h}^{(4)} + \mathbf{b}_4 \quad (\text{B.14})$$

The Q-value is then masked using Q-masking, explain in section 5.2

$$\mathbf{Q} = \mathbf{Q}_{approx} \mathbf{Q}_{mask} \quad (\text{B.15})$$

the optimal policy π^* is then given by taking the action that gives the highest Q-value

$$\pi^*(s_t) = \arg \max_{a_t} Q^*(s_t, a_t) \quad (\text{B.16})$$

5.2 Q-masking

Q-masking [15] helps the learning process by reducing the actions space by disabling actions the agent does not need to explore. If there are less than N cars, it would then be meaningless to choose to follow a car that does not exist. Which motivates masking off cars that does not exist. In previous work [4], a high negative reward was given when an action to follow a car that did not exist was chosen, while the algorithm continued with a default action take way. The agent quickly learned to not choose cars that did not exist, but with Q-masking, the agent does not even have to explore these options. For other details about the training see [4].

5.3 Simulation environment

All agents are spawned with random initial speed $v_0 \in [10, 30]\text{m/s}$, position $p_0^i \in [10, 55]\text{m}$ and intention. The cars dimensions are 2 m wide and 4 m long. The ego car operates within comfort bounds and therefore has a limited maximum acceleration and deceleration of 5 m/s^2 . Two main types of crossing were investigated. One and two crossing points as shown in Fig. 5, where the distance between crossing points d_{cross} vary between $[4, 8, 12, 25, 30, 40]\text{m}$ with different scenarios.

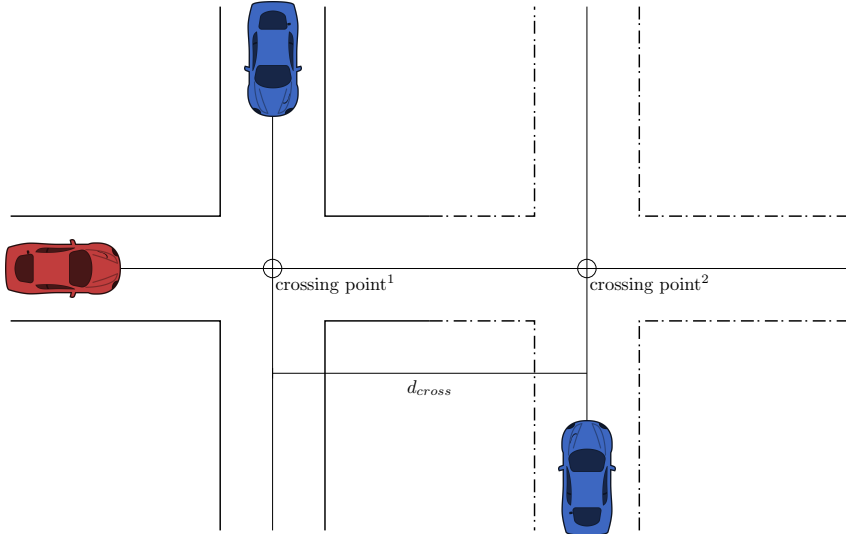


Figure 5: Illustration of a intersection scenario, where the solid line is a single crossing and together with the dashed line creates a double crossing.

The MPC agent was discretized at 30Hz, with a prediction horizon of $N = 100$ and cost tuning of

$$Q = \text{blockdiag}(0.0, 1.0, 1.0), \quad R = 1, \quad S = \mathbf{0}. \quad (\text{B.17})$$

5.4 Reward function tuning

There are three states that terminates an episode; success, failure, and timeout. Success is when the ego agent reaches the of the road defined by the scenario. Failure is when the frame of the ego agent overlaps with another road users frame, e.g., in a collision, this frame can be the size of the vehicle or a safety boundary around a vehicle. The final terminating state is timeout and that is simply when the agent cant reach the two previous terminating states before the timeout time τ_m . According to [16], the Q_π values and gradient can grow to be very large if the total reward values are too large. All rewards are therefore scaled with the episode timeout time τ_m , which is set to 25s, to keep

the total reward $r_t \in [-2, 1]$. The reward function is defined as follows:

$$r_t = \begin{cases} 1 & \text{on success,} \\ -1 & \text{on failure,} \\ 0.5 & \text{on timeout, i.e. } \tau \geq \tau_m, \\ f(p_{\text{crash}}, p_{\text{comf}}) & \text{on non-terminating updates,} \end{cases}$$

where $f(p_{\text{crash}}, p_{\text{comf}})$ consists of

$$f(p_{\text{crash}}, p_{\text{comf}}) = \alpha p_{\text{crash}} \frac{\tau_m}{\tau - t_{\text{pred}}} + \beta p_{\text{comf}} \frac{\tau_m}{\tau}, \quad (\text{B.18})$$

with $\alpha \in [0, 1]$, $\beta \in [0, 1]$ being weight parameters, and $\alpha + \beta = 1$. The first term in the function corresponds to a feasibility check of Problem (B.5), which to a large extent depends on the validity of the accuracy of the prediction layer. The high-level decision from the policy-maker affects how the constraints are constructed, and may turn the control problem infeasible, e.g. if the decided action is to take way, while not being able to pass the intersection before all other obstacles. Therefore, whenever the MPC problem becomes infeasible we set $p_{\text{crash}} = 1$ to indicate that the selected action most likely will result in a collision with the surrounding environment.

The second term p_{comf} relates to the comfort of the planned trajectory, which is estimated by computing and weighting the acceleration and jerk profiles as

$$p_{\text{comf}} = \frac{1}{\sigma N} \left(\sum_{k=0}^{N-1} \bar{a}_k^2 Q^a + \bar{j}_k^2 R^j + a_N^2 Q^a \right),$$

where \bar{a} , and \bar{j} are the acceleration and jerk components of the state and control input respectively, Q^a and R^j are the corresponding weights, and σ is a normalizing factor which ensures that $p_{\text{comf}} \in [0, 1]$. For the simulation we used $Q^a = 1$ and $R^j = 1$.

The timeout reward 0.5 was set to be higher than the average accumulated reward from p_{comf} , so that the total accumulated reward would be positive in case of timeouts. Because p_{crash} usually only triggers close to a potential collision, that is why t_{pred} is set to the first time a crash prediction is triggered. This will scale the negative reward higher in collision episodes.

Table 1: Average success rates and collision to timeout rates.

Controller	Success Rate		Timeout Ratio	
	Single	Double	Single	Double
SM	96.1%	90.9%	72%	93%
MPC	97.3%	95.2%	45%	76%

6 Results

For evaluation we compared the success rate of the decision-policy together with a collision to timeout ratio (CTR). The success rate is defined as the number of times the agent is able cross the intersections without colliding with other obstacles, or exceeding the time limit to cross. Since we define a time-out to be a failure, we use the CTR to separate potential collisions with the agent being too conservative.

Fig. 6 shows a comparison in success rate between the proposed MPC architecture and the previous SM agent for scenarios with only one crossing. In this scenario, the MPC agent converges after 10^4 training episodes, while the previous SM agent converges after $4 \cdot 10^4$ training episodes. In addition, comparing the CTR metric, Fig. 7 shows that the MPC agent has 0.45 CTR while the SM agent has 0.72 CTR. Evidently, it is visible that the MPC is able to leverage future information into its planning horizon in order to achieve faster training, and also avoiding collisions as a result.

We evaluate the performance of the MPC and SM agents for the more difficult double intersection problem, where we vary the distance between the intersection points. Table 1 shows the performance of the MPC and SM agent for both the single and double scenarios. The performance drops for both agents for the double crossing scenario. However, it is visible that the MPC agent suffers less performance degradation compared to the SM agent. The CTR however more than doubles for the MPC agent for the double crossing, while the already high CTR rate for the SM agent increases above rates of 0.9.

7 Discussion

The benefit of being able to use a prediction horizon for the MPC is shown to mostly impact the training time for the traffic scenarios compared to the

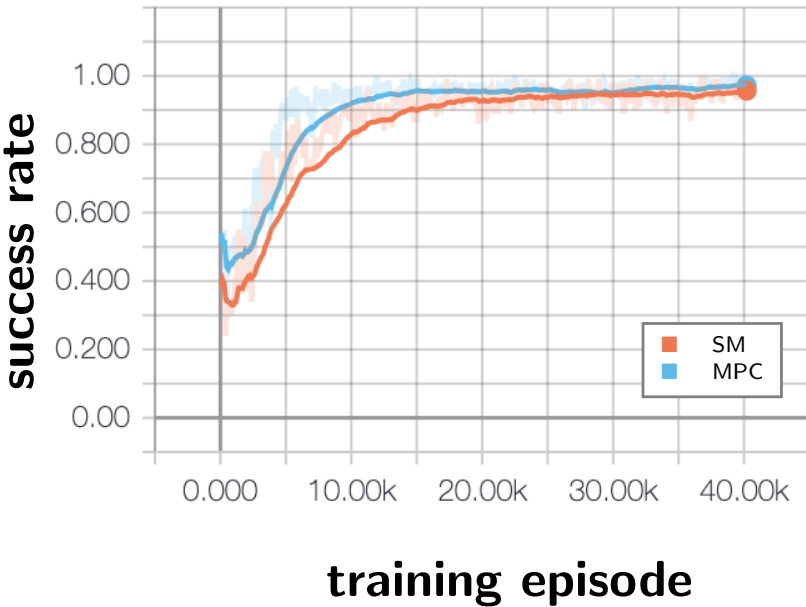


Figure 6: Average MPC and SM success rate for a single crossing after evaluating the policy 300 episodes.

SM agent. This allows the RL decision-policy to get feedback early in the training process to see whether an action most likely will lead to a collision. In addition, the lower CTR also implies that the use of a prediction horizon also makes the decision-policy more conservative, since it rather times out than risk collisions.

It is important to note little effort was put into tuning the MPC agent, and that we used very primitive prediction methods that do not hold very well in crossing scenarios, e.g. the simulated agents did not keep constant speed profiles while approaching the intersections. However, under these circumstances, the decision algorithm still managed to obtain a success rate above 95% for the double crossings.

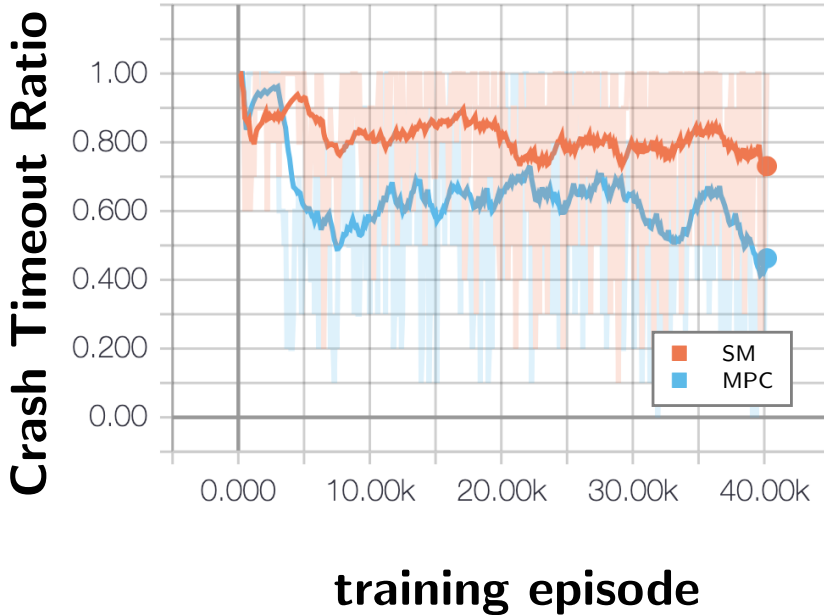


Figure 7: Average MPC and SM crash to timeout ratio for a single crossing after evaluating the policy in 300 episodes. A CTR of 0 means that all failures are timeouts, while a CTR of 1 means that all failures are collisions.

8 Conclusion

In this paper, we proposed a decision making algorithm for intersections which consists of two components: a high-level decision maker that uses Deep Q-learning to generate decisions for how the vehicle should drive through the intersection, and a low-level planner that uses MPC to optimize safe trajectories. We tested the framework in a traffic simulation with randomized intent of other road users for both single and double crossings. Results showed that the proposed MPC agent outperforms the previous SM agent by almost 5% in scenarios with double crossings and in cases of failure, more often timeout than colliding.

References

- [1] M. Liebner, M. Baumann, F. Klanner, and C. Stiller, “Driver intent inference at urban intersections using the intelligent driver model,” in *IEEE Intelligent Vehicles Symposium, Proceedings*, 2012.
- [2] M. Bansal, A. Krizhevsky, and A. Ogale, “ChauffeurNet: Learning to Drive by Imitating the Best and Synthesizing the Worst,” 2018.
- [3] A. Zyner, S. Worrall, J. Ward, and E. Nebot, “Long short term memory for driver intent prediction,” in *IEEE Intelligent Vehicles Symposium, Proceedings*, 2017.
- [4] T. Tram, A. Jansson, R. Grönberg, M. Ali, and J. Sjöberg, “Learning negotiating behavior between cars in intersections using deep Q-learning,” in *IEEE International Conference on Intelligent Transportation Systems (ITSC)*, 2018.
- [5] S. Brechtel, T. Gindele, and R. Dillmann, “Probabilistic decision-making under uncertainty for autonomous driving using continuous POMDPs,” in *Proceedings of the 17th IEEE International Conference on Intelligent Transportation Systems (ITSC)*, 2014.
- [6] M. Bouton, J. Karlsson, A. Nakhaei, K. Fujimura, M. J. Kochenderfer, and J. Tumova, “Reinforcement learning with probabilistic guarantees for autonomous driving,” in *Workshop on Safety Risk and Uncertainty in Reinforcement Learning, Conference on Uncertainty in Artificial Intelligence (UAI)*, 2018.
- [7] R. Hult, M. Zanon, S. Gros, and P. Falcone, “Optimal coordination of automated vehicles at intersections: Theory and experiments,” *IEEE Transactions on Control Systems Technology*, pp. 1–16, 2018.
- [8] X. Qian, J. Gregoire, A. de La Fortelle, and F. Moutarde, “Decentralized model predictive control for smooth coordination of automated vehicles at intersection,” in *European Control Conference (ECC)*, Jul. 2015.
- [9] R. Bellman, “A markovian decision process,” English, *Journal of Mathematics and Mechanics*, vol. 6, no. 5, pp. 679–684, 1957.
- [10] I. Batkovic, M. Zanon, M. Ali, and P. Falcone, “Real-time constrained trajectory planning and vehicle control for proactive autonomous driving with road users,” in *European Control Conference (ECC)*, 2019.

- [11] S. Lefèvre, D. Vasquez, and C. Laugier, “A survey on motion prediction and risk assessment for intelligent vehicles,” *ROBOMECH journal*, vol. 1, no. 1, p. 1, 2014.
- [12] I. Batkovic, M. Zanon, N. Lubbe, and P. Falcone, “A computationally efficient model for pedestrian motion prediction,” in *European Control Conference (ECC)*, Jun. 2018.
- [13] C. J. Hoel, K. Wolff, and L. Laine, “Automated speed and lane change decision making using deep reinforcement learning,” in *IEEE International Conference on Intelligent Transportation Systems (ITSC)*, 2018.
- [14] S. Hochreiter and J. Urgen Schmidhuber, “Long short-term memory,” *Neural Computation*, vol. 9, no. 8, pp. 1735–1780, 1997.
- [15] M. Mukadam, A. Cosgun, A. Nakhaei, and K. Fujimura, “Tactical decision making for lane changing with deep reinforcement learning,” in *NIPS Workshop on Machine Learning for Intelligent Transportation Systems*, 2017.
- [16] H. V. Hasselt, A. Guez, M. Hessel, V. Mnih, and D. Silver, “Learning values across many orders of magnitude,” in *Advances in Neural Information Processing Systems (NIPS)*, 2016.

PAPER C

Reinforcement Learning with Uncertainty Estimation for Tactical Decision-Making in Intersections

Carl-Johan Hoel, Tommy Tram, and Jonas Sjöberg

*Published in 2020 IEEE 23rd International Conference on Intelligent Transportation Systems (ITSC),
pp. 1-7, Sep. 2020.*
©2020 IEEE DOI: 10.1109/ITSC45102.2020.9294407.

The layout has been revised.

Abstract

This paper investigates how a Bayesian reinforcement learning method can be used to create a tactical decision-making agent for autonomous driving in an intersection scenario, where the agent can estimate the confidence of its decisions. An ensemble of neural networks, with additional randomized prior functions (RPF), are trained by using a bootstrapped experience replay memory. The coefficient of variation in the estimated Q -values of the ensemble members is used to approximate the uncertainty, and a criterion that determines if the agent is sufficiently confident to make a particular decision is introduced. The performance of the ensemble RPF method is evaluated in an intersection scenario and compared to a standard Deep Q-Network method, which does not estimate the uncertainty. It is shown that the trained ensemble RPF agent can detect cases with high uncertainty, both in situations that are far from the training distribution, and in situations that seldom occur within the training distribution. This work demonstrates one possible application of such a confidence estimate, by using this information to choose safe actions in unknown situations, which removes all collisions from within the training distribution, and most collisions outside of the distribution.

1 Introduction

To make safe, efficient, and comfortable decisions in intersections is one of the challenges of autonomous driving. A decision-making agent needs to handle a diverse set of intersection types and layouts, interact with other traffic participants, and consider uncertainty in sensor information. The fact that around 40% of all traffic accidents during manual driving occur in intersections indicates that decision-making in intersections is a complex task [1]. To manually predict all situations that can occur and tailor a suitable behavior is not feasible. Therefore, a data-driven approach that can learn to make decisions from experience is a compelling approach. A desired property of such a machine learning approach is that it should also be able to indicate

how confident the resulting agent is about a particular decision.

Reinforcement learning (RL) provides a general approach to solve decision-making problems [2], and could potentially scale to all types of driving situations. Promising results have been achieved in simulation by applying a Deep Q-Network (DQN) agent to intersection scenarios [3], [4], and highway driving [5], [6], or a policy gradient method to a lane merging situation [7]. Some studies have trained an RL agent in a simulated environment and then deployed the agent in a real vehicle [8], [9], and for a limited case, trained the agent directly in a real vehicle [10].

Generally, a fundamental problem with the RL methods in previous work is that the trained agents do not provide any confidence measure of their decisions. For example, if an agent that was trained for a highway driving scenario would be exposed to an intersection situation, it would still output a decision, although it would likely not be a good one. A less extreme example involves an agent that has been trained in an intersection scenario with nominal traffic, and then faces a speeding driver. McAllister et al. further discuss the importance of estimating the uncertainty of decisions in autonomous driving [11].

A common way of estimating uncertainty is through Bayesian probability theory [12]. Bayesian deep learning has previously been used to estimate uncertainty in autonomous driving for image segmentation [10] and end-to-end learning [13]. Dearden et al. introduced Bayesian approaches to RL that balances the trade off between exploration and exploitation [14]. In recent work, this approach has been extended to deep RL, by using an ensemble of neural networks [15]. However, these studies focus on creating an efficient exploration method for RL, and do not provide a confidence measure for the agents' decisions.

This paper investigates an RL method that can estimate the uncertainty of the resulting agent's decisions, applied to decision-making in an intersection scenario. The RL method uses an ensemble of neural networks with randomized prior functions that are trained on a bootstrapped experience replay memory, which gives a distribution of estimated Q -values (Sect. 2). The distribution of Q -values is then used to estimate the uncertainty of the recommended action, and a criterion that determines the confidence level of the agent's decision is introduced (Sect. 2.3). The method is used to train a decision-making agent in different intersection scenarios (Sect. 3), in which the results show that the

introduced method outperforms a DQN agent within the training distribution. The results also show that the ensemble method can detect situations that were not present in the training process, and thereby choose safe fallback actions in such situations (Sect. 4). Further characteristics of the introduced method is discussed in Sect. 5. This work is an extension to a recent paper, where we introduced the mentioned method, but applied to a highway driving scenario [16].

2 Approach

This section gives a brief introduction to RL, describes how the uncertainty of an action can be estimated by an ensemble method, and introduces a measure of confidence for different actions. Further details on how this approach was applied to driving in an intersection scenario follows in Sect. 3.

2.1 Reinforcement learning

Reinforcement learning is a branch of machine learning, where an agents explores an environment and tries to learn a policy $\pi(s)$ that maximizes the future expected return, based on the agent's experiences [2]. The policy determines which action a to take in a given state s . The state of the environment will then transitions to a new state s' and the agent receives a reward r . A Markov Decision Process (MDP) is often used to model the reinforcement learning problem. An MDP is defined by the tuple $(\mathcal{S}, \mathcal{A}, T, R, \gamma)$, where \mathcal{S} is the state space, \mathcal{A} is the action space, T is a state transition model, R is a reward model, and γ is a discount factor. At each time step t , the agent tries to maximize the future discounted return

$$R_t = \sum_{k=0}^{\infty} \gamma^k r_{t+k}. \quad (\text{C.1})$$

In a value-based branch of RL called Q -learning [17], the objective of the agent is to learn the optimal state-action value function $Q^*(s, a)$. This function is defined as the expected return when the agent takes action a from state s and then follow the optimal policy π^* , i.e.,

$$Q^*(s, a) = \max_{\pi} \mathbb{E} [R_t | s_t = s, a_t = a, \pi]. \quad (\text{C.2})$$

The Q -function can be estimated by a neural network with weights θ , i.e., $Q(s, a) \approx Q(s, a; \theta)$. The weights are optimized by minimizing the loss function

$$L(\theta) = \mathbb{E}_M \left[(r + \gamma \max_{a'} Q(s', a'; \theta^-) - Q(s, a; \theta))^2 \right], \quad (\text{C.3})$$

which is derived from the Bellman equation. The loss is obtained from a mini-batch M of training samples, and θ^- represents the weights of a target network that is updated regularly. More details on the DQN algorithm are presented by Mnih et al. [18].

2.2 Bayesian reinforcement learning

One limitation of the DQN algorithm is that only the maximum likelihood estimate of the Q -values is returned. The risk of taking a particular action can be approximated as the variance in the estimated Q -value [19]. One approach to obtain a variance estimation is through statistical bootstrapping [20], which has been applied to the DQN algorithm [21]. The basic idea is to train an ensemble of neural network on different subsets of the available replay memory. The ensemble will then provide a distribution of Q -values, which can be used to estimate the variance. Osband et al. extended the ensemble method by adding a randomized prior function (RPF) to each ensemble member, which gives a better Bayesian posterior [15]. The Q -values of each ensemble member k is then calculated as the sum of two neural networks, f and p , with equal architecture, i.e.,

$$Q_k(s, a) = f(s, a; \theta_k) + \beta p(s, a; \hat{\theta}_k). \quad (\text{C.4})$$

Here, the weights θ_k of network f are trainable, and the weights $\hat{\theta}_k$ of the prior network p are fixed to the randomly initialized values. A parameter β scales the importance of the networks. With the two networks, the loss function in Eq. C.3 becomes

$$\begin{aligned} L(\theta_k) = \mathbb{E}_M & \left[(r + \gamma \max_{a'} (f_{\theta_k^-} + \beta p_{\hat{\theta}_k})(s', a') \right. \\ & \left. - (f_{\theta_k} + \beta p_{\hat{\theta}_k})(s, a))^2 \right]. \end{aligned} \quad (\text{C.5})$$

Algorithm 2 outlines the complete ensemble RPF method, which was used in this work. An ensemble of K trainable and prior neural networks are

Algorithm 2 Ensemble RPF training process

```

1: for  $k \leftarrow 1$  to  $K$  do
2:   Initialize  $\theta_k$  and  $\hat{\theta}_k$  randomly
3:    $m_k \leftarrow \{\}$ 
4:    $i \leftarrow 0$ 
5:   while networks not converged do
6:      $s_i \leftarrow$  initial random state
7:      $\nu \sim \mathcal{U}\{1, K\}$ 
8:     while episode not finished do
9:        $a_i \leftarrow \text{argmax}_a Q_\nu(s_i, a)$ 
10:       $s_{i+1}, r_i \leftarrow \text{STEPENVIRONMENT}(s_i, a_i)$ 
11:      for  $k \leftarrow 1$  to  $K$  do
12:        if  $p \sim \mathcal{U}(0, 1) < p_{\text{add}}$  then
13:           $m_k \leftarrow m_k \cup \{(s_i, a_i, r_i, s_{i+1})\}$ 
14:         $M \leftarrow$  sample mini-batch from  $m_k$ 
15:        update  $\theta_k$  with SGD and loss  $L(\theta_k)$ 
16:       $i \leftarrow i + 1$ 

```

first initialized randomly. Each ensemble member is also assigned a separate experience replay memory buffer m_k (although in a practical implementation, the replay memory can be designed in such a way that it uses negligible more memory than a shared buffer). For each new training episode, a uniformly sampled ensemble member, $\nu \sim \mathcal{U}\{1, K\}$, is used to greedily select the action with the highest Q -value. This procedure handles the exploration vs. exploitation trade-off and corresponds to a form of approximate Thompson sampling. Each new experience $e = (s_i, a_i, r_i, s_{i+1})$ is then added to the separate replay buffers m_k with probability p_{add} . Finally, the trainable weights of each ensemble member are updated by uniformly sample a mini-batch M of experiences and using stochastic gradient descent (SGD) to backpropagate the loss of Eq. C.5.

2.3 Confidence criterion

The agent's uncertainty in choosing different actions can be defined as the coefficient of variation¹ $c_v(s, a)$ of the Q -values of the ensemble members. In

¹Ratio of the standard deviation to the mean.

previous work, we introduced a confidence criterion that disqualifies actions with $c_v(s, a) > c_v^{\text{safe}}$, where c_{safe} is a hard threshold [16]. The value of the threshold should be set so that (s, a) combinations that are contained in the training distribution are accepted, and those which are not will be rejected. This value can be determined by observing values of c_v in testing episodes within the training distribution, see Sect. 4.1 for further details.

When the agent is fully trained (i.e., not during the training phase), the policy chooses actions by maximizing the mean of the Q -values of the ensemble members, with the restriction $c_v(s, a) < c_v^{\text{safe}}$, i.e.,

$$\begin{aligned} \operatorname{argmax}_a \frac{1}{K} \sum_{k=1}^K Q_k(s, a), \\ \text{s.t. } c_v(s, a) < c_v^{\text{safe}}. \end{aligned} \quad (\text{C.6})$$

In a situation where no possible action fulfills the confidence criterion, a fallback action a_{safe} is chosen.

3 Implementation

The ensemble RPF method, which can obtain an uncertainty estimation of different actions, is tested on different intersection scenarios. In this work, the uncertainty information is used to reject unsafe actions and reduce the number of collisions. This section describes how the simulation of the scenarios is set up, how the decision-making problem is formulated as an MDP, the architecture of the neural networks, and the details on how the training is performed.

3.1 Simulation setup

The simulated environment consists of different intersection scenarios, and is based on previous work [22]. For completeness, an overview is presented here. Each episode starts by randomly selecting a single or bi-directional intersection, shown in Fig. 1, and placing the ego vehicle to the left with a random distance $p_e^{c,j}$ to the intersection and a speed of 10 m/s. A random number N of other vehicles are positioned along the top and bottom roads with a random distance $p_o^{c,j}$ to the intersection, and a random desired speed v_d^j . The other vehicles follow the Intelligent Driver Model (IDM) [23], with a set time gap of $t_d^j = 1$ s.

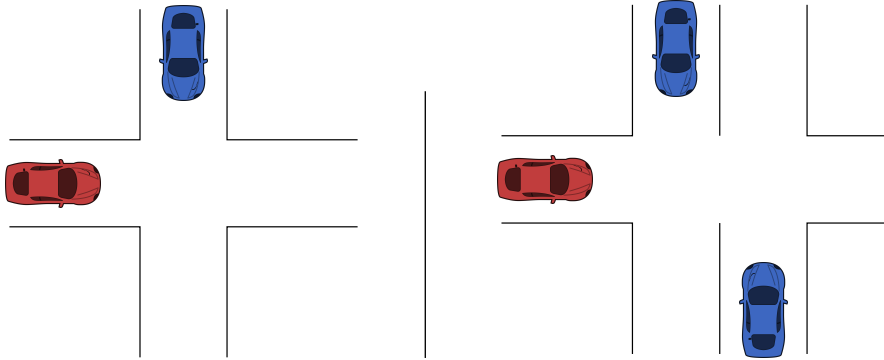


Figure 1: The two intersection scenarios considered in this work; single directional to the left and bidirectional to the right. The agent controls the red car.

Table 1: Parameters for simulator

Number of other vehicles, N	$\{1, 2, 3, 4\}$
Starting position ego, $p_e^{c,j}$	[50, 60] m
Starting position target, $p_o^{c,j}$	[10, 55] m
Desired velocity, v_d^j	[8, 12] m/s

One quarter of the vehicles stop at the intersection and three quarters continue through the intersection, regardless of the behavior of the ego vehicle. When a vehicle has passed the intersection and reached the end of the road, it is moved back to the other side of the intersection, which creates a constant traffic flow. The simulator is updated at 25 Hz, and decisions are taken at 4 Hz. The goal of the ego vehicle is to reach a position that is located 10 m to the right of the last crossing point.

3.2 MDP formulation

The following Markov decision process is used to model the decision-making problem. The full state is not directly observable, since the intentions of the surrounding vehicles are not known to the agent. Therefore, the problem is a Partially Observable Markov Decision Process (POMDP) [24]. However,

by using a k -Markov approximation, where the state consists of the k last observations, the POMDP can be approximated as an MDP [18]. For the scenarios that were considered in this work, it proved sufficient to simply use the last observation.

State space, \mathcal{S}

The design of the state of the system,

$$s = (p_e^g, v_e, a_e, \{p_e^{s,j}, p_e^{c,j}, p_o^{s,j}, p_o^{c,j}, v_o^j, a_o^j\}_{j=0,\dots,N}), \quad (\text{C.7})$$

allows the description of intersections with different layouts [4]. The state, illustrated in Fig. 2, consists of the distance from the ego vehicle to the goal p_e^g , the velocity and acceleration of the ego vehicle, v_e , a_e , and the other vehicles, v_o^j , a_o^j , where j denotes the index of the other vehicles. Furthermore, $p_e^{s,j}$ and $p_e^{c,j}$ are the distances from the ego vehicle to the start of the intersection and crossing point, relative to target vehicle j respectively. The distances $p_o^{s,j}$ and $p_o^{c,j}$ are the distance from the other vehicles to the start of the intersection and the crossing point.

Action space, \mathcal{A}

The action space consists of six tactical decisions: $\{\text{'take way'}, \text{'give way'}, \text{'follow car } \{1, \dots, 4\}\}$, which set the target of the IDM controller. The ‘take way’ action treats the situation as an empty road, whereas the ‘give way’ action sets a target distance of $p_e^{s,j}$ and a target speed of 0 m/s. The ‘follow car j ’ actions sets the target distance to $p_e^{c,j} - p_o^{c,j}$ and target speed to v_o^j . In cases where $p_o^{c,j} > p_e^{c,j}$, the target distance is set to a value that corresponds to timegap 0.5 s. The output of the IDM model is further limited by a maximum jerk $j_{\max} = 5 \text{ m/s}^3$ and maximum acceleration $a_{\max} = 5 \text{ m/s}^2$. If less than four vehicles are present, the actions that correspond to choosing an absent vehicle are pruned by using Q-masking [25].

Reward model, R

The objective of the agent is to reach the goal on the other side of the intersection, without colliding with other vehicles and for comfort reasons, with as little jerk j_t as possible. Therefore, the reward at each time step r_t is

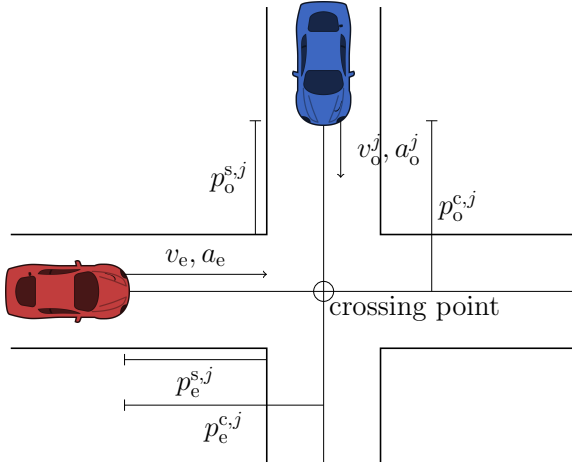


Figure 2: The state space definitions for a single crossing scenario, where subscript e and o denotes ego and other vehicle, respectively.

defined as

$$r_t = \begin{cases} 1 & \text{at reaching the goal,} \\ -1 & \text{at a collision,} \\ -\left(\frac{j_t}{j_{\max}}\right)^2 \frac{\Delta\tau}{\tau_{\max}} & \text{at non-terminating steps.} \end{cases}$$

The non-terminating reward is scaled with the maximum time of an episode, τ_{\max} , and the step time $\Delta\tau = 0.04$ s, to ensure $\sum_{t=0}^{t=\tau_{\max}} \in [-1, 0]$. Further details about the reward function can be found in previous research [22].

Transition model, T

The state transition probabilities are not known to the agent. However, the true transition model is defined by the simulation model, described in Sect. 3.1.

3.3 Fallback action

As mentioned in Sect. 2.3, a fallback action a_{safe} is used when $c_v > c_v^{\text{safe}}$ for all available actions. This fallback action is set to ‘give way’, with the

difference that no jerk limitation is applied and with a higher acceleration limit $a_{\max} = 10 \text{ m/s}^2$.

3.4 Network architecture

In previous studies, we have showed that a network architecture that applies the same weights to the input that describes the surrounding vehicles results in a better performance and speeds up the training process [6], [4]. Such an architecture can be constructed by applying a one-dimensional convolutional neural network (CNN) structure to the surrounding vehicles' input. The network architecture that is used in this work is shown in Fig. 3. The first convolutional layer has 32 filters, with size and stride set to six, which equals the number of state inputs of each surrounding vehicle, and the second convolutional layers has 16 filter, with size and stride set to one. The fully connected (FC) layer that is connected to the ego vehicle input has 16 units, and the joint fully connected layer has 64 units. All layers use rectified linear units (ReLUs) as activation functions, except for the last layer, which has a linear activation function. The final dueling structure of the network separates the estimation of the state value $V(s)$ and the action advantage $A(s, a)$ [26]. The input vector is normalized to the range $[-1, 1]$. The input vector contains slots for four surrounding vehicles, and if less vehicles are present in the traffic scene, the empty input is set to -1 .

3.5 Training process

Algorithm 2 is used to train the agent. The loss function of Double DQN is applied, which subtly modifies the maximization operation of Eq. C.3 to $\gamma Q(s', \text{argmax}_{a'} Q(s', a'; \theta_i); \theta_i^-)$ [27]. The Adam optimizer is used to update the weights [28], and K parallel workers are used for the backpropagation step. The hyperparameters of the training process are shown in Table 2, and the values were selected by an informal search, due to the computational complexity.

If the current policy of the agent decides to stop the ego vehicle, an episode could continue forever. Therefore, a timeout time is set to $\tau_{\max} = 20 \text{ s}$, at which the episode terminates. The last experience of such an episode is not added to the replay memory. This trick prevents the agent to learn that an episode can end due to a timeout, and makes it seem like an episode can

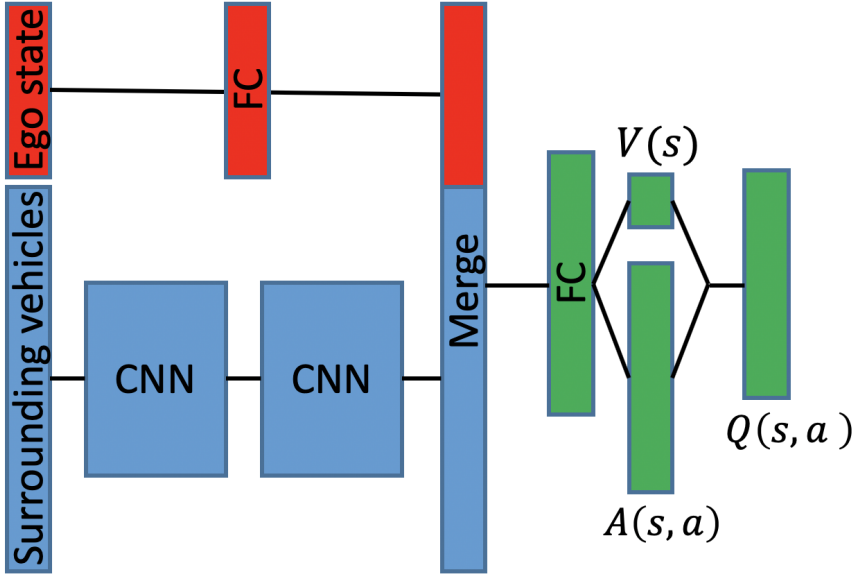


Figure 3: The neural network architecture that was used in this work.

continue forever, which is important, since the terminating state due to the time limit is not part of the MDP [6].

3.6 Baseline method

The Double DQN method, hereafter simply referred to as the DQN method, is used as a baseline. For a fair comparison, the same hyperparameters as for the ensemble RPF method is used, with the addition of an annealing ϵ -greedy exploration schedule, which is shown in Table 2. During test episodes, a greedy policy is used.

4 Results

The results show that the ensemble RPF method outperforms the DQN method, both in terms of training speed and final performance, when the resulting

Table 2: Hyperparameters of Algorithm 2 and baseline DQN.

Number of ensemble members, K	10
Prior scale factor, β	1
Experience adding probability, p_{add}	0.5
Discount factor, γ	0.99
Learning start iteration, N_{start}	50,000
Replay memory size, M_{replay}	500,000
Learning rate, η	0.0005
Mini-batch size, M_{mini}	32
Target network update frequency, N_{update}	20,000
Huber loss threshold, δ	10
Initial exploration constant, ϵ_{start}	1
Final exploration constant, ϵ_{end}	0.05
Final exploration iteration, $N_{\epsilon-\text{end}}$	1,000,000

agents are tested on scenarios that are similar to the training scenarios. When the fully trained ensemble RPF agent is exposed to situations that are outside of the training distribution, the agent indicates a high uncertainty and chooses safe actions, whereas the DQN agent collides with other vehicles. More details on the characteristics of the results are presented and briefly discussed in this section, whereas a more general discussion follows in Sect. 5.

The ensemble RPF and DQN agents were trained in the simulated environment that was described in Sect. 3. After every 50,000 training steps, the performance of the agents were evaluated on 100 random test episodes. These test episodes were randomly generated in the same way as the training episodes, but kept fixed for all the evaluation phases.

4.1 Within training distribution

The average return and the average proportion of episodes where the ego vehicle reached the goal, as a function of number of training steps, is shown in Fig. 4, for the test episodes. The figure also shows the standard deviation

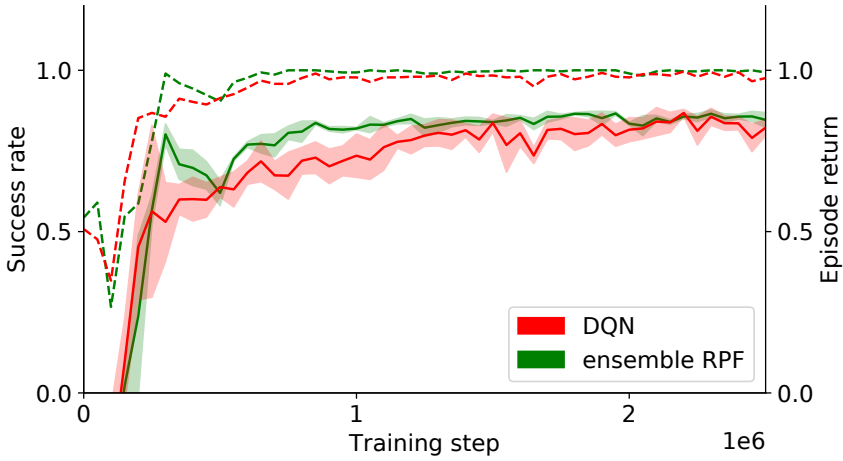


Figure 4: Proportion of test episodes where the ego vehicle reached its goal (dashed), and episode return (solid), over training steps for the ensemble RPF and DQN methods. The shaded areas show the standard deviation for 5 random seeds.

for 5 random seeds, which generates different sets of initial parameters of the networks and different training episodes, whereas the test episodes are kept fixed. The results show that the ensemble RPF method both learns faster, yields a higher return, and causes less collisions than the DQN method.

Fig. 5 shows how the coefficient of variation c_v of the chosen action varies during the testing episodes. Note that the uncertainty of actions that are not chosen can be higher, which is often the case. After around one million training steps, the average value of c_v settles at around 0.04, with a 99 percentile value of 0.15, which motivates the choice of setting $c_v^{\text{safe}} = 0.2$.

As shown in Fig. 4, occasional collisions still occur during the test episodes when deploying the fully trained ensemble RPF agent. The reasons for these collisions are further discussed in Sect. 5. In one particular example of a collision, the agent fails to brake early enough and ends up in an impossible situation, where it collides with another vehicle in the intersection. However, the estimated uncertainty increases significantly during the time before the collision, when the incorrect actions are taken, see Fig. 6. When applying the

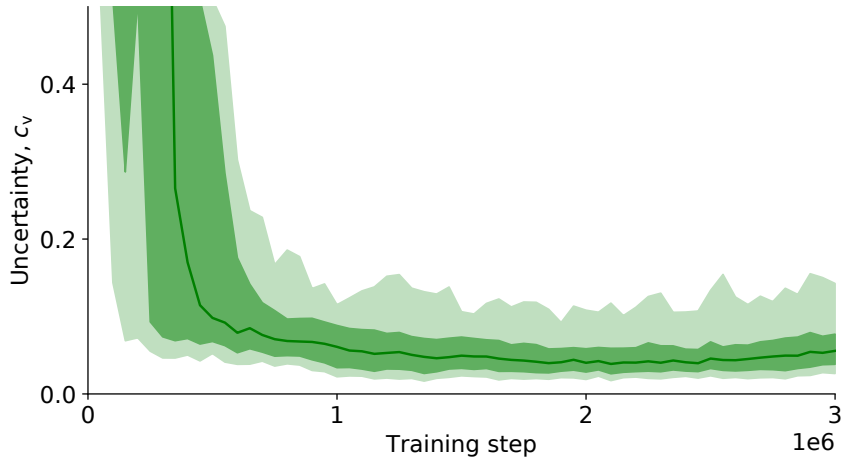


Figure 5: Mean coefficient of variation c_v for the chosen action during the test episodes. The dark shaded area shows percentiles 10 to 90, and the bright shaded area shows percentiles 1 to 99.

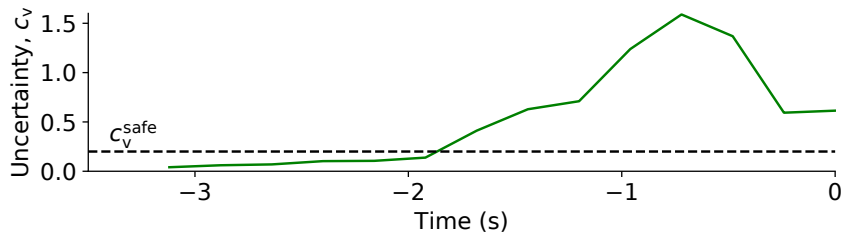


Figure 6: Uncertainty c_v during the time steps before one of the collisions in the test episodes, within the training distribution. The collision occurs at $t = 0$ s.

confidence criterion (Sect. 2.3), the agent instead brakes early enough, and can thereby avoid the collision. The confidence criterion was also applied to all the test episodes, which removed all collisions.

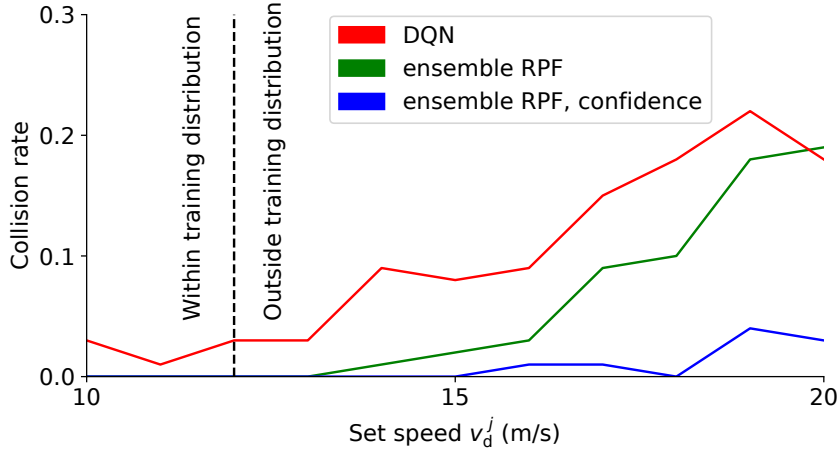
4.2 Outside training distribution

The ensemble RPF agent that was obtained after three million training steps was tested in scenarios outside of the training distribution, in order to evaluate the agent’s ability to detect unseen situations. The same testing scenarios as for within the distribution was used, with the exception that the speed of the surrounding vehicles was set to a single deterministic value, which was varied during different runs in the range $v_d^j = [10, 20]$ m/s. The proportion of collisions as a function of set speed of the surrounding vehicles is shown in Fig. 7, together with the proportion of episodes where the confidence criterion was violated at least once. The figure shows that when the confidence criterion is used, most of the collisions can be avoided. Furthermore, the violations of the criterion increase when the speed of the surrounding vehicles increase, i.e., the scenarios move further from the training distribution.

An example of a situation that causes a collision is shown in Fig. 8, where an approaching vehicle drives with a speed of 20 m/s. The Q -values of both the trained ensemble RPF and DQN agents indicate that the agents expect to make it over the crossing before the other vehicle. However, since the approaching vehicle drives faster than what the agents have seen during the training, a collision occurs. When the confidence criterion is applied, the uncertainty rises to $c_v > c_v^{\text{safe}}$ for all actions when the ego vehicle approaches the critical region, where it has to brake in order to be able to stop, and a collision is avoided by choosing action a_{safe} .

5 Discussion

The results show that the ensemble RPF method can indicate an elevated uncertainty for situations that the agent has been insufficiently trained for, both within and outside of the training distribution. In previous work by the authors of this paper, we observed similar results when using the ensemble RPF method to estimate uncertainty outside of the training distribution in a highway driving scenario [16]. In contrast, this paper shows that, in some cases, the ensemble RPF method can even detect situations with high uncertainty within the training distribution. Such situations include rare events that seldom or never occur during the training process, which makes it hard for the agent to provide an accurate estimate of the Q -values for the corresponding states. Since these states are seldom used to update the neural networks of the



(a) Proportion of collisions.

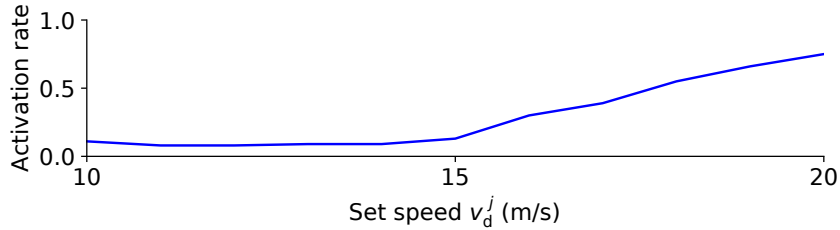
(b) Proportion of episodes where a_{safe} was used at least once.

Figure 7: Performance of the ensemble RPF agent, with and without the confidence criterion, and the DQN agent, in test episodes with different set speeds v_d^j for the surrounding vehicles.

ensemble, the weights of the trainable networks will not adapt to the respective prior networks, and the uncertainty measure c_v will remain high for these rare events. This information is useful to detect edge cases within the training set and indicate when the decision of the trained agent is not fully reliable.

In this work, the estimated uncertainty is used to choose a safe fallback action if the uncertainty exceeds a threshold value. For the cases that are considered here, this confidence criterion removes all collisions within the

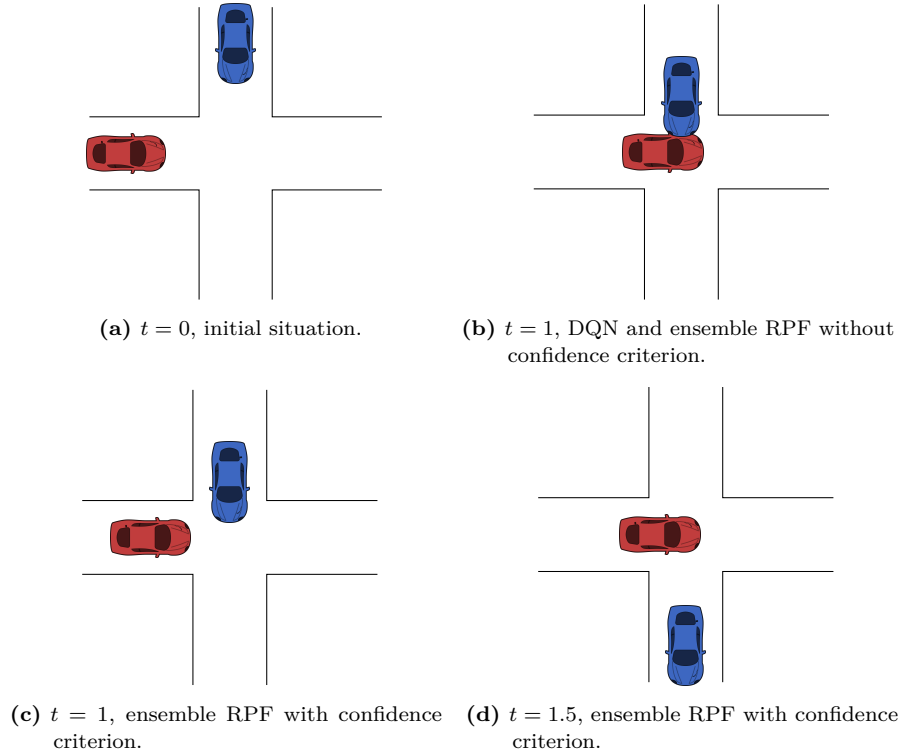


Figure 8: Example of a situation outside of the training distribution, where there would be a collision if the confidence criterion is not used. The vehicle at the top is here approaching the crossing at 20 m/s.

training distribution, and almost all collisions when the speed of the surrounding vehicles is increased to levels outside of the training distribution. However, to guarantee safety by using a learning-based method is challenging, and an underlying safety layer is often used [29]. The presented method could decrease the number of activations of such a safety layer, but possibly more importantly, the uncertainty measure could also be used to guide the training process to focus on situations that the current agent needs to explore further. Moreover, if an agent is trained in simulation and then deployed in real traffic, the uncertainty estimation of the agent could detect situations that should be added to the simulated world, in order to better match real-world driving.

The results show that the ensemble RPF method performs better and more stable than a standard DQN method within the training distribution. The main disadvantage is the increased computational complexity, since K neural networks need to be trained. This disadvantage is somewhat mitigated in practice, since the design of the algorithm allows an efficient parallelization. Furthermore, the tuning complexity of the ensemble RPF and DQN methods are similar. Hyperparameters for the number of ensemble members K and prior scale factor β are introduced, but the parameters that control the exploration of DQN are removed.

6 Conclusion

The results of this paper demonstrates the usefulness of using a Bayesian RL technique for tactical-decision making in an intersection scenario. The ensemble RPF method can be used to estimate the confidence of the recommended actions, and the results show that the trained agent indicates high uncertainty for situations that are outside of the training distribution. Importantly, the method also indicates high uncertainty for rare events within the training distribution. In this work, the confidence information was used to choose a safe action in situations with high uncertainty, which removed all collisions from within the training distribution, and most of the collisions in situations outside of the training distribution.

The uncertainty information could also be used to identify situations that are not known to the agent, and guide the training process accordingly. To investigate this further is a topic for future work. Another subject for future work involves how to set the parameter value c_v^{safe} in a more systematic way, and how to automatically update the value during training.

References

- [1] “Traffic safety facts,” National Highway Traffic Safety Administration, Tech. Rep. DOT HS 812 261, 2014.
- [2] R. S. Sutton and A. G. Barto, *Reinforcement Learning: An Introduction*, 2nd ed. MIT Press, 2018.

- [3] D. Isele, R. Rahimi, A. Cosgun, K. Subramanian, and K. Fujimura, “Navigating occluded intersections with autonomous vehicles using deep reinforcement learning,” in *IEEE International Conference on Robotics and Automation (ICRA)*, 2018.
- [4] T. Tram, A. Jansson, R. Grönberg, M. Ali, and J. Sjöberg, “Learning negotiating behavior between cars in intersections using deep Q-learning,” in *IEEE International Conference on Intelligent Transportation Systems (ITSC)*, 2018.
- [5] P. Wang, C. Chan, and A. d. L. Fortelle, “A reinforcement learning based approach for automated lane change maneuvers,” in *IEEE Intelligent Vehicles Symposium (IV)*, 2018.
- [6] C. J. Hoel, K. Wolff, and L. Laine, “Automated speed and lane change decision making using deep reinforcement learning,” in *IEEE International Conference on Intelligent Transportation Systems (ITSC)*, 2018.
- [7] S. Shalev-Shwartz, S. Shammah, and A. Shashua, “Safe, multi-agent, reinforcement learning for autonomous driving,” arXiv:1610.03295, 2016.
- [8] X. Pan, Y. You, Z. Wang, and C. Lu, “Virtual to real reinforcement learning for autonomous driving,” in *Proc. of the Brit. Machine Vision Conf. (BMVC)*, 2017.
- [9] M. Bansal, A. Krizhevsky, and A. S. Ogale, “ChauffeurNet: Learning to drive by imitating the best and synthesizing the worst,” *Robotics: Science and Systems*, 2019.
- [10] A. Kendall, V. Badrinarayanan, and R. Cipolla, “Bayesian SegNet: Model uncertainty in deep convolutional encoder-decoder architectures for scene understanding,” in *Proc. of the Brit. Machine Vision Conf. (BMVC)*, 2017.
- [11] R. McAllister *et al.*, “Concrete problems for autonomous vehicle safety: Advantages of Bayesian deep learning,” in *International Joint Conference on Artificial Intelligence (IJCAI)*, 2017.
- [12] M. J. Kochenderfer, *Decision Making Under Uncertainty: Theory and Application*. MIT Press, 2015.
- [13] R. Michelmore, M. Kwiatkowska, and Y. Gal, “Evaluating uncertainty quantification in end-to-end autonomous driving control,” *CoRR*, vol. abs/1811.06817, 2018.

- [14] R. Dearden, N. Friedman, and S. Russell, “Bayesian Q-learning,” in *AAAI Conference on Artificial Intelligence (AAAI)*, 1998.
- [15] I. Osband, J. Aslanides, and A. Cassirer, “Randomized prior functions for deep reinforcement learning,” in *Advances in Neural Information Processing Systems (NIPS)*, 2018.
- [16] C.-J. Hoel, K. Wolff, and L. Laine, “Tactical decision-making in autonomous driving by reinforcement learning with uncertainty estimation,” in *IEEE Intelligent Vehicles Symposium (IV)*, 2020.
- [17] C. J. C. H. Watkins and P. Dayan, “Q-learning,” *Machine Learning*, vol. 8, no. 3, pp. 279–292, 1992.
- [18] V. Mnih *et al.*, “Human-level control through deep reinforcement learning,” *Nature*, vol. 518, no. 7540, pp. 529–533, 2015.
- [19] J. García and F. Fernández, “A comprehensive survey on safe reinforcement learning,” *Journal of Machine Learning Research*, vol. 16, no. 42, pp. 1437–1480, 2015.
- [20] B. Efron, *The Jackknife, the Bootstrap and Other Resampling Plans*. Society for Industrial and Applied Mathematics, 1982.
- [21] I. Osband, C. Blundell, A. Pritzel, and B. Van Roy, “Deep exploration via bootstrapped DQN,” in *Advances in Neural Information Processing Systems (NIPS)*, 2016.
- [22] T. Tram, I. Batkovic, M. Ali, and J. Sjöberg, “Learning when to drive in intersections by combining reinforcement learning and model predictive control,” in *IEEE International Conference on Intelligent Transportation Systems (ITSC)*, Oct. 2019.
- [23] M. Treiber, A. Hennecke, and D. Helbing, “Congested traffic states in empirical observations and microscopic simulations,” *Physical Review E*, vol. 62, pp. 1805–1824, 2 2000.
- [24] L. P. Kaelbling, M. L. Littman, and A. R. Cassandra, “Planning and acting in partially observable stochastic domains,” *Artificial Intelligence*, vol. 101, no. 1-2, pp. 99–134, 1998, ISSN: 0004-3702.
- [25] M. Mukadam, A. Cosgun, A. Nakhaei, and K. Fujimura, “Tactical decision making for lane changing with deep reinforcement learning,” in *NIPS Workshop on Machine Learning for Intelligent Transportation Systems*, 2017.

- [26] Z. Wang, T. Schaul, M. Hessel, H. Hasselt, M. Lanctot, and N. Freitas, “Dueling network architectures for deep reinforcement learning,” in *International Conference on Machine Learning (ICML)*, vol. 48, 2016.
- [27] H. van Hasselt, A. Guez, M. Hessel, V. Mnih, and D. Silver, “Learning values across many orders of magnitude,” in *Advances in Neural Information Processing Systems (NIPS)*, 2016.
- [28] D. P. Kingma and J. Ba, “Adam: A method for stochastic optimization,” *International Conference on Learning Representations (ICLR)*, Dec. 2014.
- [29] S. Underwood, D. Bartz, A. Kade, and M. Crawford, “Truck automation: Testing and trusting the virtual driver,” in *Road Veh. Automat. 3*, G. Meyer and S. Beiker, Eds., Springer, 2016, pp. 91–109.

PAPER D

Belief State Reinforcement Learning for Autonomous Vehicles in Intersections

Tommy Tram, Maxime Bouton, Jonas Fredriksson, Jonas Sjöberg, and
Mykel Kochenderfer

Submitted to IEEE Transactions on Intelligent Vehicles,
©2023 IEEE DOI: TBD.

The layout has been revised.

Abstract

This paper investigates different approaches to find a safe and efficient driving strategy through an intersection with other drivers. Because the intentions of the other drivers to yield, stop, or go are not observable, we use a particle filter to maintain a belief state. We study how a reinforcement learning agent can use these representations efficiently during training and evaluation. This paper shows that an agent trained without any consideration of the intentions of others is both slower at reaching the goal and results in more collisions. Four algorithms that use a belief state generated by a particle filter are compared. Two of the algorithms have access to the intention only during training while the others do not. The results show that explicitly trying to predict the intention gave the best performance in terms of safety and efficiency.

1 Introduction

Advancements in autonomous vehicles (AV) technology is expected to create a paradigm shift in how we transport ourselves in the near future and even where we choose to live [1]. However, one of the major concerns is how to tackle the high social demand for traffic safety under various conditions and scenarios. Replacing the human driver with a computer to make all tactical and operational decisions is a difficult task to design. In particular, decision-making in scenarios that require interaction with other road participants, as summarized in a review paper [2].

In recent years, decision-making for AVs in structured scenarios like intersections has attracted a lot of attention in the research society and the automotive industry. A skilled engineer can sometimes solve the decision-making problem for structured traffic scenarios using rule-based methods, e.g., [3] and [4]. Rule-based decision-making is commonly implemented using hierarchical state machines to switch between predefined behaviors, as shown in [3]. However, it can be difficult for an engineer to anticipate every situation and design a suitable strategy that can solve all of them, in particular when drivers are not following the law [5], and statistics from the Insurance Institute for Highway

Safety estimated in 2019 that 143,000 people in the US were injured in red light running crashes and 846 of them were killed [6]. Hence, decision-making for AVs cannot only rely on traffic rules to be safe, but they also need to be prepared when other traffic participants do not follow them. Furthermore, rule-based approaches has difficulty generalizing to unknown situations and deal with uncertainties, such as the uncertainty of whether other traffic participants intend to follow the rules or not.

In order to handle the uncertainty of predicting other traffic participants' behaviors or intentions, the literature formulates the problem of driving under uncertainty as a partially observable Markov decision process (POMDP), e.g., with intentions as a non-observable state. POMDPs can be solved by simulating all possible future motions given different potential behaviors and/or intentions [7], [8], e.g. Monte Carlo tree search (MCTS). Unfortunately, MCTS requires extensive online computation and can be hard to scale in complex traffic situations with an increasing number of traffic participants, especially when a participant's actions are interdependent on all other participants' actions. Learning-based approaches, like reinforcement learning (RL) [9], [10], can help relieve the burden of designing hand-crafted solutions for all possible scenarios and Deep recurrent Q-network (DRQN) approaches, [11], [12], showed some promise solving POMDP with non-observable states by leveraging past observations or actions. One such approach was proposed in our previous work [13], where a decision-making policy that identifies and chooses a gap in-between cars in an intersection scenario by using a deep Q-learning [14] method and an long short-term memory (LSTM) network architecture [15]. The results showed that the policy solved the decision-making problem up to 97% of the time under perfect sensing conditions. The few cases where the AV ended up in collisions occurred when the AV and another vehicle had the same velocity and the same distance to the intersection, i.e., the policy had difficulties sorting out the situation because the estimation of the hidden state (intention) was embedded in the neural network architecture. The prediction of surrounding vehicles was especially difficult for low velocities.

To explicitly estimate the intention of other drivers is not an easy task [16]. Liebner *et al.* [17] proposed to estimate driver behavior using a driver model, the so-called intelligent driver model (IDM) [18], to infer driver intent in urban intersections, and Hoermann *et al.* [19] used a particle filter to estimate the parameters of the IDM, both works showed promising results when evaluated on

real-world data. Another approach to estimating the intention is to introduce belief states to capture uncertainties in the environment [20]. The belief state can be used to model the probability distribution over the uncertain world states, e.g., the intention of other road users. Wang *et al.* [21] decoupled the belief state modeling (via unsupervised learning) from policy optimization (via RL) and claimed that having full observability at learning time, combined with knowing what will not be observable at deployment time, enables an RL agent to learn a policy that is more robust to its unobservable states. Another approach using full observability at learning time is QMDP [22], where a model is first trained on the full state space, including the unobservable states, and later evaluated the model on the belief state. Training on full observability can only be done when the unobservable state can be obtained, e.g., using ground truth data and labeling.

In this paper, we propose a decoupled approach, similar to [21], but model the belief state using a particle filter that is tailor-made for the intersection and use the IDM to model the possible behavior of different intentions similar to [17] and [19]. The policy optimization uses the deep Q-learning approach from [13], but without the LSTM layer. More specifically, we introduce two novel approaches that are safer than their respective baseline by maintaining a belief state using a particle filter and estimating the unobservable states from the belief state before feeding it to the deep Q-network (DQN), which gives the final action. The first approach uses the probability distribution of the intention as input to the DQN and the second approach uses a likelihood estimate with a threshold value for the intention decision to make an estimate of the intention before feeding it to the DQN. The proposed approaches are compared with a naive approach that trains on the entire belief state, a standard approximation method from the literature, QMDP [22], and a DQN with full observability. The latter approach represents an upper bound of what a DQN is capable of if it has perfect sensing and is referred to as the Oracle DQN.

The main contributions of this paper are:

- A decoupled approach that separates belief state modeling, using a particle filter, and policy optimization, using deep Q-learning;
- a tailor-made particle filter implementation with a separate transition model for each intention state;
- representing the intention state as a probability distribution and two

approaches for using the distribution in DQN.

2 Mathematical preliminaries

This section describes the relevant parts of the POMDP framework and the notations used in the problem formulation. It also briefly introduces deep Q-learning, which is used to find the driving policy, and the approximation method QMDP used to handle the unknown intention of the other drivers. Finally, a driving model that describes the behaviors of other drivers is presented. The driver model is later used on multiple occasions in this paper, both as the transition model of all vehicles in the simulation environment and the prediction model in the particle filter.

2.1 Partially observable Markov decision process

A POMDP is a mathematical framework for modeling sequential decision making problems under uncertainty. It is a generalization of the Markov Decision Process (MDP) that satisfies the Markov property, which requires that the probability distribution of the next state only depends on the current state and the action taken by the agent, not the history of states. A POMDP consists of a set of states \mathcal{S} , a set of actions \mathcal{A} , a transition model T , a reward function R , a set of observations Ω , an observation model O , and a discount factor $\gamma \in [0, 1]$. Together they create the tuple $(\mathcal{S}, \mathcal{A}, T, R, \Omega, O, \gamma)$ that formally defines a POMDP [23]. The goal is to find a policy that maximizes the expected return.

In this paper, we denote the driving policy π , i.e., the driving decision, which in a POMDP is formally defined as a mapping from a belief state to an action, where the action corresponds to the decision. The probability of transitioning to a future state s' , given a current state $s \in \mathcal{S}$ and action $a \in \mathcal{A}$, is described by the transition model $T(s' | s, a)$, while the reward r for transitioning to the new state s' is given by the reward function $R(s, a)$. Note that, in the POMDP framework, the agent only has access to partial information contained in its observation o distributed according to $\Pr(o | s', a) = O(o, s', a)$.

To accommodate for the missing information, the agent maintains a belief state. A belief state b is a probability distribution such that

$$b(s) = \Pr(s | o_{1:t}) \tag{D.1}$$

is the probability of being in state s at time t , given observations $o_{1:t} := \{o_1, o_2, \dots, o_t\}$ up to time t . At each time step t , the agent updates its belief using a Bayesian filtering approach given the previous belief and the current observation as follows:

$$b'(s') \propto O(o | s', a) \int_{s \in S} T(s' | s, a) b(s). \quad (\text{D.2})$$

To evaluate different actions a , an action-value function $Q(b, a)$ is used

$$\begin{aligned} Q(b, a)^\pi &= R(b, a) + \\ &\gamma \int_o \max_{a \in \mathcal{A}} \int_s b(s) \int_{s'} O(o | s', a) T(s' | s, a) \alpha(s'). \end{aligned} \quad (\text{D.3})$$

The action-value function $Q(b, a)^\pi$ represents the expected discounted accumulated reward received by following policy π after taking action a from belief state b . The optimal policy π^* can be found by maximizing the reward

$$\pi^*(b) = \operatorname{argmax}_a Q(b, a). \quad (\text{D.4})$$

For real-world problems, finding the optimal policy from a belief state is intractable, especially when the state space is continuous [23]. In this case, the belief state can be represented as a collection of particles, which simply are samples from the state space, and an approximation referred to as QMDP can be used:

$$Q(b, a) \approx \sum_s b(s) Q_{\text{MDP}}(s, a) \quad (\text{D.5})$$

where Q_{MDP} is the optimal value function of the MDP version of the problem that assumes that the agent has full observability.

While finding the optimal $Q^*(b, a)$, in (D.4), may be hard, finding $Q_{\text{MDP}}(s, a)$ is usually easier. When the transition function is explicitly defined and the state space is finite, dynamic programming can be used to compute $Q_{\text{MDP}}(s, a)$. However, the transition function is often only accessible in the form of a generative model (*e.g.* a simulator), and the state space is high-dimensional and continuous. In such settings, deep Q-learning to approximate $Q_{\text{MDP}}(s, a)$ can be used, [22].

In deep Q-learning, the action-value function is represented by a neural network. The function approximating the optimal value function is given by

minimizing the loss function derived from the Bellman equation:

$$J(\theta) = \mathbb{E}_{s'}[(r + \gamma \max_{a'} Q(s', a'; \theta) - Q(s, a; \theta))^2] \quad (\text{D.6})$$

where θ represents the weights of the neural network and (s, a, r, s') is obtained from one simulation step in the environment.

2.2 Behavior model

The general behavior of surrounding vehicles is modeled using IDM. Besides describing the behavior of all vehicles, including the ego vehicle, the IDM is also used in the prediction model of the particle filter. The IDM models a vehicle n 's position and velocity as

$$\dot{p}_n = v_n \quad (\text{D.7})$$

$$\dot{v}_n = a_{\max} \left(1 - \left(\frac{v_n}{v_n^{\text{desired}}} \right)^{\delta} - \left(\frac{d^*(v_n, \Delta v_n)}{d_n} \right)^2 \right) \quad (\text{D.8})$$

$$\text{with } d^*(v_n, \Delta v_n) = d_0 + v_n T_{\text{gap}} + \frac{v_n \Delta v_n}{2\sqrt{a_{\max} \alpha_b}}$$

where v_n^{desired} is the desired velocity, d_0 is the minimum distance between cars, T_{gap} is the desired time gap to the vehicle in front, a_{\max} is the maximum vehicle acceleration, d_n is the distance to the vehicle in front, $\Delta v_n = v_n - v_{n-1}$ is the velocity difference between vehicle n and the vehicle directly in front $n-1$, and α_b and δ are model parameters for comfortable deceleration or acceleration.

The acceleration can be simplified into two terms: an interaction term for when there is a vehicle in front

$$\begin{aligned} a_n^{\text{int}} &= -a_{\max} \left(\frac{d^*(v_n, \Delta v_n)}{d_n} \right)^2 \\ &= -a_{\max} \left(\frac{d_0 + v_n T_{\text{gap}} + \frac{v_n \Delta v_n}{2\sqrt{a_{\max} \alpha_b} d_n}}{d_n} \right)^2 \end{aligned} \quad (\text{D.9})$$

and free road term, when there is no leading vehicle

$$a_n^{\text{free}} = a_{\max} \left(1 - \left(\frac{v_n}{v_n^{\text{desired}}} \right)^{\delta} \right). \quad (\text{D.10})$$

3 Proposed approach

In this section, the intersection problem is modeled as a POMDP, and the particle filter used to estimate the belief state and its uncertainty is introduced. Finally, we present the RL algorithms that are used to train the agent, controlling the ego vehicle.

3.1 POMDP formulation

The problem setting considered in this work is an intersection shown in 1, and here we outline a general overview of the POMDP formulation, whereas 4 specifies the numerical values. The ego vehicle approaches an intersection with at least one other vehicle on the perpendicular lane with about the same time-to-intersection assuming they keep a constant velocity. The goal for the ego vehicle is to reach the other side of the intersection as fast as possible without colliding with the other cars. With only onboard sensors on the ego vehicle, it can observe the physical state of other vehicles but not the drivers' intention.

Such an intersection problem can be described as a POMDP with $(\mathcal{S}, \mathcal{A}, T, R, \Omega, O, \gamma)$ as:

State space, \mathcal{S}

The states of the system,

$$s = (p_{\text{ego}}^{\text{goal}}, p_{\text{ego}}^{\text{int}}, v_{\text{ego}}, t_{\text{stop}}, \{p_n, v_n, \zeta_n\}_{n=1}^N), \quad (\text{D.11})$$

consists of the ego vehicle state and the states of the surrounding vehicles. The ego vehicle state is described by the distance to the intersection $p_{\text{ego}}^{\text{int}}$, the distance to the goal $p_{\text{ego}}^{\text{goal}}$, and the velocity v_{ego} . Stop time t_{stop} is the time the ego vehicle is at a standstill $v_{\text{ego}} = 0$. This state tracks the amount of time the ego vehicle has been standing still at the intersection and how far it is from potentially reaching a terminal state, defined later in 4.1. The states of the surrounding vehicles, indexed by $n \in \{1, \dots, N\}$, are described by the distance to the intersection p_n , the velocity v_n , and the intention ζ_n . The intentions are defined as one-hot vectors and can either be yield, $\zeta_n^{\text{yd}} = [0 \ 1]$, which means that the vehicle will stop before the intersection, or take way, $\zeta_n^{\text{tw}} = [1 \ 0]$, which means that the vehicle will drive through the intersection. These intentions control the behavior of the surrounding vehicles.

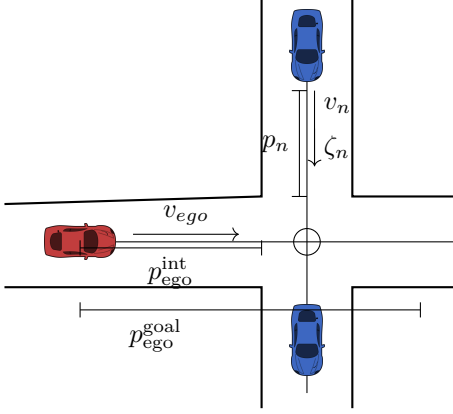


Figure 1: State definitions for the intersection. The red vehicle is the ego vehicle.

Action space, \mathcal{A}

The motion of the ego vehicle is controlled by changing the acceleration according to the IDM (D.8). This is done by two high-level actions *take way* and *yield*. The take way action sets the acceleration of the ego vehicle $a = a^{\text{free}}$ according to (D.10). While the yield action calculate a^{yield} by using (D.9) to slow down and stop at the intersection with $d_n = p_{ego}^{\text{int}}$ and $v_{n-1} = 0$. If there is a car in front, the acceleration becomes $a = \min(a^{\text{int}}, a^{\text{yield}})$.

Transition model, T

The state transition probabilities are defined by the dynamics and intentions of the crossing and ego vehicles. However, the dynamics of crossing vehicles are not known to the ego vehicle. The dynamics in this work are described by the IDM, and implemented as a simulation model defined in 4.1.

Reward function, R

The reward function is designed to encourage safety and time efficiency. The agent's main goal is to reach the other side of the intersection without colliding with other traffic participants. There are one non-terminal state and four terminal states: (i) goal, (ii) safe stop, (iii) collision, and (iv) deadlock. While goal and collision are self-explanatory, safe stop and deadlock are reached when

the agent chooses to stop at the intersection for T_{stop} consecutive seconds. To distinguish whether a stop was efficient, there are two different outcomes. If the other vehicles are at standstill and waiting for the ego vehicle, deadlock is reached, while a safe stop is reached if all other vehicles are in motion. All states other than the terminal state give a small negative reward to incentivize reaching a terminal state as quickly as possible.

Observation space, Ω

An observation o consists of the ego vehicle's state and the physical state of the surrounding vehicles, (p_n, v_n) , while the intentions of the surrounding vehicles ζ_n are not observed. An observation is described by

$$o = (p_{\text{ego}}^{\text{goal}}, p_{\text{ego}}^{\text{int}}, v_{\text{ego}}, t_{\text{stop}}, \{\hat{p}_n, \hat{v}_n\}_{n=1}^N). \quad (\text{D.12})$$

where the $\hat{\cdot}$ notation represents the observed states with noise.

Observation model, O

The ego vehicle observes its own states without noise, while it observes noisy measurements of the positions and speeds of the surrounding vehicles

$$\hat{p}_n = p_n + \epsilon_p, \quad (\text{D.13})$$

$$\hat{v}_n = v_n + \epsilon_v \quad (\text{D.14})$$

where, $\epsilon_p \sim \mathcal{N}(0, \sigma_p^2)$ and $\epsilon_v \sim \mathcal{N}(0, \sigma_v^2)$.

3.2 Belief state representation using a particle filter

This section describes how the belief state is estimated using a particle filter. The algorithm is described, along with the assumptions made on the interaction behaviors of the other vehicles in the intersection scenario. When the state space is continuous and not well approximated by a linear Gaussian model, as it is in (D.11), a sampling-based approach can be used to perform belief updates, where the belief state is represented as a collection of particles with weights [23].

The key idea is to initialize a set of particles with a uniform distribution of intention states ζ . Then, predict the future state of these particles, using a prediction model depending on ζ (D.9, D.10). Finally, sample a new set

Algorithm 3 Initialize particle state for new car

Input: $(\hat{p}_n, \hat{v}_n) \in o$
Output: $\{x_{n[m]}, w_{n[m]}\}_{m=1}^M$

- 1: **for** $m = 1, \dots, M$ **do**
- 2: $p_{n[m]} \sim \mathcal{N}(\hat{p}_n, \sigma_p^2)$,
- 3: $v_{n[m]} \sim \mathcal{N}(\hat{v}_n, \sigma_v^2)$,
- 4: $\zeta_{n[m]} \leftarrow \begin{cases} \zeta_{\text{tw}}, & \text{if } m \leq M/2 \\ \zeta_{\text{yd}}, & \text{otherwise} \end{cases}$
- 5: $x_{n[m]} = (\tilde{p}_{n[m]}, \tilde{v}_{n[m]}, \tilde{\zeta}_{n[m]})$,
- 6: $w_{n[m]} = 1/M$

of particles using the observation and the predicted states. The new set of particles will then have a better distribution of intentions.

Let s_n be the three-dimensional state, (p_n, v_n, ζ_n) , of an observed car n from the state space in (D.11). Then one particle $x_{n[m]} = (p_{n[m]}, v_{n[m]}, \zeta_{n[m]})$ represents one *belief* of s_n , i.e., one sample of the estimated distribution, where $p_{n[m]}$ is the particle position, $v_{n[m]}$ the particle velocity, $\zeta_{n[m]}$ the particle intention and m the particle index out to the M total number of particles.

When a car is observed for the first time, the particle position $p_{n[m]}$ and velocity $v_{n[m]}$ state are sampled around the first observation $o_n = (\hat{p}_n, \hat{v}_n)$ with variance σ_p^2 and σ_v^2 . The particle intention states are initialized with 50% yield and 50% take way with the same particle weight $w_{n[m]}$. The initialization of the particles for a new car is summarized in 3. The particles for each car are then combined into a joint particle state

$$x_m = \{x_{1[m]}, \dots, x_{N[m]}\} \quad (\text{D.15})$$

and as the observation on ego vehicle $s_{\text{ego}} = (p_{\text{ego}}^{\text{goal}}, p_{\text{ego}}^{\text{int}}, v_{\text{ego}}, t_{\text{stop}})$ has no noise, the belief state $b(s)$ then becomes

$$b(s) = (s_{\text{ego}}, \{x_m\}_{m=1}^M). \quad (\text{D.16})$$

The order of cars is set to $n = 1, \dots, N$, and the motion of each car n is assumed to depend on the car directly in front $n - 1$ and independent of all other cars, allowing us to factor the joint distribution transition model as:

$$\Pr(s'_{1:N} | s_{1:N}) = \Pr(s'_1 | s_1) \prod_{n=2}^N \Pr(s'_n | s_n, s_{n-1}). \quad (\text{D.17})$$

In addition, the observations of each vehicle $o_n = (\hat{p}_n, \hat{v}_n)$ are assumed to only depend on its own true state s_n and independent of the states of the other cars. Then the joint observation distribution is:

$$\Pr(o_{1:N} | s_{1:N}) = \prod_{n=1}^N \Pr(o_n | s_n). \quad (\text{D.18})$$

Given these two assumptions, we can define the full particle filter procedure for updating the joint particle state.

At each update step, the standard particle filter operations of prediction and measurement updates are performed with a few modifications. For each particle, x_m , simulate one step forward using the transition model defined in (D.9) or (D.10) depending on the particle intention state $\zeta_{n[m]}$. Noise is added to the particle state to help prevent particle depletion. This is done in two ways. First, the intention of each particle has a slight probability ξ_i to change its intention state. Second, acceleration noise σ_a is added to the prediction model. The observation weights $w_{n[m]}$ for each individual particle are generated using a Gaussian sensor model for the position and velocity, as the observation noise is assumed to be normally distributed, according to (D.13) and (D.14). The weight of a joint particle w_m is then given by multiplying each of the individual vehicle weights $w_{n[m]}$ as described in D.18. The weights w are then normalized and together with the particle set $x' = \{x'_m\}_{m=1}^M$, a new set of particles is resampled, using sequential importance resampling [25]. The new set of joint particles x'_m are then used to represent the belief state b according to (D.16). The full particle update process is summarized in 4.

3.3 Belief state reinforcement learning algorithms

Building upon the belief state $b(s)$ introduced in the previous chapter, our goal is to get an optimal policy π^* according to (D.4) by training a DQN using this belief. This section describes our two proposed approaches, QID (intention distribution) and QMDP-IE (intention estimation). The proposed approaches are compared with both a naive approach, henceforth referred to as QPF, and an established approximation approach QMDP [22]. To compare the different approaches fairly, a common DQN architecture is used for all four. The DQN uses a combination of improvement suggestions from [26], e.g., double DQN [27] and experience replay [28], but from here on out is referred

to DQN for simplicity. The DQN used in this work is inspired by the network architecture from our previous work [29], shown in 2.

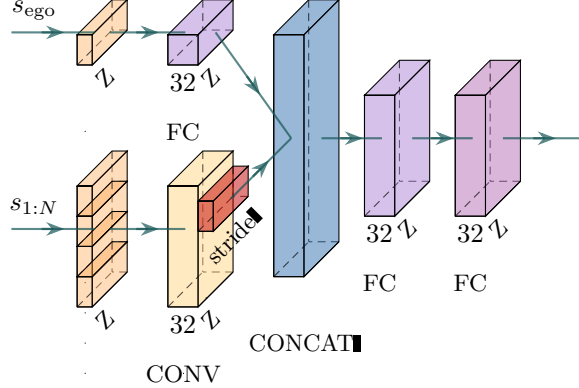


Figure 2: Common network architecture, where ego input s_{ego} represents the input features for the ego vehicle, and input of all other vehicles $s_{1:N}$. The layers consist of one convolution (Conv), three fully connected (FC), and one concatenation (CONCAT) layer. Finally, the depth of the layers Z represents the belief size. The network illustrations in this work are generated using [30]

Firstly, the naive approach, QPF, is trained on the entire belief state b , as shown in 3. The observation o , is divided into the ego state $s_{\text{ego}} = (p_{\text{ego}}^{\text{goal}}, p_{\text{ego}}^{\text{int}}, v_{\text{ego}}, t_{\text{stop}})$ and the observation of the other vehicles $o_{1:N} = \{\hat{p}_n, \hat{v}_n\}_{n=1}^N$. The observation of the other vehicles $o_{1:N}$ is sent to the particle filter to update the belief state b and we get the updated particles x according to 4. Both s_{ego} and x are sent to the DQN, where the number of particles M determines the depth Z of the DQN, which in turn increases the number of weights as a function of Z . The output of the DQN is then sent to a dimension-reducing layer, by calculating the mean value for each action and in turn outputs a single Q vector, denoted as Q_{PF} . As mentioned in the introduction, one challenge with this approach is that the number of particles representing the belief can be very large and this in turn requires more weights which leads to problems for training to converge.

This leads us to our first proposed approach, QID, shown in 4. To reduce

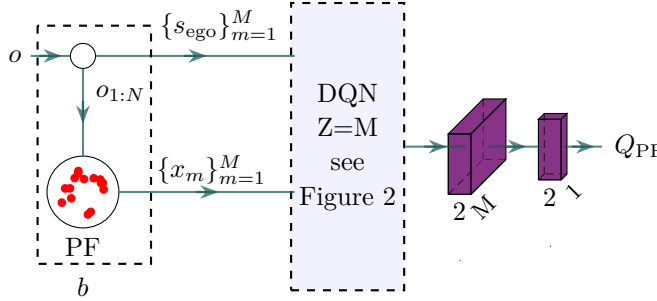


Figure 3: Block diagram of the QPF algorithm. The belief state b (D.16) consists of the observation o and the particles $\{x_m\}_{m=1}^M$ from the particle filer. From the belief state, the ego state s_{ego} is extracted separately from the state of the other vehicles $s_{1:N} = \{x_m\}_{m=1}^M$ for all cars $1 : N$ and feed to the DQN, where the depth of the DQN is given by the number of particles M . After the DQN is a depth-reducing layer that reduces the depth M to 1.

the input dimensions Z compared to QPF, we propose that the non-observable intention state ζ_n^{ID} is derived from the belief state using an approximator $D(b)$, while the observable states \hat{p}_n and \hat{v}_n are fed directly to the DQN. By doing this, the required depth of the DQN can be reduced to 1 and is no longer dependent on the number of particles M . For this method, $\tilde{\zeta}_n^{\text{ID}}$ is simply the marginal distribution of intention from the set of particles $\{x_m\}_{m=1}^M$:

$$D^{\text{ID}}(b) = \zeta_n^{\text{ID}} = \sum_{m=1}^M w_{n[m]} [\zeta_{\text{tw}} \ \zeta_{\text{yd}}]_{n[m]}, \quad (\text{D.19})$$

where $w_{n[m]}$ is the weight of the particle m and $[\zeta_{\text{tw}}, \zeta_{\text{yd}}]$ is the one-hot vector specifying intention.

Another way to reduce the depth of the DQN and still consider the uncertainty of non-observable states is the approximation method QMDP [22]. Where the weights θ_{MDP} are trained in an environment with full observability. This can be used when the non-observable states can be identified offline e.g., using ground truth labeling. During evaluation time, each particle represents one belief state $b_m = \{s_{\text{ego}}, \{x_{n[m]}\}_{n=1}^N\}$ and is evaluated using θ_{MDP} and the

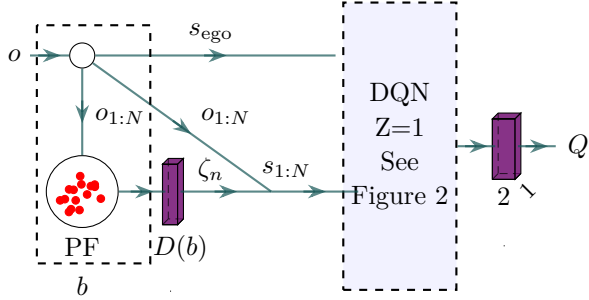


Figure 4: Our proposed approaches, QID and QMDP-IE. From an observation o , the observable states s_{ego} and $o_{1:N} = \{\hat{p}_n, \hat{v}_n\}_{n=1}^N$ are fed directly to the network. While an approximator $D(b)$ approximates the non-observable intention state ζ_n , so that $s_{1:N} = \{\hat{p}_n, \hat{v}_n, \zeta_n\}_{n=1}^N$.

approximated Q-value of the entire belief state is given by D.5

$$Q(b, a) \approx \frac{1}{M} \sum_m Q_{\text{MDP}}(b_m, a; \theta_{\text{MDP}}). \quad (\text{D.20})$$

While QMDP reduces the required depth of the network, all M particles are still processed through the network and require M number of operations more than QID. This leads us to our final proposed approach, QMDP-IE. If we had access to θ_{MDP} , instead of averaging the Q-values of all the particles, a threshold $\zeta_{\text{threshold}}$ is set on the intention distribution from the particle filter and then use it as the true intention state. Similar to QID, the particle filter is only used to generate the intention and is represented as a one-hot vector

$$D^{\text{IE}}(b) = \hat{\zeta}_n^{\text{IE}} = \begin{cases} [0 \ 1] & \text{if } \tilde{\zeta}_n^{\text{yd}} > \zeta_{\text{threshold}}, \\ [1 \ 0] & \text{otherwise,} \end{cases} \quad (\text{D.21})$$

where $\zeta_{\text{threshold}}$ is a design parameter that can be adjusted offline without any retraining of the DQN and directly correlates with the aggressiveness of the policy, e.g., a high value on $\zeta_{\text{threshold}}$ makes the agent more passive.

All four approaches are shown in 1 and the weights θ_{PF} , θ_{ID} and θ_{MDP} are obtained using double deep Q-learning [27], described in 5, where step 10 is

	Particles b	State Approximation $D(b)$
Training weights θ	QPF, θ_{PF}	QID , θ_{ID}
Weights θ_{MDP} from ground truth	$QMDP, \theta_{MDP}$	QMDP-IE , θ_{MDP}

Table 1: The difference between the **investigated algorithms**, while the other two are used as benchmarks. The columns show the algorithm’s input to the neural network, where the first column contains the *baseline algorithms* that use the belief state b with all M particles and the second column contains algorithms that use an estimate of the intention. The first row shows the algorithms that train the weights with the given input and the second row shows algorithms that use weights trained on full observability.

different between the algorithms. Step 12 is the simulator described in the next section while step 13 is the particle filter update described in 4. \mathcal{D} in step 14 – 15, is an experience replay buffer that makes the convergence of DQN more robust [31]. The loss function in step 16 modifies (D.6) to

$$J(\theta, \theta^-) = \mathbb{E}_{\alpha}[(r + \gamma Q(s, \text{argmax } Q(s, a; \theta); \theta^-))], \quad (\text{D.22})$$

where θ^- is the weight of the target network.

All algorithms are trained and evaluated on the same simulator and are described in the next section.

4 Experiments

The main goal of the experiments is to show the performance difference between the algorithms described in the previous chapter. In this section, we present the experiment setup in three parts. First, we describe how the simulator generates the different traffic scenarios. Second, the design of the reward function with some motivation to its values is described. Finally, we define the common network architecture, shown in Figure 2.

4.1 Simulator setup

Starting with the simulator, at the start of each episode, up to N vehicles are spawned with some initial values. The number of vehicles simultaneously in the other lane is the same thing as the traffic density of the lane. The initial positions p_n^0 are distributed along the intersecting lane with the furthest distance from the intersection being p_{lim} , a starting velocity v_n^0 , and a desired velocity v_n^{desired} . Each vehicle is spawned with a deterministic policy that represents its intention ζ_n , which can either be ζ_n^{tw} *take way* or ζ_n^{yd} *yield*. These intentions follow the same transition model as the actions described in 3.1 for the ego vehicle and the time between simulation steps is dt_{decision} seconds. The ego vehicle is spawned last with an initial speed v_{ego} and desired speed $v_{\text{ego}}^{\text{desired}}$, i.e., v_n^{desired} from (D.8).

Every time a vehicle in the perpendicular lane crosses the intersection, they are removed and a new vehicle is spawned at the start of the lane at a random time with new initial values $p_n^0, v_n^0, v_n^{\text{desired}}$ and intention ζ_n .

As mentioned in the introduction, the scenario from our previous work [29] that had the most difficulty solving was a *conflict scenario*, i.e., when another vehicle in the crossing lane has the same velocity and the same distance to the intersection. To create these conflict scenarios, the starting position of ego p_{ego}^0 is set based on the time to intersection τ_{tti} of one of the other vehicles. This "other car" is referred to as the conflict car and is randomly chosen. This increases the probability that the ego will be in conflict with at least one other car.

Each episode is simulated until a terminal state, (i) goal, (ii) collision, (iii) safe stop, (iv) or deadlock, and a reward is given according to the reward function.

4.2 Designing the reward function

The reward function R is part of the POMDP defined in 3.1 and the reward for each terminal state determines the behavior of the optimal policy π^* from (D.4). According to [32], large reward values would result in large Q-values, which can cause the gradients to grow. With some trial and error, the rewards

for each terminal state for this POMDP are defined as

$$r = \begin{cases} 8 & \text{reaching the goal,} \\ -10 & \text{collision,} \\ 0.4 & \text{safe stop,} \\ -0.6 & \text{deadlock,} \\ -0.01 & \text{non-terminal states.} \end{cases}$$

To get a policy that can cross the intersection when possible, a high reward of $r = 8$ is received whenever the agent reaches the goal. A high negative reward of $r = -10$ is received when the agent collides with another car to ensure that it avoids collisions.

When the agent instead chooses to yield and stop for longer than T_{stop} seconds, the received reward depends on what the other vehicle did. While the agent has stopped and the cars on the intersecting lane are crossing the intersection, the agent has made a safe stop and receives the reward $r = 0.4$. To disincentivize deadlock situations, where two cars are waiting for each other, a small negative reward is received $r = -0.6$.

Finally, to incentivize the agent to quickly reach a terminal state, a small negative reward is given for each decision step when the agent has not reached a terminal state combined with the discount factor γ .

5 Results / Results and discussion

This section presents the evaluation metrics and results from the experiments, described in 4.1. Each algorithm is evaluated on 2000 episodes. The metrics of interest are the average time it takes for the agent to reach the success state and how often each terminal state is reached. A success state refers to either reaching the goal or a safe stop. An ideal agent would cause no collisions or deadlocks, and pass the junction with the smallest possible success time.

Another way to describe the algorithms' performance is by using aggressive and passive, which are not completely complementary to each other. An agent is considered aggressive if it has a low success time but a higher collision percentage, when compared to the Oracle DQN. An agent that does not collide often but instead ends up in deadlock more often is considered passive. So an agent that has low success time and high no collisions is neither aggressive nor

passive, just a good agent. We start with analyzing how well a DQN agent that does not consider intentions, performs in scenarios with different traffic densities.

5.1 Traffic density experiment

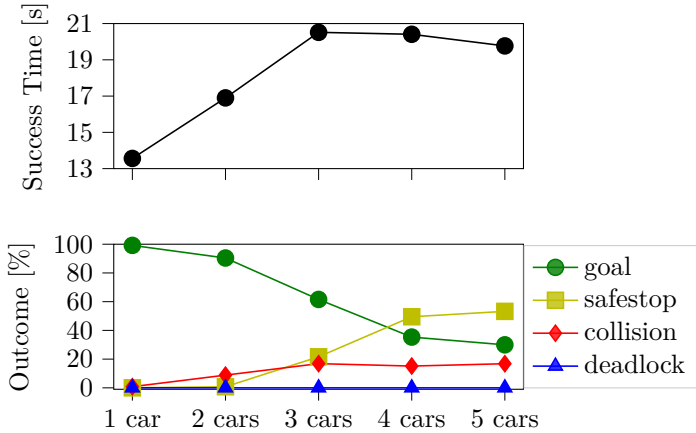


Figure 5: Performance results for DQN without intention state ζ , showing success time and outcome percentage for scenarios with increasing numbers of other cars.

Traffic density affects the problem at hand. 5 shows the results from an experiment with DQN trained agents that do not consider intentions in scenarios with different traffic densities. The 1-car scenario corresponds to traffic densities up to 1 car or vehicle per 50 m, or 20 vehicles/km; 2 cars correspond to 2 cars per 50 m, 40 vehicles/km, and so on. The results presented in 5 clearly show that for low traffic densities, the problem can relatively easily be solved without needing intention estimation. The agent can solve the problem without collisions, deadlocks, or safe stops. As the traffic density increases, the performance significantly drops. For traffic densities larger than 60 vehicles/km (4 cars), the agent only reaches the goal in approximately 35 % of the cases, makes safe stops before the intersection in 50 % of the cases, and collides in 15 %, which makes them the scenarios that can be most improved upon with algorithms that consider intentions. This experiment also gives

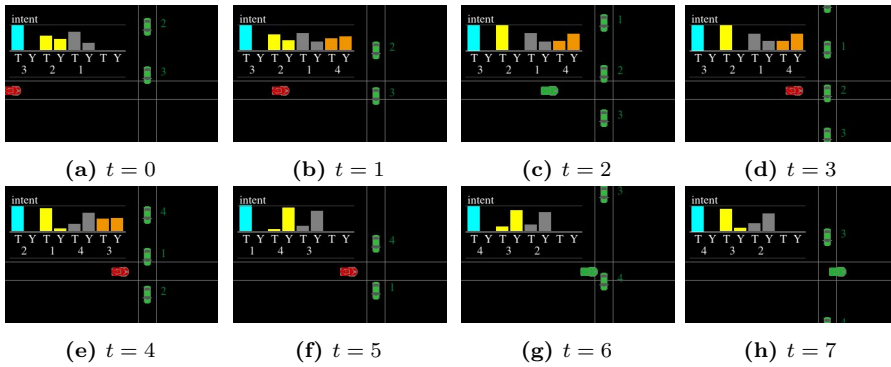


Figure 6: Example with a QMDP agent. The numbers on the right of the vertical cars are the cars id number n . The intention bar figure in each image shows the intention distribution for each other car. Each car has two bars grouped by the same color and the car id number, starting with the take way probability on the left and marked by a "T" and yield probability on the right marked with a "Y".

a sense of the limit of how a DQN can perform when not considering the intention state ζ .

As traffic densities in OECD countries according to [33] is around 60 vehicles/km, the rest of the experiments will focus on the 4 cars scenario.

5.2 Probability distribution of the intention state

The particle filter generates the probability distribution of the non-observable intention state ζ , which can be used to make the algorithms from 3.3 possible to implement.

In 6, an example of a QMDP agent with the intention distribution from the particle filter is shown. Looking at the first car with id 3 at $t = 0 - 3$, we can observe that the particle filter correctly predicts the take way intention and has some uncertainty about the intention for car id 2 and 1 crossed the intersection. It is also interesting to observe car id 4, as it temporarily has a higher probability of yielding when following car id 1 for $t = 1 - 5$, but could quickly switch to take way once car 1 crossed the intersection at $t = 6$.

The example from 6 shows that the proposed particle filter performs well at estimating the probability distribution of the intention. However, it relies on

an accurate prediction model and could make some mistakes. Because we want to investigate if the approximation of the DQN could compensate for the noisy states of the particles and utilize the change of intention probability between states, the focus in this paper is not to make the particle filter prediction as correct as possible. It is possible to improve the estimate by increasing the number of particles at the expense of additional computation.

5.3 Oracle DQN



Figure 7: Example scenario of an Oracle DQN agent trying to drive through a gap between cars. The agent is on the horizontal lane and is red when choosing the yield action and green when choosing the take way action.

The results from the previous experiment gave us a sense of the lower limit of a DQN when not considering the intention state ζ . To give a sense of an upper limit, we trained a DQN agent on the true state (D.11), this is referred to as the Oracle DQN. 3 shows results of the oracle DQN and all four other agents described in 3.3. Looking at the results, we see that even with full observability the oracle DQN has 1.05 % collisions. This shows that there are still some corner cases that the oracle DQN agent had difficulty navigating. One such case is shown in 7, where the agent found a possible gap between cars in the picture on the left, but was hit on the tail end of ego in the figure to the right.

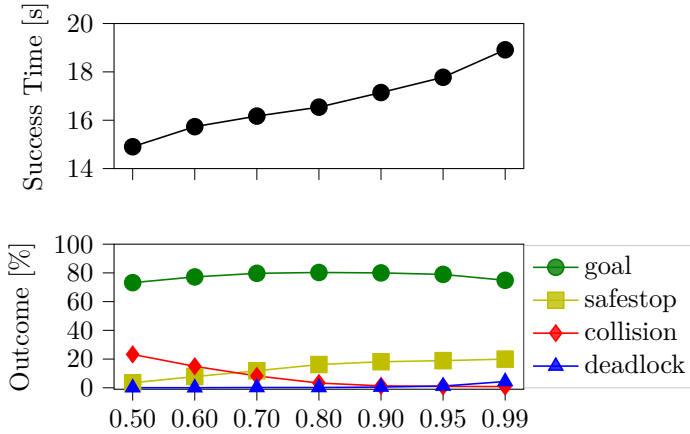


Figure 8: QMDP-IE performance (aggressiveness) for different $\zeta_{\text{threshold}}$ values. Increasing $\zeta_{\text{threshold}}$ lowers the collision rate while at the same time increasing the safe stop rate and the time it takes to reach a success state.

5.4 QMDP-IE and QMDP results

Starting with QMDP-IE, we first demonstrate how the $\zeta_{\text{threshold}}$ is chosen and then compare its results with QMDP. Both algorithms use the same network weights as the Oracle DQN, but QMDP-IE is less computational than QMDP since the threshold $\zeta_{\text{threshold}}$ transforms the set of particles into a point estimate of the intention state, as described in 3.3. Therefore, the choice of $\zeta_{\text{threshold}}$ is an important hyperparameter that directly correlates with the aggressiveness of the agent.

The threshold value $\zeta_{\text{threshold}}$, used in QMDP-IE, is determined by evaluating the agent with different $\zeta_{\text{threshold}}$ and observing the outcome percentage and success time. The results are shown in 8. The lowest threshold $\zeta_{\text{threshold}} = 0.5$ is equivalent to just taking the most likely estimation of the intention and resulting in an aggressive agent. At the same time, threshold values that are too large result in a passive agent. In summary, the parameter $\zeta_{\text{threshold}}$ directly correlates with the agent's aggressiveness, and a good trade-off between aggressiveness and passiveness is around $\zeta_{\text{threshold}} = 0.9$. With $\zeta_{\text{threshold}} = 0.9$, QMDP-IE performs significantly better on most evaluation metrics than QMDP, see 3. Moreover, QMDP-IE performs almost the same as the Oracle DQN,

particularly regarding collision avoidance and success time. The method is slightly more passive than the Oracle DQN but less passive than QMDP. A feature with QMDP-IE is that the aggressiveness/passiveness can be adjusted using threshold $\zeta_{\text{threshold}}$ and can be changed without re-training the network weights. However, the network weights need to be trained using the true states.

5.5 QPF and QID results

As opposed to QMDP-IE and QMDP, QID and QPF algorithms do not require access to the true intent during training time. While QPF trains a network using all particles, QID only uses the intention distribution from the particles, which reduces the size of the network while keeping information about the uncertainty of the intention state. Looking at 3, QPF has the highest collision rate at 12.15 % and the second lowest success time out of all considered algorithms, making it the most aggressive policy out of all four algorithms. QID collided more than QMDP-IE but still less than QMDP. This shows that training on ground truth is preferred, but QID is a good algorithm to use when ground truth data is not available. One downside is that QID and QPF took much longer time to train than the Oracle DQN, with up to 5 days of training. Since QID and QPF have comparable training times, this hints that the particle filter used by both algorithms is the main explanation for the computational time and that the large state space of QPF is of minor importance.

5.6 Overtake agent

To investigate how the algorithms perform when exposed to a behavior they are not trained for, we introduce a new scenario where the conflict car is allowed to overtake the car in front. This is done by only using the free road term (D.10) for the conflict car even when there are other cars in front. The overtake scenario aims to demonstrate how adaptable the agent is to situations outside of the training set. All algorithms are evaluated on the new overtake scenario without any retraining. The performance for all four algorithms, including the Oracle DQN, is summarized in 4. The collision rate for the Oracle DQN is the highest with 10.05 %, this is expected since the method is trained on intention states ζ_n outside of its training set.

In the overtake scenario, both QID and QPF have relatively low collision

rates at 2.53 % and 3.7% respectively, which is lower when compared to the trained scenarios in 3. While the collision rate for QMDP-IE and QMDP is 4.6 % and 5.95 % respectively, which is higher than what they got on the trained scenario but it is also higher than QID and QPF. This indicates that QID and QPF are better at handling some scenarios outside the training set than QMDP-IE and QMDP. QMDP also has the highest safe stop and deadlock rate at 10.2 % and 4.15 %, making it the most passive policy.

5.7 Discussion

When comparing QMDP-IE with QID, it is observed that the algorithms trained on ground truth (QMDP-IE) outperform the algorithms that were trained using the belief state (QPF) or even just an estimate of the belief distribution (QID).

The particle filter was used to create the belief state and filter the noisy observations. Hoping the flexibility of the neural network would be able to compensate for some of the inaccuracy when estimating the distribution. The higher collision rate for the QPF compared to the Oracle DQN shows that training on the full belief state can make finding a good policy difficult.

8 shows that the aggressiveness of the policy from QMDP-IE is correlated with $\zeta_{\text{threshold}}$ and by choosing a relatively high value, it could get a collision rate close to the Oracle DQN, and in this case could, to some extent, compensate for the not fully optimized particle filter. The ability to adjust the aggressiveness of the policy by changing $\zeta_{\text{threshold}}$ is also a strength of QMDP-IE compared to QMDP and our previous black box methods that use an LSTM to estimate the latent state [13]. The downside with QMDP-IE is that, in practice, they require the true intention during training, this can be obtained by either human labeling or auto labeling techniques, which can be either expensive or tedious to generate.

The other agents' possible actions were simplified to take way or yield. These actions could be expanded to left turn, right turn, or accelerate. But these actions would mainly affect the velocity profile of these cars coming into the intersection and slightly limit how fast ego can accelerate after a car that has turned into its lane. Looking at the overtake scenario, we can assume that these actions would not perform worse than using an overtake agent, shown in 4.

6 Conclusion

In this study, we explored the application of reinforcement learning for safe intersection navigation, emphasizing the importance of accounting for uncertainty and planning over the distribution of intentions. Specifically, we proposed two methods for representing belief over drivers' intentions using a particle-based approach and a compact parametric representation, which can manifest as a probability distribution (QID) or a point estimate (QMDP-IE).

Our proposed particle filter exhibited promising results in estimating intention probabilities. We leveraged these intention probability estimates in QMDP-IE and QID algorithms, which demonstrated superior performance compared to respective baseline approaches QMDP and QPF. QMDP-IE, in particular, offered adjustable aggressiveness post-training, yielding a collision rate close to the Oracle DQN with an optimal threshold value $\zeta_{\text{threshold}}$. Furthermore, QID policies collision rate was comparable to QMDP-IE for conflict scenarios. However, in an additional experiment involving a scenario with overtaking maneuvers, all algorithms exhibited higher collision rates compared to the standard scenario. Interestingly, QID and QPF demonstrated relatively lower collision rates, indicating adaptability to unforeseen behaviors, while QMDP displayed a more passive approach. A downside to QID and QPF is that the training times were considerably longer, highlighting the computational demands of the particle filter.

Overall, our findings underline the importance of accounting for uncertain intentions in autonomous driving scenarios and highlight the effectiveness of leveraging intention prediction for informed decision-making. Future research could improve the computational demand from the particle filter by focusing on network structure that can better learn the intention state and compare the results with the QMDP-IE and QID.

References

- [1] K. Heineke, N. Laverty, T. Möller, and F. Ziegler, *The future of mobility: Mobility evolves*, Apr. 2023.
- [2] W. Schwarting, J. Alonso-Mora, and D. Rus, “Planning and decision-making for autonomous vehicles,” *Annual Review of Control, Robotics, and Autonomous Systems*, vol. 1, no. 1, pp. 187–210, 2018.

- [3] L. Fletcher *et al.*, “The mit–cornell collision and why it happened,” *Journal of Field Robotics*, vol. 25, pp. 775–807, Oct. 2008.
- [4] S. Kammel *et al.*, “Team annieway’s autonomous system for the 2007 darpa urban challenge,” *Journal of Field Robotics*, vol. 25, pp. 615–639, Sep. 2008.
- [5] L. Gressenbuch and M. Althoff, “Predictive monitoring of traffic rules,” in *IEEE International Conference on Intelligent Transportation Systems (ITSC)*, 2021.
- [6] “2019 traffic safety culture index,” AAA Foundation for Traffic Safety, Washington DC, Tech. Rep. 202-638-5944, 2019.
- [7] C. Hubmann, M. Becker, D. Althoff, D. Lenz, and C. Stiller, “Decision making for autonomous driving considering interaction and uncertain prediction of surrounding vehicles,” in *IEEE Intelligent Vehicles Symposium (IV)*, 2017.
- [8] Z. N. Sunberg, C. J. Ho, and M. J. Kochenderfer, “The value of inferring the internal state of traffic participants for autonomous freeway driving,” in *American Control Conference (ACC)*, 2017.
- [9] R. S. Sutton and A. G. Barto, *Reinforcement Learning: An Introduction*, 2nd ed. MIT Press, 2018.
- [10] D. Isele, R. Rahimi, A. Cosgun, K. Subramanian, and K. Fujimura, “Navigating occluded intersections with autonomous vehicles using deep reinforcement learning,” in *IEEE International Conference on Robotics and Automation (ICRA)*, 2018.
- [11] M. J. Hausknecht and P. Stone, “Deep recurrent q-learning for partially observable mdps,” in *AAAI Conference on Artificial Intelligence (AAAI)*, 2015.
- [12] P. Zhu, X. Li, P. Poupart, and G. Miao, *On improving deep reinforcement learning for pomdps*, 2018.
- [13] T. Tram, A. Jansson, R. Grönberg, M. Ali, and J. Sjöberg, “Learning negotiating behavior between cars in intersections using deep Q-learning,” in *IEEE International Conference on Intelligent Transportation Systems (ITSC)*, 2018.
- [14] V. Mnih *et al.*, *Playing atari with deep reinforcement learning*, 2013.

- [15] S. Hochreiter and J. Schmidhuber, “Long short-term memory,” *Neural computation*, vol. 9, no. 8, pp. 1735–1780, 1997.
- [16] S. B. Amsalu, A. Homaifar, A. Karimoddini, and A. Kurt, “Driver intention estimation via discrete hidden markov model,” in *IEEE International Conference on Systems, Man, and Cybernetics (SMC)*, 2017.
- [17] M. Liebner, M. Baumann, F. Klanner, and C. Stiller, “Driver intent inference at urban intersections using the intelligent driver model,” in *IEEE Intelligent Vehicles Symposium (IV)*, 2012.
- [18] M. Treiber, A. Hennecke, and D. Helbing, “Congested traffic states in empirical observations and microscopic simulations,” *Physical Review E*, vol. 62, pp. 1805–1824, 2 2000.
- [19] S. Hoermann, D. Stumper, and K. Dietmayer, “Probabilistic long-term prediction for autonomous vehicles,” in *IEEE Intelligent Vehicles Symposium (IV)*, 2017.
- [20] M. Bouton, A. Cosgun, and M. J. Kochenderfer, “Belief state planning for autonomously navigating urban intersections,” in *IEEE Intelligent Vehicles Symposium (IV)*, 2017.
- [21] A. Wang, A. C. Li, T. Q. Klassen, R. T. Icarte, and S. A. Mcilraith, “Learning belief representations for partially observable deep RL,” vol. 202, Jul. 2023.
- [22] M. L. Littman, A. R. Cassandra, and L. P. Kaelbling, “Learning policies for partially observable environments: Scaling up,” in *International Conference on Machine Learning (ICML)*, 1995.
- [23] M. J. Kochenderfer, *Decision Making Under Uncertainty: Theory and Application*. MIT Press, 2015.
- [24] A. Kong, J. S. Liu, and W. H. Wong, “Sequential imputations and bayesian missing data problems,” *Journal of the American Statistical Association*, vol. 89, no. 425, pp. 278–288, 1994.
- [25] “Novel approach to nonlinear/non-gaussian bayesian state estimation,” vol. 140, no. 2, pp. 107–113, 1993.
- [26] M. Hessel *et al.*, “Rainbow: Combining improvements in deep reinforcement learning,” *AAAI Conference on Artificial Intelligence (AAAI)*, vol. 32, no. 1, Apr. 2018.

- [27] H. van Hasselt, A. Guez, and D. Silver, “Deep reinforcement learning with double Q-learning,” in *AAAI Conference on Artificial Intelligence (AAAI)*, 2016.
- [28] L.-J. Lin, “Reinforcement learning for robots using neural networks,” UMI Order No. GAX93-22750, Ph.D. dissertation, USA, 1992.
- [29] T. Tram, I. Batkovic, M. Ali, and J. Sjöberg, “Learning when to drive in intersections by combining reinforcement learning and model predictive control,” in *IEEE International Conference on Intelligent Transportation Systems (ITSC)*, Oct. 2019.
- [30] H. Iqbal, *Harisiqbal88/plotneuralnet v1.0.0*, version v1.0.0, Dec. 2018.
- [31] V. Mnih *et al.*, “Human-level control through deep reinforcement learning,” *Nature*, vol. 518, no. 7540, pp. 529–533, 2015.
- [32] H. van Hasselt, A. Guez, M. Hessel, V. Mnih, and D. Silver, “Learning values across many orders of magnitude,” in *Advances in Neural Information Processing Systems (NIPS)*, 2016.
- [33] OECD, *Road traffic, vehicles and networks*. 2015.

Algorithm 4 Update the joint particle state

Current particle state: $\{x_m, w_m\}_{m=1}^M$
New observation: o'
Updated particle state: $\{x'_m, w'_m\}_{m=1}^M$

```

1:  $w_{\text{sum}} = 0$ 
2: for  $m = 1, \dots, M$  do
3:   for  $n = 1, \dots, N$  do
4:     if  $x_{n[m]}$  is new then
5:       See Algorithm 3
6:     else
7:       if  $\mathcal{U}(0, 1) < \xi_i$  then
8:          $\zeta_{n[m]} = \begin{cases} \zeta^{\text{tw}}, & \text{if } \zeta_{n[m]} = \zeta^{\text{yd}} \\ \zeta^{\text{yd}}, & \text{otherwise} \end{cases}$ 
9:          $v'_{n[m]} \leftarrow v_{n[m]} + \sigma_a + \begin{cases} a^{\text{int}} dt, & \text{if } \zeta_{n[m]} = \zeta^{\text{yd}} \\ a^{\text{free}} dt, & \text{otherwise} \end{cases}$ 
10:         $p'_{n[m]} = p_{n[m]} + v_{n[m]} dt$ 
11:         $x'_{n[m]} = \{p'_{n[m]}, v'_{n[m]}, \zeta_{n[m]}\}$ 
12:         $w_{n[m]} \propto \mathcal{N}([p_n, v_n]^T; [\hat{p}_n, \hat{v}_n]^T, \text{diag}[\sigma_p^2, \sigma_v^2])$ 
13:         $x'_m = \{x'_{1,m}, \dots, x'_{N,m}\}$ 
14:         $w_m = \prod_{n=1}^N w_{n[m]}$ 
15:         $w_{\text{sum}} = w_{\text{sum}} + w_m$ 
16: for  $m = 1, \dots, M$  do                                 $\triangleright$  normalize weights
17:    $w_m = w_m / w_{\text{sum}}$ 
18:    $M_{\text{eff}} = \frac{1}{\sum_{i=1}^M (w^i)^2}$                                  $\triangleright$  from [24]
19: if  $M_{\text{eff}} < M_{\text{threshold}}$  then
20:    $x' = \text{Resample}(x, w)$                                  $\triangleright$  from [25]
21:    $w' = 1/M$                                                $\triangleright$  reset weights

```

Algorithm 5 double Q-learning training process

```

1: Initialize  $\theta$  randomly
2:  $\mathcal{D} \leftarrow \emptyset$ 
3: for nr episodes do
4:    $o \leftarrow$  initiate environment                                ▷ (D.12)
5:    $b \leftarrow \text{INITIALIZEBELIEF}(o)$                                 ▷ Alg. 3
6:   while episode not finished do
7:     if  $e \sim \mathcal{U}(0, 1) < \epsilon$  then                                ▷ from [14]
8:        $a \leftarrow$  random action
9:     else
10:       $Q(b, a) \leftarrow \text{GETACTIONVALUES}(b, \theta)$                 ▷ S. 3.3
11:       $a \leftarrow \text{argmax}_a Q(b, a)$                                 ▷ (D.4)
12:       $o', r \leftarrow \text{STEPENVIRONMENT}(a)$                             ▷ S. 4.1
13:       $b' \leftarrow \text{UPDATEBELIEF}(b, o', a)$                             ▷ Alg. 4
14:       $\mathcal{D} \leftarrow \mathcal{D} \cup \{(b, a, r, b')\}$ 
15:       $E \leftarrow$  sample from  $\mathcal{D}$                                 ▷ from [28]
16:      update  $\theta^-$  with SGD and loss  $J(\theta, \theta^-)$                 ▷ (D.22)
17:      for every  $N_{\text{update}}$  do
18:        update  $\theta$  with  $\theta^-$                                 ▷ from [27]
```

Table 2: Hyperparameters of Simulator

decision time [s],	dt	2
maximum initial distance [m],	p_{lim}	50
initial speed [m/s],	v_n^0	2 – 7
initial acceleration [m/s ²],	a_n^0	0
desired speed [m/s],	v_n^{desired}	2 – 7
time gap [s],	T_{gap}	1.5
Stop time limit [s],	T_{stop}	10
ego initial speed [m/s],	v_{ego}	5
ego desired speed [m/s],	$v_{\text{ego}}^{\text{desired}}$	5
noise position [m],	σ_p	2
noise velocity [m/s],	σ_v	1
max observed vehicles,	N	4
IDM max acceleration [m/s ²],	α^{max}	0.73
IDM deceleration [m/s ²],	α_b	0.5 – 4.0
IDM acceleration exponent,	δ	4
IDM minimum distance [m],	d_0	2
IDM vehicle length [m],	l_n	4
number of particles	M	100
min number of particles	$M_{\text{threshold}}$	75
acceleration noise [m/s ²]	σ_a	0.1
intention switch probability [%]	ξ_i	5
intention probability threshold	$\zeta_{\text{threshold}}$	0.8
Batch size	B	128
Learning rate	lr	0.0001
Discount factor	γ	0.95
Replay memory size	E_{replay}	20,000
Target network update frequency	N_{update}	1,000

Table 3: Result summary for 4 cars scenario

Experiments	Goal reached	Safe stop	Collision	Deadlock	Success time	Training time
	%	%	%	%	s	h
Oracle DQN	84.50	14.45	1.05	0.00	15.49	31h
QMDP-IE	80.00	18.15	1.35	0.50	17.14	N/A
QMDP	71.95	15.05	5.70	7.30	20.56	N/A
QID	85.60	10.40	3.70	0.30	16.64	119h
QPF	63.50	21.80	12.15	2.55	16.61	124h

Table 4: Results with an overtake agent

Experiments	Goal reached	Safe stop	Collision	Deadlock	Success time
	%	%	%	%	s
Oracle DQN	89.80	0.15	10.05	0.00	16.01
QMDP-IE	94.55	0.20	4.60	0.65	16.62
QMDP	79.70	10.20	5.95	4.15	19.84
QID	96.89	0.11	2.53	0.47	16.38
QPF	96.15	0.10	3.70	0.05	17.62

PAPER E

Reinforcement Learning in the Wild with Maximum Likelihood-based Model Transfer

Hannes Eriksson, Tommy Tram, Debabrota Basu, Mina Alibeigi, and Christos Dimitrakakis

Published in 2024 International Conference on Adaptive Agents and Multi-Agent Systems (AAMAS), pp. 516–524, May. 2024.

The layout has been revised.

Abstract

In this paper, we study the problem of transferring the available Markov Decision Process (MDP) models to learn and plan efficiently in an unknown but similar MDP. We refer to it as *Model Transfer Reinforcement Learning (MTRL)* problem. First, we formulate MTRL for discrete MDPs and Linear Quadratic Regulators (LQRs) with continuous state actions. Then, we propose a generic two-stage algorithm, MLEMTRL, to address the MTRL problem in discrete and continuous settings. In the first stage, MLEMTRL uses a *constrained Maximum Likelihood Estimation (MLE)*-based approach to estimate the target MDP model using a set of known MDP models. In the second stage, using the estimated target MDP model, MLEMTRL deploys a model-based planning algorithm appropriate for the MDP class. Theoretically, we prove worst-case regret bounds for MLEMTRL both in realisable and non-realisable settings. We empirically demonstrate that MLEMTRL allows faster learning in new MDPs than learning from scratch and achieves near-optimal performance depending on the similarity of the available MDPs and the target MDP.

1 Introduction

Deploying autonomous agents in the real world poses a wide variety of challenges. As in [1], we are often required to learn the real-world model with limited data, and use it to plan to achieve satisfactory performance in the real world. There might also be safety and reproducibility constraints, which require us to track a model of the real-world environment [2]. In light of these challenges, we attempt to construct a framework that can aptly deal with optimal decision making for a novel task, by leveraging external knowledge. As the novel task is unknown, we adopt the Reinforcement Learning (RL) [3] framework to guide an agent’s learning process and to achieve near-optimal decisions.

An RL agent interacts directly with the environment to improve its performance. Specifically, in model-based RL, the agent tries to learn a model of the

environment and then use it to improve performance [4]. In many applications, the depreciation in performance due to sub-optimal model learning can be paramount. For example, if the agent interacts with living things or expensive equipment, decision-making with an imprecise model might incur significant cost [5]. In such instances, boosting the model learning by leveraging external knowledge from the existing models, such as simulators [6], physics-driven engines, etc., can be of great value [7]. A model trained on simulated data may perform reasonably well when deployed in a new environment, given the novel environment is *similar enough* to the simulated model. Also, RL algorithms running on different environments yield data and models that can be used to plan in another similar enough real-life environment. In this work, we study the problem where we have access to multiple source models built using simulators or data from other environments, and we want to transfer the source models to perform efficient model-based RL in a different real-life environment.

Let us consider that a company is designing autonomous driving agents for different countries in the world. The company has designed two RL agents that have learned to drive well in USA and UK. Now, the company wants to deploy a new RL agent in India. Though all the RL agents are concerned with the same task, i.e. driving, the models encompassing driver behaviors, traffic rules, signs, etc., can differ for each. For example, UK and India have left-handed traffic, while the USA has right-handed traffic. However, learning a new controller *specifically* for every new geographic location is computationally expensive and time-consuming, as both data collection and learning take time. Thus, the company might use the models learned for UK and USA, to estimate the model for India, and use it further to build a new autonomous driving agent (RL agent). Hence, being able to transfer the source models to the target environment allows the company to use existing knowledge to build an efficient agent faster and resource efficiently.

We address this problem of model transfer from source models to a target environment to plan efficiently. We observe that this problem falls at the juncture of *transfer learning* and *reinforcement learning* [8]–[10]. [9] enlists three approaches to transfer knowledge from the *source tasks* to a *target task*. (i) *Instance transfer*: data from the source tasks is used to guide decision-making in the novel task [7]. (ii) *Representation transfer*: a representation of the task, such as learned neural network features, are transferred to perform

the new task [11]. (iii) *Parameter transfer*: the parameters of the RL algorithm or *policy* are transferred [12]. In our paper, the source tasks are equivalent to the source models, and the target task is the target environment. Moreover, we adopt the **model transfer reinforcement learning** approach (MTRL), which encompasses both (i) and (ii) (Section 4).

[13] describes three possible benefits of transfer learning. The first is **learning speed improvement**, i.e. decreasing the amount of data required to learn the solution. Secondly, **asymptotic improvement**, where the solution results in better asymptotic performance. Lastly, **jumpstart improvement**, where the initial proxy model serves as a better starting solution than that of one learning the true model from scratch. In this work, we propose a new algorithm to transfer RL that achieves both learning speed improvement and jumpstart improvement (Section 8). However, we might not find an asymptotic improvement in performance if compared with the best and unbiased algorithm in the true setting. Rather, we aim to achieve a model estimate that allows us to plan accurately in the target MDP (Section 6).

Contributions. We aim to answer two central questions:

1. *How can we accurately construct a model using a set of source models for an RL agent deployed in the wild?*
2. *Does the constructed model allow efficient planning and yield improvements over learning from scratch?*

In this paper, we address these questions as follows:

1. *A Taxonomy of MTRL*: First, we formulate the problem with the Markov Decision Processes (MDPs). We further provide a taxonomy of the problem depending on a discrete or continuous set of source models, and whether the target model is realisable by the source models (Section 4).
2. *Algorithm Design with MLE*: Following that, we design a two-stage algorithm MLEMTRL to plan in an unknown target MDP (Section 5). In the first stage, MLEMTRL uses a Maximum Likelihood Estimation (MLE) approach to estimate the target MDP using the source MDPs. In the second stage, MLEMTRL uses the estimated model to perform model-based planning. We instantiate MLEMTRL for discrete state-action (tabular) MDPs and Linear Quadratic Regulators (LQRs). We also derive a generic bound on the goodness of the policy computed using MLEMTRL (Section 6). We further provide a meta-algorithm, called Meta-MLEMTRL, to control the adaptation to the

non-realisable setting (Section 7).

3. Performance Analysis: In Section 8, we empirically verify whether MLEMTRL improves the performance for unknown tabular MDPs and LQRs than learning from scratch. MLEMTRL exhibits learning speed improvement for tabular MDPs and LQRs. For LQRs, it incurs learning speed improvement and asymptotic improvement. We also observe that the more similar the target and source models are, the better the performance of MLEMTRL, as indicated by the theoretical analysis. An ablation study of Meta-MLEMTRL under realisable and non-realisable settings further shows provable improvements yielded in the asymptotic and non-realisable regimes.

Before elaborating on the contributions, we posit this work in the existing literature (Section 2) and discuss the background knowledge of MDPs and MLEs (Section 3).

2 Related Work

Our work on Model Transfer Reinforcement Learning is situated in the field of Transfer RL (TRL) and also is closely related to the multi-task RL and Bayesian multi-task RL literature. In this section, we elaborate on these connections.

TRL is widely studied in Deep Reinforcement Learning. [14] introduces different ways of transferring knowledge, such as *policy transfer*, where the set of source MDPs \mathcal{M}_s has a set of expert policies associated with them. The expert policies are used together with a new policy for the novel task by transferring knowledge from each policy. [12] uses this approach, where a student learner is combined with a set of teacher networks to guide learning in multi-task RL. [15] develops an actor-critic structure to learn ways to transfer its knowledge to new domains. [16] invokes generalisation across Q-functions by learning a master policy. Here, *we focus on model transfer instead of policy*.

Another seminal work in TRL, by [8] distinguishes between *multi-task learning* and *transfer learning*. Multi-task learning deals with problems where the agent aims to learn from a distribution over scenarios, whereas transfer learning makes no specific assumptions about the source and target tasks. Thus, in transfer learning, the tasks could involve different state and action spaces and different transition dynamics. Specifically, we focus on **model-transfer** [17] approach to TRL, where the state-action spaces and also dynamics can be

different. [17] performs model transfer for a target task with an identical transition model. Thus, the main consideration is to transfer knowledge to tasks with the same dynamics but varying rewards. [10] assumes a context similar to that of [17], where the model dynamics are identical across environments. In our work, we rather assume that the reward function is the same, but the transition models are different. We believe this is an interesting question as the harder part of learning an MDP is learning the transition model. These works explicate a deep connection between the fields of *multi-task learning* and *TRL*. In general, TRL can be viewed as an extension of multi-task RL, where multiple tasks can either be learned simultaneously or have been learned *a priori*. This flexibility allows us to learn even in settings where the state-actions and transition dynamics are different among tasks. [18] describes a multi-task Maximum Likelihood Estimation procedure for optimal control of an aircraft. They identify a mixture of Gaussians, where the mixture is over each of the tasks. Here, we adopt an MLE approach to TRL to optimise performance for the target MDP (or a target task) rather than restricting to a mixture of Gaussians.

The Bayesian approach to multi-task RL [19], [20] tackles the problem of learning jointly how to act in multiple environments. [20] handles the *open-world assumption*, i.e. the number of tasks is unknown. This allows them to transfer knowledge from existing tasks to a novel task, using value function transfer. However, this is significantly different from our setting, as we are considering model-based transfer. Further, *we adopt an MLE-based framework in lieu of the full Bayesian procedure described in their work*. In Bayesian RL, [21] also investigates a learning technique to generalise over multiple problem instances. By sampling a large number of instances, the method is expected to learn how to generalise from the existing tasks to a novel task. We do not assume access to such prior or posterior distributions to sample from.

There is another related line of work, namely multi-agent transfer RL [22]. For example, [23] develops a TRL framework for autonomous driving using federated learning. They accomplish this by aggregating knowledge for independent agents. This setting is different from general transfer learning but could be incorporated if the source tasks are learned simultaneously with the target task. This requires cooperation among agents, which is out of the scope.

3 Background

In this section, we introduce the important concepts on which this work is based upon. Firstly, we introduce the way we model the dynamics of the tasks. Secondly, we describe the Maximum Likelihood Estimation (MLE) framework used in this work.

3.1 Markov Decision Process

We study sequential decision-making problems that can be represented as Markov Decision Processes (MDPs) [24]. An MDP μ consists of a discrete or continuous state space denoted by \mathcal{S} , a discrete or continuous action-space \mathcal{A} , a reward function $\mathcal{R} : \mathcal{S} \times \mathcal{A} \rightarrow \mathbb{R}$ which determines the quality of taking action a in state s , and a transition function $\mathcal{T} : \mathcal{S} \times \mathcal{A} \rightarrow \Delta\mathcal{S}$ inducing a probability distribution over the successor states s' given a current state s and action a . Finally, in the infinite-horizon formulation, a discount factor $\gamma \in [0, 1)$ is assigned. The overarching objective for the agent is to compute a decision-making policy $\pi : \mathcal{S} \rightarrow \Delta(\mathcal{A})$ that maximises the expected sum of future discounted rewards up until the horizon T : $V_\mu^\pi(s) = \mathbb{E}\left[\sum_{t=0}^T \gamma^t \mathcal{R}(s_t, a_t)\right]$. $V_\mu^\pi(s)$ is called the value function of policy π for MDP μ . The optimal value function is denoted as μ is $V_\mu^* = V_\mu^{\pi^*}$. The technique used to obtain the the optimal policy $\pi^* = \sup_\pi V_\mu^\pi$ depends on the MDP class. The MDPs with discrete state-action spaces are referred to as tabular MDPs. In this paper, we also study a specific class of MDPs with continuous state-action spaces, namely the Linear Quadratic Regulators (LQRs) [25]. In tabular MDPs, we employ VALUEITERATION [24] for model-based planning whereas in the LQR setting we use RICCATIITERATION [26].

The standard metric used to measure the performance of a policy π [27] for an MDP μ is *regret* $R(\mu, \pi)$. Regret is the difference between the optimal value function and the value function of π . In this work, we extend the definition of regret for MTRL, where the optimality is taken with respect to a policy class in the target MDP.

3.2 Maximum Likelihood Estimation

One of the most popular methods of constructing point estimators is the *Maximum Likelihood Estimation* (MLE) [28] framework. Given a density

function $f(x | \theta_1, \dots, \theta_n)$ and associated i.i.d. data X_1, \dots, X_t , the goal of the MLE scheme is to maximise,

$$\ell(\theta | x) \triangleq \ell(\theta_1, \dots, \theta_n | x_1, \dots, x_t) \triangleq \log \prod_{i=1}^t f(x_i | \theta_1, \dots, \theta_n). \quad (\text{E.1})$$

$\ell(\cdot)$ is called the log-likelihood function. The set of parameters maximising Equation E.1 is called the *maximum likelihood estimator* of θ given the data X_1, \dots, X_t . Maximum likelihood estimation has many desirable properties that we leverage in this work. For example, the ML estimator satisfies *consistency*, i.e. under certain conditions, it achieves optimality even for *constrained* MLE. An estimator being consistent means that if the data X_1, \dots, X_t is generated by $f(\cdot | \theta)$ and as $t \rightarrow \infty$, the estimate almost surely converges to the true parameter θ . [29] shows that MLE admits the consistency property given the following assumptions hold. The model is *identifiable*, i.e. the densities at two parameter values must be different unless the two parameter values are identical. Further, the parameter space is *compact* and *continuous*. Finally, if the log-density is *dominated*, one can establish that MLE converges to the true parameter almost surely [30]. For problems where the likelihood is unbounded, flat or otherwise unstable one may introduce a penalty term in the objective function. This approach is called *penalised maximum likelihood estimation* [31], [32]. As we in our work are mixing over known parameters, we do not need to add regularisation to our objective to guarantee convergence.

In this work, we iteratively collect data and compute new point estimates of the parameters and use them in our decision-making procedure. In order to carry out MLE, a likelihood function has to be chosen. In this work, we investigate two such likelihood functions in Section 5, one for each respective model class.

4 A Taxonomy of Model Transfer RL

Now, we formally define the Model Transfer RL problem and derive a taxonomy of settings encountered in MTRL.

4.1 MTRL: Problem Formulation

Let us assume that we have access to a set of source MDPs $\mathcal{M}_s \triangleq \{\mu_i\}_{i=1}^m$. The individual MDPs can belong to a finite or infinite but compact set depending on the setting. For example, for tabular MDPs with finite state-actions, this is always a finite set. Whereas for MDPs with continuous state-actions, the transitions can be parameterised by real-valued vectors/matrices, corresponding to an infinite but compact set. Given access to \mathcal{M}_s , we want to find an optimal policy for an unknown target MDP μ^* that we encounter while deploying RL in the wild. At each step t , we use \mathcal{M}_s and the data observed from the target MDP $D_{t-1} \triangleq \{s_0, a_0, s_1, \dots, s_{t-1}, a_{t-1}, s_t\}$ to construct an estimate of μ^* , say $\hat{\mu}^t$. Now, we use $\hat{\mu}^t$ to run a model-based planner, such as VALUEITERATION or RICCATIITERATION, that leads to a policy π^t . After completing this planning step, we interact with the target MDP using π_t that yields an action a_t , and leads to observing s_{t+1}, r_{t+1} . We update the dataset with these observations: $D_t \triangleq D_{t-1} \cup \{a_t, s_t\}$. Here, we assume that all the source and target MDPs share the same reward function \mathcal{R} . We do not restrict the state-action space of target and source MDPs.

Our goal is to compute a policy π^t that performs as close as possible with respect to the optimal policy π^* for the target MDP as the number of interactions with the target MDP $t \rightarrow \infty$. This allows us to define a notion of regret for MTRL: $R(\mu^*, \pi_t) \triangleq V_{\mu^*}^* - V_{\mu^*}^{\pi_t}$. Here, π_t is a function of the source models \mathcal{M}_s , the data collected from target MDP D_t , and the underlying MTRL algorithm. The goal of an MTRL algorithm is to minimise $R(\mu^*, \pi_t)$. For the parametric policies π_θ with $\theta \in \Theta \subset \mathbb{R}^d$, we can specialise the regret further for this parametric family: $R(\mu^*, \pi_{\theta_t}) = V_{\mu^*}^{\pi_{\theta^*}} - V_{\mu^*}^{\pi_{\theta_t}}$. For example, for LQRs, we by default work with linear policies. We use this notion of regret in our theoretical and experimental analysis.

4.2 Three Classes of MTRL Problems

We begin by illustrating MTRL using Figure 1. In the figure, the source MDPs \mathcal{M}_s are depicted in red. This green area is the convex hull spanned by the source models $\mathcal{C}(\mathcal{M}_s)$. The target MDP μ^* , the best representative within the convex hull of the source models μ , and the estimated MDP $\hat{\mu}$ are shown in blue, yellow, and purple, respectively. If the target model is *inside* the convex hull, we call it a **realisable** setting. whereas If the target model is outside (as

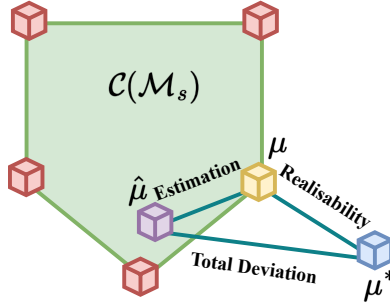


Figure 1: An illustration of the MTRL setting. The source models \mathcal{M}_s are the red boxes. The green area is the convex hull $\mathcal{C}(\mathcal{M}_s)$ spanned by the source models. The target MDP μ^* is displayed in blue, and the best proxy model is contained in the convex hull μ in yellow. Finally, the estimator of the best proxy model $\hat{\mu}$ is shown in purple.

in Figure 1), then we have a **non-realisable** setting.

Figure 1 also shows that the total deviation of the estimated model from the target model depends on two sources of errors: (i) realisability, i.e. how far is the target MDP μ^* from the convex hull of the source models $\mathcal{C}(\mathcal{M}_s)$ available to us, and (ii) estimation, i.e. how close is the estimated MDP $\hat{\mu}$ to the best possible representation μ of the target MDP. In the realisable case, the realisability gap can be reduced to zero, but not otherwise. This approach allows us to decouple the effect of the expressibility of the source models and the goodness of the estimator.

Now, we further elaborate on these three classes and the corresponding implications of performing MLE.

I. Finite and Realisable Plausible Models. If the true model μ^* is one of the target models, i.e. $\hat{\mu} \in \mathcal{M}_s$, we have to identify the target MDP from a finite set of plausible MDPs. Thus, the corresponding MLE involves a finite set of parameters, i.e. the parameters of the source MDPs \mathcal{M}_s . We compute the MLE $\hat{\mu}$ by solving the optimisation problem:

$$\hat{\mu} \in \arg \max_{\mu' \in \mathcal{M}_s} \log \mathbb{P}(D_t | \mu'), D_t \sim \mu^*. \quad (\text{E.2})$$

This method may serve as a reasonable heuristic for the TRL problem, where the target MDP is the same as or reasonably close to one of the source MDPs. However, this method will potentially be sub-optimal if the target MDP is too different from the source MDPs. Even if μ^* lies within the convex hull of the

source MDPs (the green area in Figure 1), this setting restricts the selection of a model to one of the red boxes. Thus, this setting fails to leverage the expressiveness of the source models as MLE allows us to accurately estimate models which are also in $\mathcal{C}(\mathcal{M}_s)$. Thus, we focus on the two settings described below.

II. Infinite and Realisable Plausible Models. In this setting, the target MDP μ^* is in the convex hull $\mu^* \in \mathcal{C}(\mathcal{M}_s)$ of the source MDPs. Thus, for Class I, we extend the parameter space considered in MLE to an infinite but compact parameter set.

Let us define the convex hull as $\mathcal{C}(\mathcal{M}_s) \triangleq \{\mu_1 w_1 + \dots + \mu_m w_m \mid \mu_i \in \mathcal{M}_s, w_i \geq 0, i = 1, \dots, m, \sum_{i=1}^m w_i = 1\}$. Then, the corresponding MLE problem with the corresponding likelihood function is

$$\hat{\mu} \in \arg \max_{\mu' \in \mathcal{C}(\mathcal{M}_s)} \log \mathbb{P}(D_t \mid \mu'), D_t \sim \mu^*. \quad (\text{E.3})$$

Since $\mathcal{C}(\mathcal{M}_s)$ induces a compact subset of model parameters $\mathcal{M}' \subset \mathcal{M}$, Equation (E.3) leads to a *constrained maximum likelihood estimation problem* [33]. It implies that if the parameter corresponding to the target MDP is in \mathcal{M}' , it can be correctly identified. In the case where the optimum lies inside, we can use constrained MLE to accurately identify the true parameters given enough experience from μ^* . This approach allows us to leverage the expressibility of the source models completely. However, μ^* might lie outside or on the boundary. Either of them may pose problems for the optimiser.

III. Infinite and Non-realisable Plausible Models. This class is similar to Class II with the important difference that the true parameter μ^* is outside the convex hull of source MDPs $\mathcal{C}(\mathcal{M}_s)$, and thus, the corresponding parameter is not in the induced parameter subset \mathcal{M}' . This key difference means the true parameters cannot be correctly identified. Instead, the objective is to identify the best proxy model $\mu \in \mathcal{M}'$. The performance loss for using μ instead of μ^* is intimately related to the model dissimilarity $\|\mu^* - \mu\|_1$. This allows us to describe the limitation of expressivity of the source models by defining the *realisability gap*: $\epsilon_{\text{Realise}} \triangleq \min_{\mu \in \mathcal{C}(\mathcal{M}_s)} \|\mu^* - \mu\|_1$. The realisability gap becomes important while dealing with continuous state-action MDPs with parameterised dynamics, such as LQRs.

Algorithm 6 Maximum Likelihood Estimation for Model-based Transfer Reinforcement Learning (MLEMTRL)

```

1: Input: weights  $\mathbf{w}^0$ ,  $m$  source MDPs  $\mathcal{M}_s$ , data  $D_0$ , discount factor  $\gamma$ , iterations  $T$ .
2: for  $t = 0, \dots, T$  do
3:   // STAGE 1: MODEL ESTIMATION //
4:    $\mathbf{w}^{t+1} \leftarrow \text{OPTIMISER}(\log \mathbb{P}(D_t | \sum_{i=1}^m w_i \mu_i), \mathbf{w}^t)$ 
5:   Estimate the MDP:  $\mu^{t+1} = \sum_{i=1}^m w_i \mu_i$ 
6:   // STAGE 2: MODEL-BASED PLANNING //
7:   Compute the policy:  $\pi^{t+1} \in \arg \max_{\pi} V_{\mu^{t+1}}^{\pi}$ 
8:   // CONTROL //
9:   Observe  $s_{t+1}, r_{t+1} \sim \mu^*(s_t, a_t)$ ,  $a_t \sim \pi^{t+1}(s_t)$ 
10:  Update the dataset  $D_{t+1} = D_t \cup \{s_t, a_t, s_{t+1}, r_{t+1}\}$ 
11: return An estimated MDP model  $\mu^T$  and a policy  $\pi^T$ 
```

5 MLEMTRL: MTRL with Maximum Likelihood Model Transfer

Now, we present the proposed algorithm, MLEMTRL. The algorithm consists of two stages, a *model estimation* stage, and a *planning* stage. After having obtained a plan, then the agent will carry out its decision-making in the environment to acquire new experiences. We sketch an overview of MLEMTRL in Algorithm 6. For completeness, we also provide an extension to MLEMTRL called Meta-MLEMTRL. This extension combines the MLEMTRL estimated model with the empirical model of the target task. This allows us to identify the true model even in the non-realisable setting. The details of this algorithm are available in Section 7.

5.1 Stage 1: Model Estimation

The first stage of the proposed algorithm is *model estimation*. During this procedure, the likelihood of the data needs to be computed for the appropriate MDP class. In the tabular setting, we use a product of multinomial likelihoods, where the data likelihood is over the distribution of successor states s' for a given state-action pair (s, a) . In the LQR setting, we use a linear-Gaussian likelihood, which is also expressed as a product over data observed from the

target MDP.

Likelihood for Tabular MDPs. The log-likelihood that we attempt to maximise in tabular MDPs is a product over $|\mathcal{S}| \times |\mathcal{A}|$ of pairs of multinomials, where p_i is the probability of event i , $n^{s,a}$ is the number of times the state-action pairs (s, a) appear in the data D_t , and $x_i^{s,a}$ is the number of times the state-action pair (s, a, s_i) occurs in the data. That is, $\sum_{i=1}^{|\mathcal{S}|} x_i^{s,a} = n^{s,a}$. Specifically,

$$\log \mathbb{P}(D_t | \mathbf{p}) = \log \left(\prod_{s,a} n^{s,a}! \prod_{i=1}^{|\mathcal{S}|} \frac{p_i^{x_i^{s,a}}}{x_i^{s,a}!} \right) \quad (\text{E.4})$$

Likelihood for Linear-Gaussian MDPs. For continuous state-action MDPs, we use a linear-Gaussian likelihood. In this context, let d_s be the dimensionality of the state-space, $\mathbf{s} \in \mathbb{R}^{d_s}$ and d_a be the dimensionality of the action-space. Then, the mean function \mathbf{M} is a $\mathbb{R}^{d_s} \times \mathbb{R}^{d_a+d_s}$ matrix. The mean visitation count to the successor state \mathbf{s}'_t when an action \mathbf{a}_t is taken at state \mathbf{s}_t is given by $\mathbf{M}(\mathbf{a}_t, \mathbf{s}_t)$. We denote the corresponding covariance matrix of size $\mathbb{R}^{d_s} \times \mathbb{R}^{d_s}$ by \mathbf{S} . Thus, we express the log-likelihood by

$$\log \mathbb{P}(D_t | \mathbf{M}, \mathbf{S}) = \log \prod_{i=1}^t \frac{\exp\left(-\frac{1}{2}\mathbf{v}^\top \mathbf{S}^{-1} \mathbf{v}\right)}{(2\pi)^{d_s/2} |\mathbf{S}|^{1/2}},$$

where $\mathbf{s}'_i - \mathbf{M}(\mathbf{a}_i, \mathbf{s}_i) = \mathbf{v}$.

Model Estimation as a Mixture of Models. As the optimisation problem involves weighing multiple source models together, we add a weight vector $\mathbf{w} \in [0, 1]^m$ with the usual property that \mathbf{w} sum to 1. This addition results in another outer product over the likelihoods shown above. Henceforth, μ will refer to either the parameters associated with the product-Multinomial likelihood or the linear-Gaussian likelihood, depending on the model class.

$$\begin{aligned} \min_{\mathbf{w}} \quad & \log \mathbb{P}(D_t | \sum_{i=1}^m w_i \mu_i), D_t \sim \mu^*, \mu_i \in \mathcal{M}_s, \\ \text{s.t.} \quad & \sum_{i=1}^m w_i = 1, w_i \geq 0. \end{aligned} \quad (\text{E.5})$$

Because of the constraint on \mathbf{w} , this is a constrained nonlinear optimisation problem. We can use any optimiser algorithm, denoted by OPTIMISER, for this purpose.

OPTIMISER. In our implementations, we use Sequential Least-Squares Quadratic Programming (SLSQP) [34] as the OPTIMISER. SLSQP is a quasi-Newton method solving a quadratic programming subproblem for the Lagrangian of the objective function and the constraints.

Specifically, in Line 4 of Algorithm 6, we compute the next weight vector \mathbf{w}^{t+1} by solving the optimisation problem in Eq. (E.5). Let $f(\mathbf{w}) = \log \mathbb{P}(D_t | \sum_{i=1}^m w_i \mu_i)$. Further, let $\lambda = \{\lambda_1, \dots, \lambda_m\}$ and κ be Lagrange multipliers. We then define the Lagrangian \mathcal{L} ,

$$\mathcal{L}(\mathbf{w}, \lambda, \kappa) = f(\mathbf{w}) - \lambda^\top \mathbf{w} - \kappa(1 - \mathbf{1}^\top \mathbf{w}). \quad (\text{E.6})$$

Here, \mathbf{w}^k is the k -th iterate. Finally, taking the local approximation of Eq. (E.5), we define the optimisation problem as:

$$\begin{aligned} & \min_{\mathbf{d}} \frac{1}{2} \mathbf{d}^\top \nabla^2 \mathcal{L}(\mathbf{w}, \lambda, \kappa) \mathbf{d} + \nabla f(\mathbf{w}^k)^\top \mathbf{d} + f(\mathbf{w}^k) \\ & \text{s.t. } \mathbf{d} + \mathbf{w}^k \geq 0, \mathbf{1}^\top \mathbf{w}^k = 1. \end{aligned} \quad (\text{E.7})$$

This minimisation problem yields the search direction \mathbf{d}_k for the k -th iteration. Applying this iteratively and using the construction above ensures that the constraints posed in Eq. (E.5) are adhered to at every step of MLEMTRL. At convergence, the k -th iterate, \mathbf{w}^k is considered as the next \mathbf{w}^{t+1} in Line 4 of Algorithm 6.

5.2 Stage 2: Model-based Planning

When an appropriate model μ^t has been identified at time step t , the next stage of the algorithm involves model-based planning in the estimated MDP. We describe two model-based planning techniques, VALUEITERATION and RICCATIITERATION for tabular MDPs and LQRs, respectively.

VALUEITERATION. Given the model, μ^t and the associated reward function \mathcal{R} , the optimal value function of μ^t can be computed iteratively as [3]:

$$V_{\mu^t}^*(s) = \max_a \sum_{s'} \mathcal{T}_{s,s'}^a \left(\mathcal{R}(s, a) + \gamma V_{\mu^t}^*(s') \right). \quad (\text{E.8})$$

The fixed-point solution to Eq. (E.8) is the optimal value function. When the optimal value function has been obtained, one can simply select the action maximising the action-value function. Let π^{t+1} be the policy selecting the

maximising action for every state, then π^{t+1} is the policy the model-based planner will use at time step $t + 1$.

RICCATI ITERATION. A LQR-based control system, and thus, the corresponding MDP, is defined by four system matrices [25]: $\mathbf{A}, \mathbf{B}, \mathbf{Q}, \mathbf{R}$. The matrices \mathbf{A}, \mathbf{B} are associated with the transition model $s_{t+1} - s_t = \mathbf{A}s_t + \mathbf{B}a_t$. The matrices \mathbf{Q}, \mathbf{R} dictate the quadratic cost (or reward) of a policy π under an MDP μ is

$$V_\mu^\pi = \sum_{t=0}^T \mathbf{s}_t^\top \mathbf{Q} \mathbf{s}_t + \mathbf{a}_t^\top \mathbf{R} \mathbf{a}_t.$$

Optimal policy is identified following [26] that states $a_t = -\mathbf{K}s_t$ at time t , where \mathbf{K} is computed using $\mathbf{A}, \mathbf{B}, \mathbf{Q}, \mathbf{R}$. We refer to Appendix ?? for details.

6 Theoretical Analysis of MLEMTRL

In this section, we further justify the use of our framework by deriving worst-case performance degradation bounds relative to the optimal controller. The performance loss is shown to be related to the realisability of μ^* under $\mathcal{C}(\mathcal{M}_s)$. In Figure 1, we visualise the model dissimilarities, where $\|\mu - \hat{\mu}\|_1$ is the model estimation error, $\|\mu^* - \mu\|_1$ is the realisability gap and $\|\mu^* - \hat{\mu}\|_1$ the total deviation of the estimated model. Note that by the norm on MDP, we always refer to the L_1 norm over transition matrices.

Theorem 1 (Performance Gap for Non-Realisable Models): *Let $\mu^* = (\mathcal{S}, \mathcal{A}, \mathcal{R}, \mathcal{T}^*, \gamma)$ be the true underlying MDP. Further, let $\mu = (\mathcal{S}, \mathcal{A}, \mathcal{R}, \mathcal{T}, \gamma)$ be the maximum log-likelihood*

$$\mu \in \arg \max_{\mu' \in \mathcal{C}(\mathcal{M}_s)} -\log \mathbb{P}(D_\infty | \mu'), D_\infty \sim \mu^*$$

and $\hat{\mu} = (\mathcal{S}, \mathcal{A}, \mathcal{R}, \hat{\mathcal{T}}, \gamma)$ be a maximum log-likelihood estimator of μ . In addition, let $\pi^*, \pi, \hat{\pi}$ be the optimal policies for the respective MDPs. Then, if \mathcal{R} is a bounded reward function $\forall_{(s,a)} r(s,a) \in [0,1]$ and with ϵ_{Estim} being the estimation error and

$$\epsilon_{\text{Realise}} \triangleq \min_{\mu \in \mathcal{C}(\mathcal{M}_s)} \|\mu^* - \mu\|_1$$

the realisability gap. Then, the performance gap is given by,

$$\|V_{\mu^*}^* - V_{\mu^*}^{\hat{\pi}}\|_\infty \leq \frac{3(\epsilon_{\text{Estim}} + \epsilon_{\text{Realise}})}{(1-\gamma)^2}. \quad (\text{E.9})$$

For the full proof, see Appendix A.1. This result is comparable to recent results such as [35] but here with an explicit decomposition into model estimation error and realisability gap terms.

Remark (Bound on L_1 Norm Difference in the Realisable Setting): It is known [36]–[38] that in the realisable setting, it is possible to bound the model estimation error term ϵ_{Estim} via the following argument. Let μ^* be the true underlying MDP, and $\hat{\mu}$ be an MLE estimate of μ^* , as defined in Theorem 1. If \mathcal{R} is a bounded reward function, i.e. $r(s, a) \in [0, 1], \forall (s, a)$, and ϵ_{Estim} is upper bound on the L_1 norm between \mathcal{T}^* and $\hat{\mathcal{T}}$. If $n^{s,a}$ be the number of times (s, a) occur together, then with probability $1 - SA\delta$,

$$\|\mathcal{T}^* - \hat{\mathcal{T}}\|_1 \leq \epsilon_{\text{Estim}} \leq \sum_{s \in \mathcal{S}} \sum_{a \in \mathcal{A}} \sqrt{\frac{2 \log((2^S - 2)/\delta)}{n^{s,a}}}.$$

From this, it can be said that the total L_1 norm then scales on the order of $\mathcal{O}(SA\sqrt{S + \log(1/\delta)})/\sqrt{T}$.

This result is specific to tabular MDPs. In tabular MDPs, the maximum likelihood estimate coincides with the empirical mean model. Further details are in Appendix A.2.

Remark (Performance Gap in the Realisable Setting): A trivial worst-case bound for the realisable case (Section 4.2) can be obtained by setting $\epsilon_{\text{Realise}} = 0$ because by definition of the realisable case $\mu^* \in \mathcal{C}(\mathcal{M}_s)$.

7 A Meta-Algorithm for MLEMTRL under Non-realisability

To guarantee good performance even in the non-realisable setting, we can proceed in two steps. First, we can add the target task to the set of source tasks. Second, we can construct a meta-algorithm, combining the model estimated by MLEMTRL and the empirical estimation of the target task. In this section, we propose a meta-algorithm based on the latter. We illustrate it in Algorithm 7.

The main change in Algorithm 7 compared to Algorithm 6 is internally keeping track of the empirical model, and in Line 8, computing a posterior probability distribution over the respective models by weighting the two likelihoods together with their respective priors. The resulting algorithm then trades off its bias to the prior based on the choice of prior hyperparameter

Algorithm 7 Meta-MLEMTRL

```

1: Input: prior  $p$ , weights  $\mathbf{w}^0$ ,  $m$  source MDPs  $\mathcal{M}_s$ , data  $D_0$ , discount factor
    $\gamma$ , iterations  $T$ .
2: for  $t = 0, \dots, T$  do
3:   // STAGE 1: OBTAIN MODEL WEIGHTS //
4:    $\mathbf{w}^{t+1} \leftarrow \text{MLEMTRL}(\mathbf{w}^t, \mathcal{M}_s, \mathcal{D}_t, \gamma, 1)$ 
5:   Estimate the MDP:  $\mu^{t+1} = \sum_{i=1}^m w_i \mu_i$ 
6:   Compute log-likelihood  $\ell_{\text{MLEM}}^{t+1} = \log \mathbb{P}(\mathcal{D}_t | \mu^{t+1})$ 
7:   Compute log-likelihood of empirical model  $\ell_{\text{Empirical}}^{t+1} = \log \mathbb{P}(\mathcal{D}_t | \hat{\mu}^{t+1})$ 
8:   Sample  $\tilde{\mu}^{t+1}$  as  $\mu^{t+1}$  w.p.  $\propto p \exp(\ell_{\text{MLEM}}^{t+1})$  and  $\hat{\mu}^{t+1}$  w.p.  $\propto (1 - p) \exp(\ell_{\text{Empirical}}^{t+1})$ .
9:   // STAGE 2: MODEL-BASED PLANNING //
10:  Compute the policy:  $\pi^{t+1} \in \arg \max_{\pi} V_{\tilde{\mu}^{t+1}}^{\pi}$ 
11:  // CONTROL //
12:  Observe  $s_{t+1}, r_{t+1} \sim \mu^*(s_t, a_t), a_t \sim \pi^{t+1}(s_t)$ 
13:  Update the dataset  $D_{t+1} = D_t \cup \{s_t, a_t, s_{t+1}, r_{t+1}\}$ 
14: return An estimated MDP model  $\tilde{\mu}^T$  and a policy  $\pi^T$ 

```

p . Since asymptotically the likelihood of the data under the empirical model is greater than the likelihood of the data under the MLEM-estimated model, as more and more data is collected the Meta-MLEMTRL algorithm performs similarly to the optimal planning using the empirical estimate. This is intended behaviour and allows for the algorithm to asymptotically plan optimally even in the non-realisable setting.

We experimentally study the behaviour of Meta-MLEMTRL and its dependence on the prior parameter p in the next section.

8 Experimental Analysis

To benchmark the performance of MLEMTRL, we compare ourselves to a posterior sampling method (**PSRL**) [39], equipped with a combination of product-Dirichlet and product-Normal Inverse Gamma priors for the tabular setting, and Bayesian Multivariate Regression prior [40] for the continuous setting. In PSRL, at every round, a new model is sampled from the prior, and it learns in the target MDP from scratch. Finally, for model-based planning,

we use RICCATIITERATIONS to obtain the optimal linear controller for the sampled model. In the continuous action setting, we compare the performance to the baseline algorithm multi-task soft-actor critic (**MT-SAC**) [41], [42] and a modified **MT-SAC-TRL** using data from the novel task during learning. In the tabular MDP setting, we compare against multi-task proximal policy optimisation (**MT-PPO**) [42], [43] and similarly **MT-PPO-TRL**.

The objectives of our empirical study are three-fold:

1. How does MLEMTRL impact performance in terms of **learning speed**, **jumpstart improvement** and **asymptotic convergence** compared to our baseline?
2. What is the performance loss of MLEMTRL in the **non-realisable setting**?
3. How does Meta-MLEMTRL perform in the **non-realisable setting**?

We conduct two kinds of experiments to verify our hypotheses. Firstly, in the upper row of Figure 2, we consider the realisable setting, where the novel task μ^* is part of the convex hull $\mathcal{C}(\mathcal{M}_s)$. In this case, we are looking to identify an improvement in some or all of the aforementioned qualities compared to the baselines. Further, in the bottom row of Figure 2, we investigate whether the algorithm can generalise to the case beyond what is supported by the theory in Section 4.2. We begin by recalling the goals of the transfer learning problem [13].

1. *Learning Speed Improvement*: A learning speed improvement would be indicated by the algorithm reaching its asymptotic convergence with less data.
2. *Asymptotic Improvement*: An asymptotic improvement would mean the algorithm converges asymptotically to a superior solution to that one of the baseline.
3. *Jumpstart Improvement*: A jumpstart improvement can be verified by the behaviour of the algorithm during the early learning process. In particular, if the algorithm starts at a better solution than the baseline, or has a simpler optimisation surface, it may more rapidly approach better solutions with much less data.

RL Environments. We test the algorithms in a tabular MDP, i.e. Chain [44], CartPole [45], and two LQR tasks in *Deepmind Control Suite* [46]: *dm_LQR_2_1* and *dm_LQR_6_2*. Further details on experimental setups are deferred to Appendix C.1.

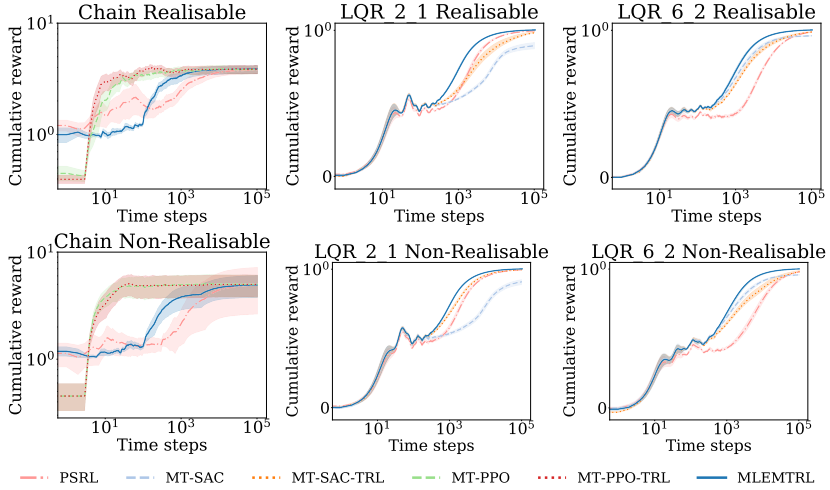


Figure 2: Depicted is the average cumulative reward at every time step computed over 10 novel tasks in the realisable/non-realisable setting. The shaded regions represent the standard error of the average cumulative reward at the time step.

(1) Impacts of Model Transfer with MLEMTRL. We begin by evaluating the proposed algorithm in the Chain environment. The results of the said experiment are available in the leftmost column of Figure 2. In it, we evaluate the performance of MLEMTRL against PSRL, MT-PPO, MT-PPO-TRL. The experiments are done by varying the slippage parameter $p \in [0.00, 0.50]$ and the results are computed for each different setup of Chain from scratch. In this experiment, we can see the baseline algorithms MT-PPO and MT-PPO-TRL perform very well. This could partially be explained by PSRL and MLEMTRL not only having to learn the transition distribution but also the reward function. The value function transfer in the PPO-based baselines implicitly transfers not only the empirical transition model but also the reward function. We can see that MLEMTRL has improved learning speed compared to PSRL in both realisable and non-realisable settings. An additional experiment with a known reward function across tasks is shown in Figure 7 in Appendix.

In the centre and rightmost columns of Figure 2, we can see the results of running the algorithms in the LQR settings with the baseline algorithms PSRL, MT-SAC and MT-SAC-TRL. The variation over tasks is given by the

randomness over the stiffness of the joints in the problem. In these experiments, we can see a clear advantage of MLEMTRL compared to all baselines in terms of learning speed improvements, and in some cases, asymptotic performance.

In Figure 2, the performance metric is the average cumulative reward at every time step, for 10^5 time steps and the shaded region represents the standard deviation, where the statistics are computed over 10 independent tasks.

(2) Impact of Realisability Gap on Regret. Now, we further illustrate the observed relation between model dissimilarity and degradation in performance. Figure 3 depicts the regret against the KL-divergence of the target model to the best proxy model in the convex set. We observe that model dissimilarity influences the performance gap in MLEMTRL. This is also justified in Section 6 where the bounds have an explicit dependency on the model difference. In this figure, only the non-zero regret experiments are shown. This is to have an idea of which models result in poor performance. As its shown, it is those models that are very dissimilar. Additional results in Figure 5 in Appendix further illustrate the dependency on model similarity.

(3) Performance of Meta-MLEMTRL under Non-realisability. In order to validate the performance of the proposed meta algorithm Meta-MLEMTRL, we perform an ablation study over the prior hyperparameter p . In Figure 4, we illustrate the results of running the Meta-MLEMTRL algorithm in the Chain environment for both the realisable and non-realisable settings. The choice of p determines how much the algorithm should be biased towards the model estimated using MLEMTRL and in the case when $p = 1$, Meta-MLEMTRL reduces to MLEMTRL. Similarly, if $p = 0$ then the algorithm will forego the MLEMTRL-estimate for the empirical estimate. Figure 4 shows that the performance of Meta-MLEMTRL is stable in long-run for different values of p . However, we identify that higher p values yield positive improvements in the cumulative reward over 10^5 steps, especially in the non-realisable setting. This indicates that the MLEMTRL-estimated model acts a good representation, while combined with the asymptotically converging empirical estimate obtained by Meta-MLEMTRL.

Summary of Results. In the experiments, we sought to identify whether the proposed algorithm shows superiority in terms of the transfer learning goals given by [13]. In the LQR-based environments, we can see a clear superiority of MLEMTRL in terms of learning speed compared to all baselines and in some cases, an asymptotic improvement. In the Chain environment, the proposed

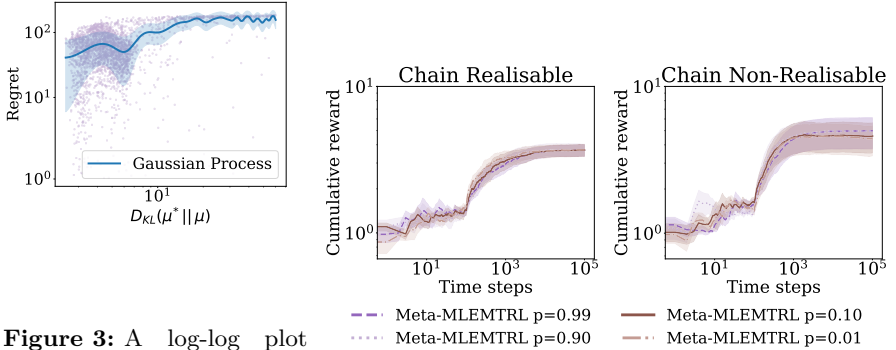


Figure 3: A log-log plot of regret vs. KL-divergence between the true MDP and the best proxy model in CartPole. The thick blue line is a Gaussian Process regression model fitted on observed data (in purple).

Figure 4: Figure depicting an ablation study of the prior parameter p in the Meta-MLEMTRL algorithm. The y-axis is the average cumulative reward at each time step computed over 10 novel tasks and the shaded region represents the standard error. When $p = 1$, the algorithm reduces to MLEMTRL and when $p = 0$ the algorithm reduces to standard maximum likelihood model estimation.

algorithm, MLEMTRL, outperforms PSRL in terms of learning speed. Also, we perform an ablation study of Meta-MLEMTRL under realisable and non-realisable settings, demonstrating provable improvements in the asymptotic and non-realisable regimes.

9 Discussions and Future Work

In this work, we aim to answer two central questions.

1. *How can we accurately construct a model using a set of source models for an RL agent deployed in the wild?*
2. *Does the constructed model allow us to perform efficient planning and yield improvements over learning from scratch?*

Our answer to the first question is by adopting the *Model Transfer Rein-*

forcement Learning framework and weighting existing knowledge together with data from the novel task. We accomplished this by following a maximum likelihood-based approach. This has led to a novel algorithm, MLEMTRL, consisting of a model identification stage and a model-based planning stage. The second question is answered by the empirical results in Section 8 and the theoretical results in Section 6. Further, the model allows generalising to novel tasks, given that the tasks are similar enough to the existing task(s).

We motivate the use of our framework in settings where an agent is to be deployed in a new domain that is similar to existing, known, domains. We verify the quick, near-optimal performance of the algorithm in the case where the new domain is similar and we prove worst-case performance bounds of the algorithm in both the realisable and non-realisable settings. As a future work, it would be interesting to study the MTRL framework under Bayesian setting [21] and to deploy it with a risk-sensitive value function [47], [48].

ACKNOWLEDGMENTS

This work was partially supported by the Wallenberg AI, Autonomous Systems and Software Program (WASP) funded by the Knut and Alice Wallenberg Foundation. D. Basu acknowledges the Inria-Kyoto University Associate Team “RELIANT” and the ANR JCJC grant for the REPUBLIC project (ANR22-CE23-0003-01).

References

- [1] G. Dulac-Arnold *et al.*, “Challenges of real-world reinforcement learning: Definitions, benchmarks and analysis,” *Machine Learning*, vol. 110, no. 9, pp. 2419–2468, 2021.
- [2] J. Skirzyński, F. Becker, and F. Lieder, “Automatic discovery of interpretable planning strategies,” *Machine Learning*, vol. 110, no. 9, pp. 2641–2683, 2021.
- [3] R. S. Sutton and A. G. Barto, *Reinforcement learning: An introduction*. MIT press, 2018.

- [4] T. M. Moerland, J. Broekens, A. Plaat, C. M. Jonker, *et al.*, “Model-based reinforcement learning: A survey,” *Foundations and Trends® in Machine Learning*, vol. 16, no. 1, pp. 1–118, 2023.
- [5] A. S. Polydoros and L. Nalpantidis, “Survey of model-based reinforcement learning: Applications on robotics,” *Journal of Intelligent & Robotic Systems*, vol. 86, no. 2, pp. 153–173, 2017.
- [6] X. B. Peng, M. Andrychowicz, W. Zaremba, and P. Abbeel, “Sim-to-real transfer of robotic control with dynamics randomization,” in *2018 IEEE international conference on robotics and automation (ICRA)*, 2018.
- [7] M. E. Taylor, N. K. Jong, and P. Stone, “Transferring instances for model-based reinforcement learning,” in *Joint European conference on machine learning and knowledge discovery in databases*, 2008.
- [8] M. E. Taylor and P. Stone, “Transfer learning for reinforcement learning domains: A survey.,” *Journal of Machine Learning Research*, vol. 10, no. 7, 2009.
- [9] A. Lazaric, “Transfer in reinforcement learning: A framework and a survey,” in *Reinforcement Learning*, Springer, 2012, pp. 143–173.
- [10] R. Laroche and M. Barlier, “Transfer reinforcement learning with shared dynamics,” in *Thirty-First AAAI Conference on Artificial Intelligence*, 2017.
- [11] A. Zhang, H. Satija, and J. Pineau, “Decoupling dynamics and reward for transfer learning,” *arXiv preprint arXiv:1804.10689*, 2018.
- [12] A. A. Rusu *et al.*, “Policy distillation,” *arXiv preprint arXiv:1511.06295*, 2015.
- [13] P. Langley, “Transfer of knowledge in cognitive systems,” in *Talk, workshop on Structural Knowledge Transfer for Machine Learning at the Twenty-Third International Conference on Machine Learning*, 2006.
- [14] Z. Zhu, K. Lin, A. K. Jain, and J. Zhou, “Transfer learning in deep reinforcement learning: A survey,” *IEEE Transactions on Pattern Analysis and Machine Intelligence*, 2023.
- [15] E. Parisotto, J. L. Ba, and R. Salakhutdinov, “Actor-mimic: Deep multi-task and transfer reinforcement learning,” *arXiv preprint arXiv:1511.06342*, 2015.

-
- [16] I. Arnekvist, D. Kragic, and J. A. Stork, “Vpe: Variational policy embedding for transfer reinforcement learning,” in *2019 International Conference on Robotics and Automation (ICRA)*, 2019.
 - [17] C. G. Atkeson and J. C. Santamaria, “A comparison of direct and model-based reinforcement learning,” in *Proceedings of international conference on robotics and automation*, vol. 4, 1997.
 - [18] C. Rommel, J. F. Bonnans, B. Gregorutti, and P. Martinon, “Aircraft dynamics identification for optimal control,” in *7th European Conference on Aeronautics and Space Sciences (EUCASS 2017)*, 2017.
 - [19] A. Wilson, A. Fern, S. Ray, and P. Tadepalli, “Multi-task reinforcement learning: A hierarchical bayesian approach,” in *Proceedings of the 24th international conference on Machine learning*, 2007.
 - [20] A. Lazaric and M. Ghavamzadeh, “Bayesian multi-task reinforcement learning,” in *ICML-27th International Conference on Machine Learning*, 2010.
 - [21] A. Tamar, D. Soudry, and E. Zisselman, “Regularization guarantees generalization in bayesian reinforcement learning through algorithmic stability,” in *Proceedings of the AAAI Conference on Artificial Intelligence*, vol. 36, 2022.
 - [22] F. L. Da Silva and A. H. R. Costa, “A survey on transfer learning for multiagent reinforcement learning systems,” *Journal of Artificial Intelligence Research*, vol. 64, pp. 645–703, 2019.
 - [23] X. Liang, Y. Liu, T. Chen, M. Liu, and Q. Yang, “Federated transfer reinforcement learning for autonomous driving,” in *Federated and Transfer Learning*, Springer, 2023, pp. 357–371.
 - [24] M. L. Puterman, *Markov decision processes: discrete stochastic dynamic programming*. John Wiley & Sons, 2014.
 - [25] R. E. Kalman, “A new approach to linear filtering and prediction problems,” 1960.
 - [26] J. Willems, “Least squares stationary optimal control and the algebraic riccati equation,” *IEEE Transactions on automatic control*, vol. 16, no. 6, pp. 621–634, 1971.
 - [27] D. E. Bell, “Regret in decision making under uncertainty,” *Operations research*, vol. 30, no. 5, pp. 961–981, 1982.

- [28] G. Casella and R. L. Berger, *Statistical inference*. Cengage Learning, 2021.
- [29] J. Kiefer and J. Wolfowitz, “Consistency of the maximum likelihood estimator in the presence of infinitely many incidental parameters,” *The Annals of Mathematical Statistics*, pp. 887–906, 1956.
- [30] W. K. Newey and J. L. Powell, “Asymmetric least squares estimation and testing,” *Econometrica: Journal of the Econometric Society*, pp. 819–847, 1987.
- [31] G. Ciuperca, A. Ridolfi, and J. Idier, “Penalized maximum likelihood estimator for normal mixtures,” *Scandinavian Journal of Statistics*, vol. 30, no. 1, pp. 45–59, 2003.
- [32] R. Ouhamma, D. Basu, and O. Maillard, “Bilinear exponential family of mdps: Frequentist regret bound with tractable exploration & planning,” in *Proceedings of the AAAI Conference on Artificial Intelligence*, vol. 37, 2023.
- [33] J. Aitchison and S. Silvey, “Maximum-likelihood estimation of parameters subject to restraints,” *The annals of mathematical Statistics*, vol. 29, no. 3, pp. 813–828, 1958.
- [34] D. Kraft, “A software package for sequential quadratic programming,” *Forschungsbericht- Deutsche Forschungs- und Versuchsanstalt fur Luft- und Raumfahrt*, 1988.
- [35] A. Zhang, S. Sodhani, K. Khetarpal, and J. Pineau, “Learning robust state abstractions for hidden-parameter block mdps,” in *International Conference on Learning Representations*, 2020.
- [36] A. L. Strehl and M. L. Littman, “A theoretical analysis of model-based interval estimation,” in *Proceedings of the 22nd international conference on Machine learning*, 2005.
- [37] P. Auer, T. Jaksch, and R. Ortner, “Near-optimal regret bounds for reinforcement learning,” *Advances in neural information processing systems*, vol. 21, 2008.
- [38] J. Qian, R. Fruin, M. Pirotta, and A. Lazaric, “Concentration inequalities for multinoulli random variables,” *arXiv preprint arXiv:2001.11595*, 2020.

- [39] I. Osband, D. Russo, and B. Van Roy, “(more) efficient reinforcement learning via posterior sampling,” in *Advances in Neural Information Processing Systems*, 2013.
- [40] T. Minka, “Bayesian linear regression,” Citeseer, Tech. Rep., 2000.
- [41] T. Haarnoja, A. Zhou, P. Abbeel, and S. Levine, “Soft actor-critic: Off-policy maximum entropy deep reinforcement learning with a stochastic actor,” in *International conference on machine learning*, 2018.
- [42] T. Yu *et al.*, “Meta-world: A benchmark and evaluation for multi-task and meta reinforcement learning,” in *Conference on robot learning*, 2020.
- [43] J. Schulman, F. Wolski, P. Dhariwal, A. Radford, and O. Klimov, “Proximal policy optimization algorithms,” *arXiv preprint arXiv:1707.06347*, 2017.
- [44] R. Dearden, N. Friedman, and S. Russell, “Bayesian q-learning,” *Aaai/iaai*, vol. 1998, pp. 761–768, 1998.
- [45] A. G. Barto, R. S. Sutton, and C. W. Anderson, “Neuronlike adaptive elements that can solve difficult learning control problems,” *IEEE transactions on systems, man, and cybernetics*, no. 5, pp. 834–846, 1983.
- [46] Y. Tassa *et al.*, “Deepmind control suite,” *arXiv preprint arXiv:1801.00690*, 2018.
- [47] H. Eriksson, D. Basu, M. Alibeigi, and C. Dimitrakakis, “Sentinel: Taming uncertainty with ensemble based distributional reinforcement learning,” in *Uncertainty in Artificial Intelligence*, 2022.
- [48] Y. Flet-Berliac and D. Basu, “Saac: Safe reinforcement learning as an adversarial game of actor-critics,” in *RLDM 2022-The Multi-disciplinary Conference on Reinforcement Learning and Decision Making*, 2022.